STUDY OF CORRELATIONS BETWEEN NUCLEAR FLOW AND STOPPING IN HEAVY-ION COLLISIONS

A THESIS

submitted to the

THAPAR INSTITUTE OF ENGINEERING AND TECHNOLOGY UNIVERSITY, PATIALA

for the degree of

DOCTOR OF PHILOSOPHY

IN THE FACULTY OF SCIENCE

By

Rubina Bansal

Regn. No. 901112005

SCHOOL OF PHYSICS AND MATERIALS SCIENCE

THAPAR INSTITUTE OF ENGINEERING AND TECHNOLOGY UNIVERSITY

PATIALA-147004, PUNJAB,

(INDIA)

Dedicated to

My papa

CANDIDATE'S DECLARATION

This is to certify that the thesis entitled " **STUDY OF CORRELATIONS BETWEEN NUCLEAR FLOW AND STOPPING IN HEAVY-ION COLLISIONS**" in partial fulfilment of the requirements for the award of Degree of Doctor of Philosophy in the School of Physics and Materials Science, Thapar institute of Engineering and Technology University, Patiala, is a record of the my own work carried out by me under the supervision of Dr. Suneel Kumar, Professor, Department of Physics, University Institute of Sciences, Chandigarh University, Gharuan (Mohali). The matter presented in this thesis has not been submitted in part or full for the award of any degree in any university or institute. I shall be responsible for plagiarism beyond the limit specified by Thapar institute of Engineering and Technology University, Patiala.

Rubina

(Rubina Bansal)

This is to certify that the above statement made by the candidate is correct to the best of our knowledge.

S Kumar
23/10/2017

Dr. Suneel Kumar
Professor
Department of Physics
University Institute of Sciences,
Chandigarh University, Gharuan
Mohali (Punjab)

Acknowledgments

Firstly, I would like to pay high regards to my Goddess Kali who gave me some intellect and wisdom to reach where I am today. She is only one, who always listen me without any argument. During the inevitable ups and downs of my research she often reminded me lifes true priorities.

I would like to express my most sincere gratitude to my thesis supervisor **Dr. Suneel Kumar** *Professor, Department of Physics, University Institute of Sciences, Chandigarh University, Gharuan.* I started my Ph.D. pursuit four years ago, with absolute no experience in theoretical research. It is the enthusiasm he has toward research that attracted me into the field of heavy-ion reactions in the first place. His intuition and persistency are the key reasons that I could successfully finish each of the research topics.

Special thanks go to **Dr. Rajeev K. Puri** *Professor, Panjab University, Chandigarh* for his enthusiasm. He has especially contributed a lot to this thesis during the data analysis. He is an inexhaustible source of intellectual and creative energy. His good sense in finding general physics laws to explain complicated theoretical data was an excellent lesson to me. I am extremely impressed by his ability to get an intuitive feel of the most difficult ideas. It is a fortunate for me being associated with them in research field.

I offer my special thanks to **Sr. Prof. O. P. Pandey**, *Dean, Research and Sponsered Projects, Thapar University, Patiala.* Words are not enough to express his ability to get an intuitive feel of the most difficult ideas. A million thanks to him, as he gave me the strength, to make my dream come true. He pushed me forward with word, "I am always here". There are no words to express his importance to fulfill my dream. I can never forget what he has done for me. I can not see the good shape of my thesis without his help and suggestions in formatting the entire thesis.

A special thanks to **Sh. Gurbinder Singh**, *Registrar, Thapar University, Patiala* and

Dr. Perakash Gopalan, *Director, Thapar University, Patiala*, who helped me a lot to complete my work. I know that I will not be able to convey full appreciation to them that they have done for me.

I would also like to thank, **Dr. Manoj Kumar Sharma, Dr. Alka Upadhyay** and **Dr. S. Jana** for serving as my committee members even at hardship. I also want to thank you for letting my defense be an enjoyable moment, and for your brilliant comments and suggestions, thanks to you.

I gratefully acknowledge **Dr. A. K. Lal**, *Associate Professor, Thapar University, Patiala* for his personal attention to solve my problems regarding the programming.

I am thankful to my labmates and friends **Sangeeta, Kamaldeep Kaur**, **Mandeep Kaur**, **Dr. Anupriya Jain**, **Dr. Karan Singh Vinayak**, **Rajni**, **Dr. Deepika Jain**, **Dr. Chandni Khurana**, **Dr. Harjinder Singh**, **Dr. Samiksha Verma** and **Dr. Mintu Tiyagi** for their constant support and encouragement. My special thanks to my friend **Navjot Kaur Virk**. I can not complete my thesis without her help. She helped me in that time, when I need her. She helped me without her benefit. She gave me her precious time that I can not return her. I admire his distinguished helping nature.

A special thanks to my family; my father **Madan Lal Bansal** and mother **Bhawana Bansal**. I can not prove my existence without their sacrifices and trust. Its your labour and patience paved the way to achieve my goal. My achievement is not this work, its your smile that comes to see me happy. I am also grateful to my mother-in law **Promila Jindal** and father-in-law **Tarsem Jindal** for all of the sacrifices that you have made on my behalf. Your prayer for me has led to sustain the pressure. I would also like to thank to my beloved husband **Amit Jindal**. Thank you for supporting me for everything, and encouraging me throughout this experience. I am grateful to you for understanding and trusting on me, fight for me and for all affords that you have made for me without my knowledge. My special thanks to my sister **Deepika Bansal** and brothers **Sumit Bansal** & **Kunal Bansal**,

who have taken my dream as their dream. You have sacrificed your future for me. There is no word to express your sacrifices to fulfil by dream. You smile with me and make it inexpressible and you weeped with me to share my grief. This thesis can not be completed without a little angel, my beloved daughter **Daanya**. I can not thank her in words, because she wept for me, without saying any word. Her smile gave me alight that nothing is impossible and no one can survive in this world without struggle. A special thanks to my uncle **Om Lalit Gupta**, who was the source of inspiration for me and gave me strength to never afraid from truth. I can not complete my thesis without his constant moral support.

Beside this, I am thankful to those people, who have knowingly and unknowingly helped me in the successful completion of my thesis.

Rubina

Date : October 2017 (Rubina Bansal)

Patiala

List of Publications :

A. Journals :

1. Isospin effects on p_t-differential flow in heavy ion collisions at intermediate energies.
   Rubina Bansal, Anupriya Jain and Suneel Kumar,
   Inter. Jour. of Mod. Phys. E 23, 1450062 (2014).

2. Correlation between directed transverse flow and nuclear stopping around the energy of vanishing flow.
   Rubina Bansal, Anupriya Jain and Suneel Kumar,
   Indian Jour. of Phys. 89, 1077 (2015).

B. Symposia/Workshops/Conferences:

3. Isospin effects on fragmentation in heavy ion collisions.
   Rubina Bansal and Suneel Kumar,
   AIP Conf. Proc. 1524, 232 (2013).

4. Effect of symmetry energy on intermediate mass fragment production.
   Rubina Bansal and Suneel Kumar,
   Proceedings of the DAE Symp. on Nucl. Phys. 56, 778 (2011).

5. On the directed transverse flow and the relation between symmetric and asymmetric collisions.
   Karan Singh Vinayak, Rubina Bansal and Suneel Kumar,
   Proceedings of the DAE Symp. on Nucl. Phys. 57, 698 (2012) .

6. Charge contents of fragment produced in heavy ion collision near Fermi energy regime.
   Rubina Bansal, Suneel Kumar and Rajeev K. Puri,
   Proceedings of the DAE Symp. on Nucl. Phys. 57, 722 (2012).

7. Effect of incident energy and mass asymmetry on the production of charge fragments.
   Rubina Bansal, Suneel Kumar and Rajeev K. Puri,
   Proceedings of the DAE Symp. on Nucl. Phys. 57, 724 (2012).

8. Influence of density dependent of symmetry energy on neutron-proton directed transverse flow.
   Rubina Bansal, Anupriya Jain and Suneel Kumar,
   Proceedings of the DAE Symp. on Nucl. Phys. 58, 346 (2013).

9. Correlation between temperature, density and nuclear stopping in heavy ion collisions.
   Suneel Kumar, Anupriya Jain and Rubina Bansal,
   Proceedings of the DAE Symp. on Nucl. Phys. 58, 344 (2013).

10. On the stability of final stage fragments obtained through transport models.
    Amandeep Kaur, Rubina Bansal and Suneel Kumar,
    Proceedings of the DAE Symp. on Nucl. Phys. 59, 448 (2014).

Contents

ABSTRACT

The present work deals with the study of collective flow and nuclear stopping for mass symmetric and asymmetric colliding nuclei in heavy-ion collisions. The simulations are carried out by using *Isospin-dependent Quantum Molecular Dynamics* (IQMD) model. The role of mass asymmetry on collective flow and nuclear stopping is studied in detail. The nuclear stopping associated with various fragments is also studied. The correlation of nuclear stopping with directed and elliptical flow is also established.

The present thesis is divided into following five chapters.

Chapter 1 presents the general introduction of heavy-ion collisions in mass symmetric and asymmetric reactions. The various observables and their correlation with nuclear equation of state have been discussed. It also presents the status of the available theoretical and experimental attempts made to understand the collective flow, nuclear stopping and correlations between them.

Chapter 2 gives the details of various theoretical models used in literature to study the heavy-ion collisions. This chapter include detailed explanation of the isospin dependent Quantum Molecular Dynamics model used to study the heavy-ion collisions. Primary model produce the phase space of the nucleons. The secondary model namely minimum spanning tree (MST) method used to analyze the phase space of nucleons generated by the primary models is also discussed.

In **Chapter 3**, the role of isospin degree of freedom in heavy-ion collisions through the transverse momentum (p_t), isospin content ratio and system mass dependence of p_t-differential transverse flow is discussed. The results are discussed for the symmetric systems. The p_t-differential transverse flow is highly sensitive towards the symmetry energy and its density dependence. The p_t-differential transverse flow dependence is found to be more sensitive towards the symmetry energy and its density dependence compared to the

energy of vanishing flow. The effect of density dependent symmetry energy under different rapidity bins are discussed and compared the theoretical calculations with the experimental data of FOPI collaboration.

Chapter 4, author has studied the effect of mass asymmetry on nuclear stopping $\langle R \rangle$ by keeping the total mass fixed. A reasonable significance has found in fragments stopping over the nucleons stopping by comparing the theoretical results with experimental data of INDRA collaboration for nearly symmetric reactions. Correlations between directed transverse flow $\langle P_x^{dir} \rangle$ and nuclear stopping $\langle R \rangle$ for mass asymmetric reactions have been studied. The study reveals that at high incident energy, correlation between the directed transverse flow and nuclear stopping follows a linear behavior, while at low incident energy, it follows a parabolic behavior. The positive value of elliptical flow signifies the in-plane particles emission, whereas negative value signifies the out-of-plane particles emission. Author has also studied the behavior of nuclear stopping for different fragments in out-of-plane and in-plane emitted particles by studying the nuclear stopping at and around the transition energy.

Finally, the results along with an outlook is summarized in **Chapter 5**.

Chapter 1

Introduction

1.1 Introduction of nuclear physics

It was assumed by John Dalton that atoms were the smallest part of any element [1]. But Rutherford scattering experiment in 1906 proved that 99.9% mass of an atom is contained in a nucleus [2]. The science of nuclear physics is associated with the properties of nuclear matter that makes up massive center of atoms, which accounts for 99.95% of the matter. Nuclear physics deals with the structure of nucleons, interactions among the nucleons and nucleon-nucleon scattering. Apart from basic research, it has remarkable contributions in the field of nuclear medicine [3], energy production [4], agriculture [5] and medical diagnosis [6].

The most challenging question in nuclear physics is to address the behavior of nuclear matter at extreme situations [7]. In early fifties of last century, due to the availability of light ions/particles accelerators, one can only studied the fission or fussion like processes by shooting the light ions/particles on heavy nuclei [8]. At low energy, one can study the nuclear interactions, cluster radioactivity, fusion-fission, formation of halo nuclei and radioactive heavy nuclei [9] etc. At low energies the reaction cross-section comprise of three categories i.e. deep inelastic scattering, fusion-fission and fussion evaporation [8]. The reaction dynamics are mainly governed by projectile-target combination, bombarding energy as well as by angular momentum of colliding nuclei. In due course of time, due to advanced technological development, one is able to accelerate heavy ions ($A \geq 4$) with colliding energies comparable to their mass. Thus a new branch of nuclear physics came into existence termed as intermediate energy heavy ion physics [10, 11, 12].

The intermediate energy heavy ion collisions (HICs) are proved to be a excellent tool to

explore the complex nuclear interactions inside the highly dense and hot compressed nuclear matter having density 3-4 times the normal nuclear matter density (0.15-0.17 fm^{-}3). The behavior of nuclear matter at different densities and temperature can be further analysed by studying the phase diagram of nuclear matter.

1.2 The phase transition of nuclear matter

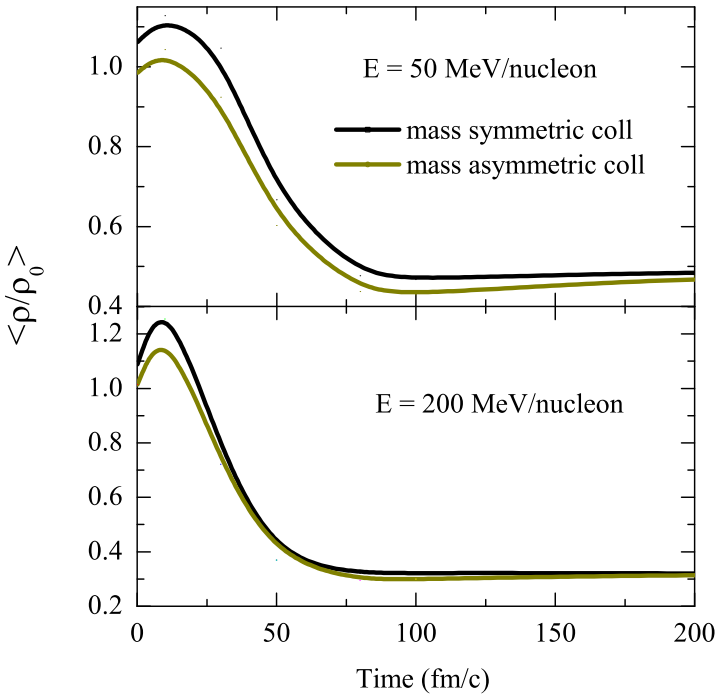

Figure 1.1: *Time evolution of density $\langle\rho/\rho_o\rangle$ at E = 50 MeV/nucleon (upper panel) and E = 200 MeV/nucleon (lower panel) for mass symmetric and asymmetric collisions.*

In HIC both target and projectile nuclei collide with each other and produce compressed and hot nuclear matter. The chattels of nuclear matter are highly influenced by pressure, temperature and density. The study of density and temperature dependence of hadronic systems for mass asymmetric collision is an interesting topic in nuclear physics. Mass asymmetry of colliding nuclei is represented by $\eta = |\ \frac{A_T - AP}{A_T + AP}\ |$, where A_T and A_P are masses of target and projectile, respectively. The physical mechanism and behavior behind of mass symmetric as well as asymmetric nucleus-nucleus collisions are entirely different from each other. This happens due to different form of thermal and compressional energy. In symmetric reactions, energy is deposited into system in the form of compressional en-

ergy, whereas in case of asymmetric collisions, the energy deposited is in the form of thermal excitation energy. In symmetric collisions, the compression is more due to the large interaction zone while in asymmetric collisions, the compression decreases due to increase in η. Moreover, in symmetric collisions due to large interaction zone large number of nucleons interacts with each other and large dissipation of energy take place, whereas in asymmetric collisions due to small interaction zone, low energy dissipation takes place.

In Fig. 1.1, the time evolution of density $\langle\rho/\rho_o\rangle$ at low energy (upper panel) and at intermediate energy (lower panel) have been displayed. One can see that mass symmetric and asymmetric reactions behave differently. Peak as well as saturation density reached in both type of nuclear reactions are different. The maximum density is reached around 10-30 fm/c and density become saturates above 100 fm/c. Moreover, the compressed nuclear matter saturate earlier at the high incident energy than low incident energy. Due to different density achieved in both type of reactions, different phenomena at same energy and collision geometry exhibit different behaviour.

Maximum and saturation density decide the fate of a reaction e.g. multifragmentation depends on saturation density, while nuclear flow and stopping depend on maximum density. Fig. 1.2 represents the mass asymmetry dependence of $\langle\rho/\rho_o\rangle^{max}$ and $\langle\rho/\rho_o\rangle^{sat}$ at different incident energies (E = 50 and 200 MeV/nucleon). One can see that the max density ($\langle\rho/\rho_o\rangle^{max}$) decreases with increase in mass asymmetry of colliding nuclei, whereas the saturation density $\langle\rho/\rho_o\rangle^{sat}$ is changes slowly at larger mass asymmetric collisions. This happens due to least destruction of non colliding nuclear matter in large mass asymmetric heavy-ion reactions. The variation of $\langle\rho/\rho_o\rangle^{max}$ and $\langle\rho/\rho_o\rangle^{sat}$ with mass asymmetry reflects that the density achieved during the collision depends on the size of colliding nuclei. The behaviour of density and temperature in various reaction conditions help to extract the properties of nuclear matter, which can be inferred by phase diagram.

The phase diagram of hot dense nuclear matter helps to understand the various reaction mechanisms in HIC. Fig. 1.3 shows the phase diagram of hot and dense nuclear matter. The x-axis represents the scaled density (ρ/ρ_0) of baryons, whereas y-axis represents the temperature (T) in MeV. The ground state represented at $\rho = \rho_0$ and T = 0. The nucleon-nucleon interactions behave similar as the Vander Waal forces, having short range repulsive

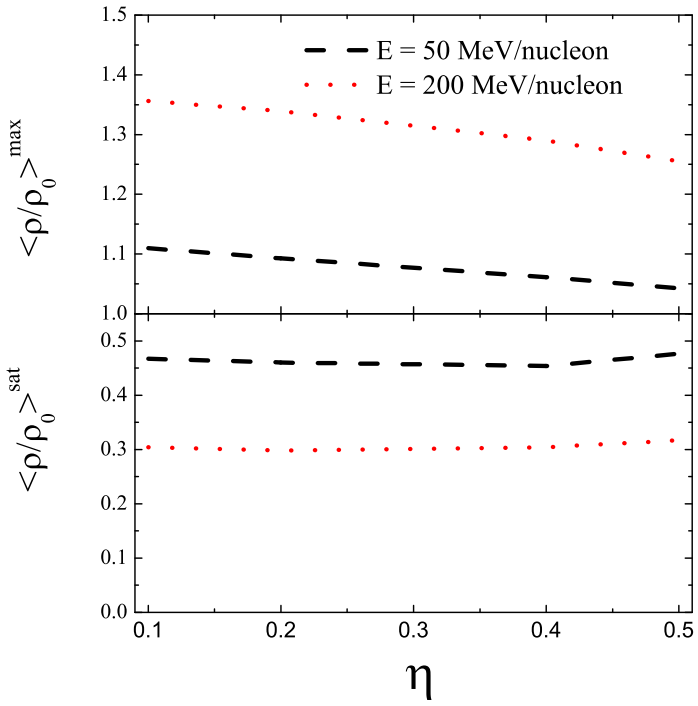

Figure 1.2: $\langle\rho/\rho_o\rangle^{max}$ *in upper panel and* $\langle\rho/\rho_o\rangle^{sat}$ *in lower panel as a function of mass asymmetry of colliding nuclei at* $E = 50$ *and 200 MeV/nucleon.*

and a long range attractive components. Thus, at ground state nuclear matter behave similar to the liquid drop. On increasing the temperature up to 15 MeV and decreasing the density from normal nuclear matter density, the liquid phase changes into gas phase. This phase transition region is named as liquid gas (LG) phase [13]. The region of very high temperature and density is dubbed as quark gluon plasma (QGP) phase [14, 15, 16]. The nuclear matter phase having density and temperature in between the LG and QGP phase is known as hadron gas (HG) phase. The region with density upto 10 times more than the normal nuclear matter density is considered as neutron star (NS) density region. The red dashed line corresponds to the path followed by the early Universe in first few minutes of its existence. The region separates the HG phase from the QGP phase is the phase of co-existence transition region [17, 18]. The pink dashed lines starting from the ground state represents the head-on collisions. After collision the compressed nuclear matter expands due to the internal collisions and cool down. The cooled nuclear matter dive into different regions of phase diagram. The maximum density and temperature achieved throughout the reaction depends on colliding energy, mass of the colliding nuclei and collision geometry.

The different phases shown on the diagram having different characteristics. The as-

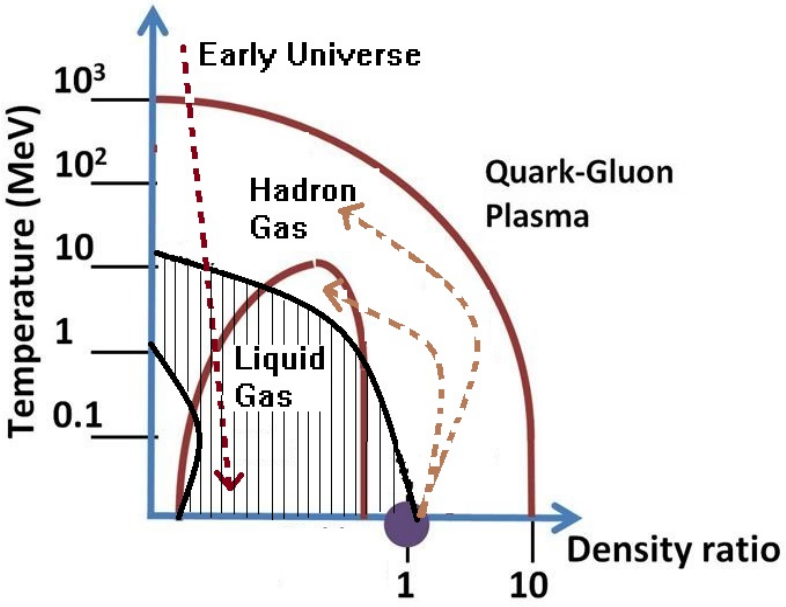

Figure 1.3: *Phase diagram of nuclear matter. The y-axis indicates the temperature (in MeV) and the x-axis indicates the baryons density normalized to the density of the ground state of nuclear matter [19].*

trophysical observable like NS give indirect information about the hot and dense nuclear matter. The HG and QGP phases subsisted in initial stage of universe formation, which is inaccessible today. The study of nuclear structure give information regarding the phenomena that takes place around the normal nuclear matter density and at low temperature. Both density as well as temperature decreases at freeze out point. However, nuclear matter can transform in any phase from higher density and temperature to lower one. Researchers are still continuing their attempts to extract the nuclear equation of state (EOS) for isospin symmetric as well as isospin asymmetric colliding nuclei. From all the above methods, HIC give a good opportunity to study the nuclear matter under extreme conditions of temperature and density. Maximum density of 2-3 times the normal nuclear matter density with maximum temperature of T = 100 MeV can be achieved in HIC. The present work deals with the mass symmetric as well as the mass asymmetric collisions in Fermi and intermediate energy region. According to the selected reaction conditions used in this work, the density is vary from 0.3 to 1.4 and temperature is goes up to 18 MeV, which is shown by shaded portion in phase diagram. The HICs involves many topics of interest like multi-

fragmentation, collective flow, nuclear stopping and their isospin dependence. The study of these observables describe the nuclear equation of state under extreme conditions of temperature.and density.

1.3 Nuclear equation of state

In intermediate energies the HICs are most eligible for the investigation of nuclear equation of state (NEOS) [10, 11, 12]. The knowledge of correct information of NEOS is vital to understand various models of early universe, neutron stars and supernova explosion etc. The elementary information of NEOS is extracted from the Weizsäcker binding energy formula and from the density profile of nuclear matter. The NEOS of symmetric nuclear matter is well recognized to study the giant dipole resonance, multifragmenation, collective flow, nuclear stopping etc [20]-[27].

Nuclear equation of state describes the energy and the density relation. The compressibil-

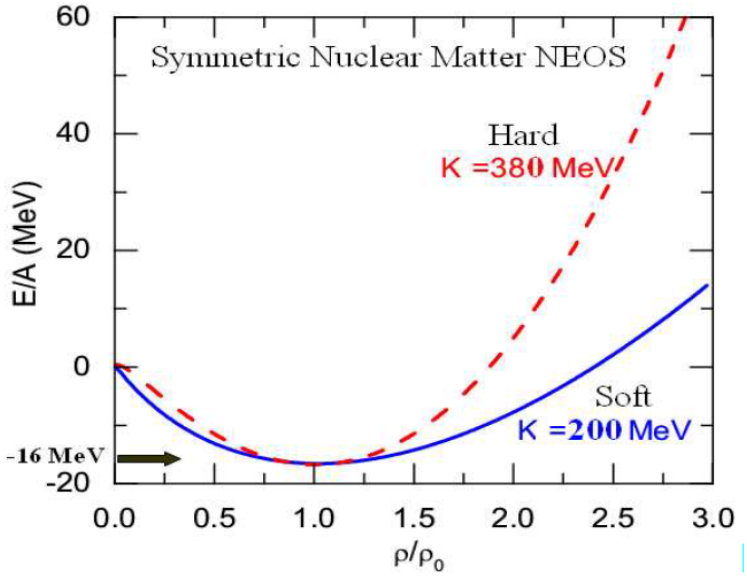

Figure 1.4: *The density dependence of compressional energy per nucleon. Different lines represent for the hard and soft NEOS. The figure is taken from the Ref. [7].*

ity of nuclear matter is characterized by the curvature of energy per nucleon, which depend on ρ. A well defined compressibility factor which describes the stiffness of symmetric nuclear

matter is defined as [28, 29]:

$$K = 9\rho_0^2 \frac{\partial^2}{\partial \rho^2} \left(\frac{E}{A} \right). \tag{1.1}$$

To get an idea from the (in)compressibility factor, one might run a parabola through two known points on the curve of E/A vs $\left(\frac{\rho}{\rho_0}\right)$ as shown in Fig. 1.4. Different equations of state have been suggested based on different parameterizations. The exact form of NEOS cannot be proposed with complete accuracy [7]. The only way to know the NEOS is through various observables associated with the phenomena like multifragmentation, nuclear stopping and nuclear flow, etc. On comparing the theoretical results with experimental data, one can guess which parameterization of NEOS is suitable. If the actual value of K is less than the standard value, then one consider it as soft EOS (represented by solid line) and if it overestimates the standard value, then it can be considered as hard EOS (represented by dashed line). Some attempts also have been made to understand the NEOS for isospin asymmetric nuclear matter [30, 31]. The NEOS of isospin asymmetric nuclear matter, particularly in regards to density dependent symmetry energy is recently under way [32, 33].

1.4 Reaction dynamics

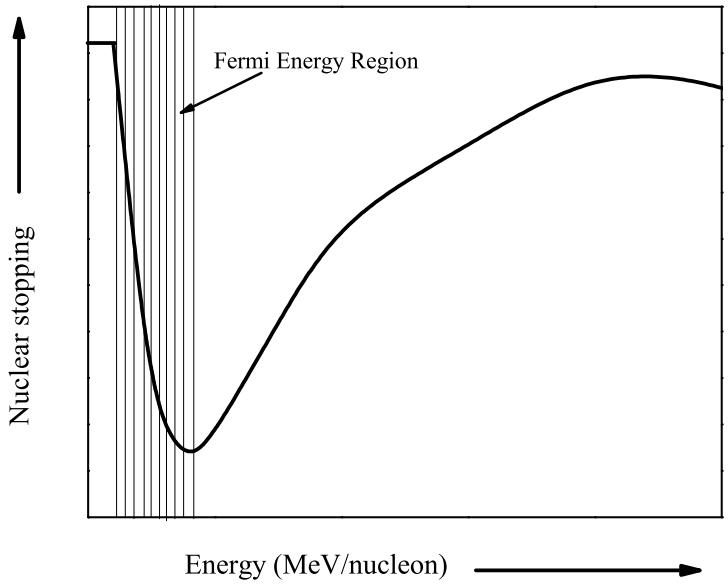

Figure 1.5: *Energy dependence of nuclear stopping.*

In earlier studies, due to the lack of technology, one has to work in limited energy and mass domain and these studies were limited to the process like fussion, fission, cluster radioactivity etc. But, now a days, due to the advancement in technical knowledge, it is possible to collide two mass asymmetric nuclei from few MeV/nucleon to several TeV/nucleon. On the basis of incident energy, the nuclear reactions can be classified into three regions: high energy region, intermediate energy region and low energy region. The phenomena (cluster-radioactivity, fussion, fission, formation of super-heavy nuclei and halo nuclei) that take place below 10 MeV/nucleon are lying in low energy region. In this energy region, one is mainly concerned about the study of nuclear structure. In low energy region, attractive mean field effects dominates and the nucleon-nucleon (NN) collisions are strongly restrained by Fermionic nature of nucleons and this phenomena is named as Pauli blocking [34, 35, 36]. The Pauli blocking and internuclear potential play a momentous role in this energy region. The influence of Pauli blocking decreases as incident energy increases.

The part of nuclear physics that corresponds to the formation of quark-gluon plasma

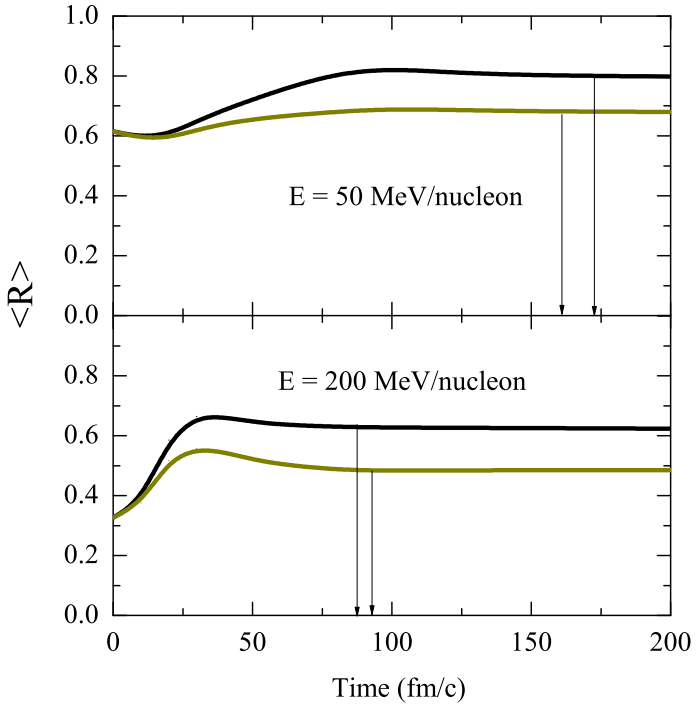

Figure 1.6: *The time evolution of nuclear stopping $\langle R \rangle$ for mass symmetric and asymmetric collisions in Fermi (upper panel) and intermediate (lower panel) energy region. Meaning of different lines are same as in Fig. 1.1.*

(QGP) [37] and breaking of nucleons into their constituents (quarks and gluons) is known

as high energy physics. The nuclear reactions that take place above 2 GeV/nucleon are considered to lie in high energy region. The energy region which lies between 50 MeV/nucleon $\leq$ E $\leq$ 2 GeV/nucleon is known as intermediate energy region. In this energy region, one can study the reactions under extreme conditions of density and temperature. The phenomena like multifragmentation, collective flow and nuclear stopping take place in this energy region. In intermediate energy region NN collisions play a crucial role.

The shaded energy region (shown in Fig. 1.5) between 20 to 100 MeV/nucleon, NN collisions (two-body correlation) try to superimpose on the mean field. Due to different characteristics, this region is dubbed as Fermi energy region. The Fermi energy region considers the mean field approach with realistic NN interactions. One can study the significance of Fermi energy region via study the energy dependence of nuclear stopping in central collisions. In Fig. 1.5, below Fermi energy region, the mean field governs the reaction dynamics and shows maximum stopping. However, above the Fermi energy region, NN collisions govern the reaction dynamics. In Fermi energy region both mean field and NN collisions contribute.

Incident energy changes the reaction dynamics significantly. In Fig. 1.6, the time evolu-

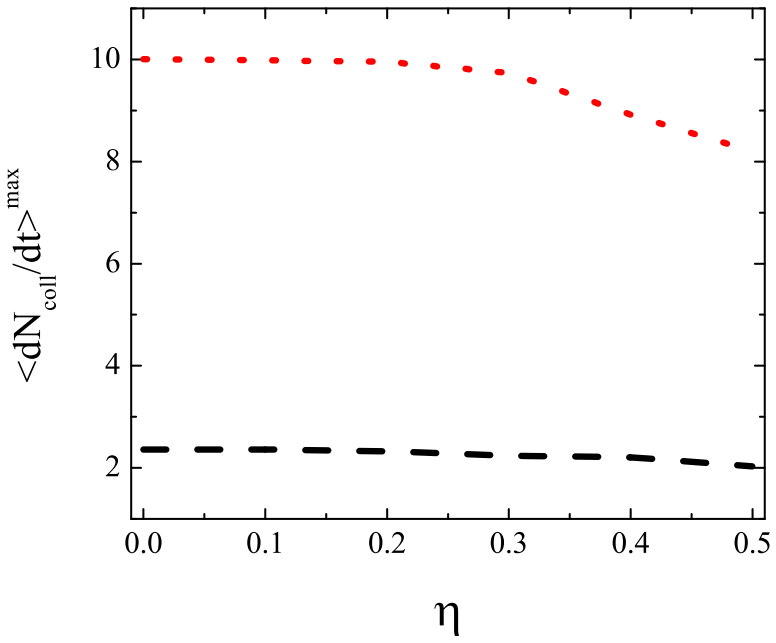

Figure 1.7: *The mass asymmetry dependence of maximum collisions suffered by colliding nuclei at E = 50 and 200 MeV/nucleon. The meaning of different lines are same as in Fig.1.2.*

tion of anisotropic ratio $\langle R \rangle$ for different values of mass asymmetry is displayed. In Fermi energy region, due to the dominant role of attractive mean field over NN collisions, the mean free path between successive NN collisions is large. Hence, $\langle R \rangle$ takes longer time to saturate at low energy. Moreover, at high energy (E = 200 MeV/nucleon), $\langle R \rangle$ increases till the time of maximum density. After that nuclear stopping gets saturated as the high density phase is over. This shows that NN collisions that takes place after high density region, do not alter their position in the momentum space. From both the panels, one can conclude that nuclear stopping saturate after t = 100 fm/c irrespective of mass asymmetry.

To study the mass asymmetry under different reaction conditions, Stöcker *et al.* [38] showed a pictorial view of colliding light projectile (Ne) on heavy target (U) at incident energies between E = 250 and 800 MeV/nucleon at different colliding geometries. For head on (central) collisions, projectile directly hit the target near the collision axis (z-axis) and generates a highly compressed and excited participant (stock) zone. In this case, the projectile fully merges into the target and both (target and projectile) suffer forward momentum which leads to the achievement of maximum stopping. However, at peripheral collisions residue of both the nuclei (target and projectile) kicked apart by highly compressed zone (participant zone). Due to the velocity effect, the projectile residue is deflected to forward angles, while target residue is azimuthally anticorrelated with projectile residue. Moreover, the excited target nucleus decay into fragments. With further increase in impact parameter, the projectile fragments originated from the bounce off region have large transverse as well as forward momentum, whereas, target residue moves slowly with parallel and perpendicular directions (near the initial position of target) i.e. the flow reduces as one consider heavy target and lighter projectile.

The maximum number of collisions ($\langle dn/dt \rangle$) suffered by colliding nuclei is also decreases with increase in mass asymmetry of colliding nuclei (shown in Fig. 1.7). In mass asymmetric collisions, the energy impelled into the system is dissipated in the rotational motion and correlations remain unaltered in non-colliding part. The study of mass asymmetric reactions is of great importance these days, because this technique can be used to produce radioactive nuclide. Also this information is important from the point of view of astrophysics because one can understand the mechanism of collisions among the galaxies in the universe. One

can use this information to interpret, why after so many billion years, the universe is still in non-equilibrium state. Isospin contents of colliding nuclei affect the reaction dynamics and can also be helpful to us to estimate the equation of state (EOS) of isospin asymmetric nuclear matter.

1.5 Isospin physics

Symmetries have been introduced in nuclear and particle physics to understand the complex interactions. Isospin is related to identical behavior of protons and neutrons. Isospin enter into the calculations through Coulomb interactions, symmetry potential and nucleon-nucleon (NN) cross-section. The term isospin refers to those particles (neutrons and protons), which are having similar properties, but differ only in electric charge. Availability of radioactive beams make possible to accelerate the nuclei with neutron number larger than the proton number. The interactions among the proton-proton (pp), neutron-neutron (nn) and neutron-proton (np) depend on their isospin. Thus, NEOS for the isospin symmetric nuclear matter (N = Z) shows different behavior from that of isospin asymmetric nuclear matter (N $\neq$ Z) [39]. Giant monopole resonance, collective flow and multifragmentation help us to estimate the NEOS of isospin symmetric or asymmetric nuclear matter [23, 40, 41]. The role of symmetry energy becomes more prominent in case of neutron-rich isospin asymmetric nuclear matter. The concept of symmetry energy inferred from Fig. 1.8.

In this figure, lower line represents the symmetric nuclear matter, while upper line represents the pure neutron matter. The difference between these two lines reflects the symmetry energy. The behavior of symmetry energy is repulsive for neutrons and attractive for protons [42]. In order to form a heavy nucleus, one has to bind large number of neutrons within the nucleus. However, to compensate the repulsive interactions between the neutrons (due to symmetry potential) large number of protons has to be added in the nucleus [42]. The large protons content tend to increase the Coulomb interactions, which are long range interactions. Both the symmetry energy as well as the Coulomb interactions are necessary to decide the fate of a nuclear reaction. The repulsive behavior of symmetry energy at all densities affect the reaction dynamics. However Coulomb interactions is an important asymmetry term that effect the observables of heavy ion reactions. Symmetry energy and

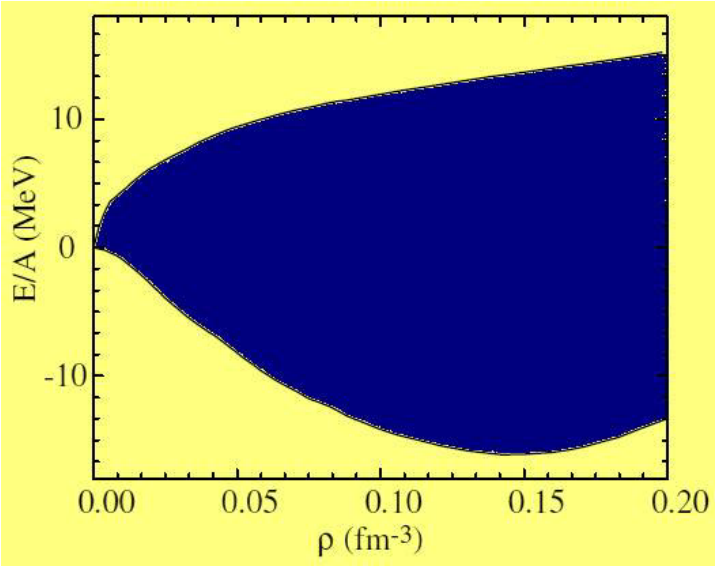

Figure 1.8: *The schematic view of symmetry energy. The two lines represent the energy density of pure neutron (upper line) and symmetric nuclear (lower line) matter. The difference of two lines reflects the symmetry energy. The figure is taken from the Ref. [43].*

its density dependence is one of the important feature of HIC these days.

1.5.1 Density dependence of symmetry energy

Information about the symmetry energy term is crucial for the nuclear physics community, as it emphasized the reaction dynamics induced by rare isotopes, on structure of radioactive nuclei, but also on the astrophysics community as it provide essential understanding about the evolution of supernova explosion and massive stars [44, 45]. The symmetry potential can not be directly measured, one has to be estimate through other observables such as [46], the neutron-proton differential flow [47], the t/^{3}He [48, 49], π^-/π^+ [50, 51, 52], Σ^-/Σ^+ [53], and K^0/K^+ [54].

The symmetry energy basically accounts for the large neutron content in the isospin asymmetric systems [55]. The variation of energy per nucleon in nuclear matter with density ρ and isospin asymmetry parameter γ can be estimated through parabolic function given by Heiselberg and Hjorth-Jensen [56] defined as:

$$E_{sym}(\rho) = E^0_{sym}(\rho_0)\left[\frac{\rho}{\rho_0}\right]^{\gamma}. \tag{1.2}$$

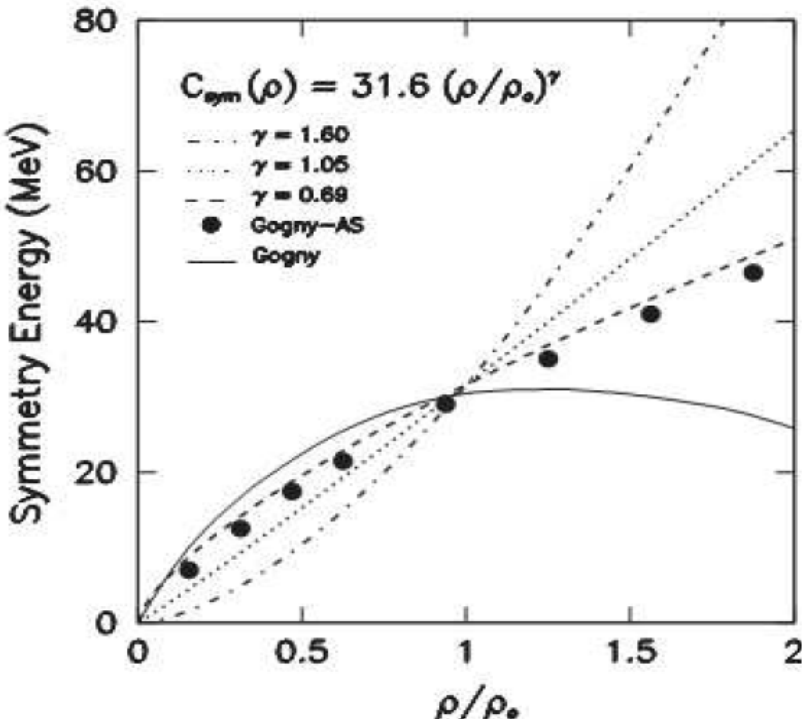

Figure 1.9: *Schematic representation of the density dependent symmetry energy for different γ values. This figure has been taken from the Ref. [57, 58].*

$E^0_{sym}(\rho_0)$ is the symmetry energy at normal nuclear matter density and $\frac{\rho}{\rho_0}$ is the scaled density. Hjorth-Jensen proposed the parameterized value of $E^0_{sym}(\rho_0) = 32$ MeV and stiffness parameter $\gamma = 0.66$. Till now, various forms of symmetry energy (values of stiffness factor γ) are proposed in the literature [59, 60, 61].

The γ gives strength (stiffness) value of symmetry energy at different densities as shown in Fig. 1.9. The symmetry energy whose strength increases till normal nuclear matter density ($\frac{\rho}{\rho_0} = 1$) followed by decrease afterwards at high densities is named as soft form of density dependent symmetry energy. However, for the case in which strength of symmetry energy increases monotonically with density is known as stiff form of density dependence symmetry energy. In chapter 3, author has discussed the influence of density dependent symmetry energy on nuclear flow under different reaction conditions.

1.5.2 Isospin dependence of NN cross-section

The another important parameter influenced by isospin of the nucleons is NN cross-section [40, 41]. In nuclear physics, the possibility of collision among nucleons are expressed

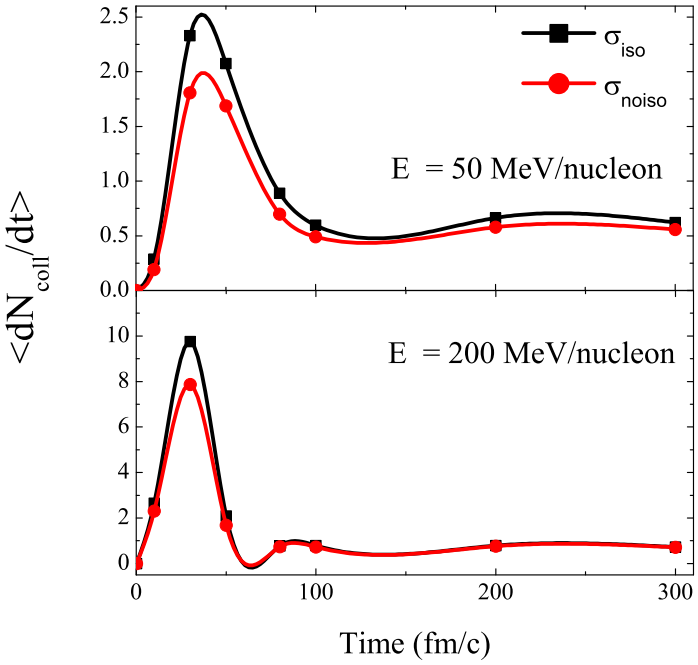

Figure 1.10: *The time evolution of ($\langle dN_{coll}/dt \rangle$) for isospin dependent (σ_{iso}) and independent (σ_{noiso}) NN cross-section. The different panels represented at different incident energies.*

by interaction cross-section. Basically, the cross-section is a imaginary area around the colliding nucleon that characterize the probability of collision. Transition matrices of isospin dependent channels, both channels (iso-singlet and -triplet) contribute to the np scattering, thus their interaction cross-section in free space is higher than the nn and pp, where only iso-triplet channel is contribute [55]. The scattering cross-section between np is about 3 times larger than the nn and pp cross-section.

In literature, various theoretical evidence have discussed the significance of various form of NN cross-section [62]-[66]. Cugnon *et al.* [62] developed the energy dependent cross-section. The energy dependent cross-section involved both elastic and inelastic contributions, which in supported by the center-of-mass energy available between two colliding nucleons. Faessler and co-workers [63, 64] first time reported the in-medium NN cross-section which is connected with the mean free path of nucleons in hot and dense nuclear matter and also gave a strong modification in free NN cross-section with density profile. Later on, Li *et al.* [65] studied the density dependence of in-medium NN cross-section. Cassing *et al.* [66] through G-Matrix estimated the in-medium NN cross-section.

In order to have the proper understanding of isospin dependent part of NEOS, one should

explicitly consider the isospin degree of freedom w.r.t the observables that affects the NEOS. In Fig. 1.10, the time evolution of collisions suffered by colliding nucleons is displayed for whole time span. For isospin independent cross section $\sigma_{pp} = \sigma_{nn} = \sigma_{np}$ and labeled as σ_{noiso}. One can see that larger number of collisions are suffered for the isospin dependent (σ_{iso}) cross-section compared to the isospin independent (σ_{noiso}) cross-section. The interplay between symmetry energy and isospin dependent NN cross-section on collective flow will be discussed in chapter 3. The next section carry a brief introduction of various observables (multifragmentation, collective flow and nuclear stopping) in HIC to study the isospin effects.

1.6 Various phenomena at intermediate energies

1.6.1 Multifragmentation

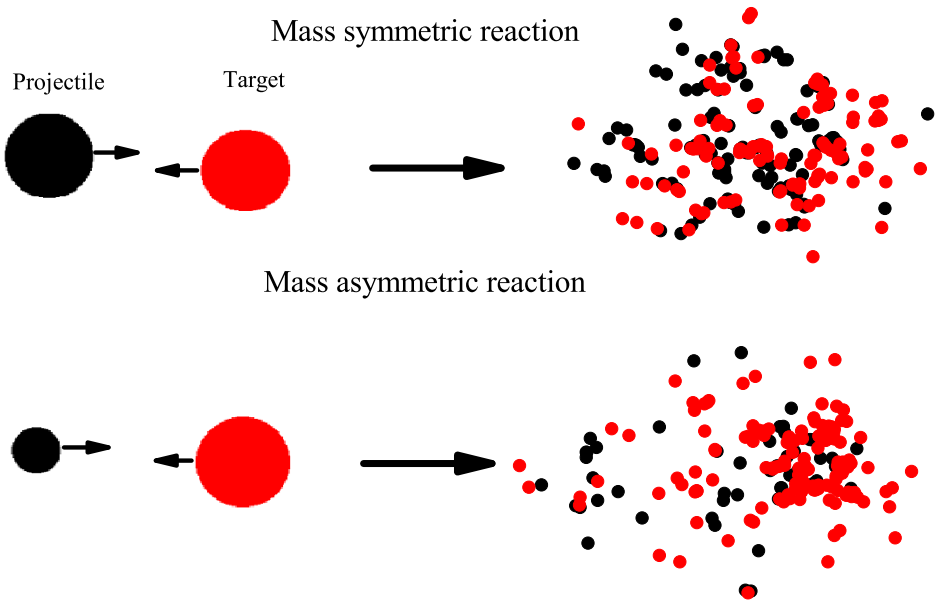

Figure 1.11: *Schematic view of the multi-fragmentation process for mass symmetric and asymmetric collisions.*

When two two heavy mass nuclei (target and projectile) collide with each other, an excited system is formed. The excited system breaks into many fragments of different masses. The phenomena of breaking of excited system into different mass fragments is known as "multifragmentation" [20, 21]. The pictorial view of multi-fragmentation process for mass

symmetric and mass asymmetric collisions is shown in Fig. 1.11. From figure, one can see that in initial stages of reaction, nuclear matter is highly dense for both mass symmetric and asymmetric collisions. During collision, nucleons of both nuclei (target and projectile) interact with each other. Due to NN interactions nuclear matter begin to expand from high pressure region to low pressure. The symmetric collision leads to a spherical distribution of nucleons. In symmetric collisions the colliding nucleons have sufficient energy to stop each other and the initial correlations are broken to a maximum level in symmetric collisions, as a result more randomization is observed. Moreover, in mass asymmetric collisions, emission of nucleons is not uniformly distributed in all the directions (as shown in Fig. 1.11). In mass asymmetric collisions, due to the smaller projectile, most of the projectile nucleons penetrates through the target nucleus. Thus, mass asymmetric collisions show different fragments distribution than the mass symmetric collisions.

To understand the phenomena of multifragmentation is an interesting study in current nuclear physics research. Theoretically, multifragmentation is considered to be very feasible to study the liquid-gas phase (LGP) [13]. The phenomena of multiplicity based on entrance channel parameters such as colliding geometry, incident energy, mass of the colliding nuclei, reaction cross-section, etc. Due to the violent phase of collisions in central collision lighter mass fragments are produced. However, in peripheral collisions, colliding nuclei interact partially with each other. Due to this, large mass fragments are emitted.

1.6.2 Collective flow

When two nuclei collide with each other at non central geometries, the achieved density is higher than the normal nuclear matter density, a flow pattern is developed during the subsequent expansion of the system. During the expansion of compressed system, the speed and direction of the constituent nucleons is influenced by the pressure gradient i.e. the emitted particles tend to move toward the low pressure region.

The phenomenon of collective flow is directly related to the pressure build up during the compression stage and gives information about the nuclear density and pressure (i.e. NEOS) [67]. The collective flow helps to understand the concept of thermalization and phase transition at high density [67]. On the basis of experimental findings and theoretical

calculations, there are different type of flows in intermediate HIC: radial [22], directed [23] and elliptic flow [68] etc.

Radial Flow

Radial flow is generated in central collisions and leads to an isotropic distribution of the emitted nucleons in transverse plane. The radial flow is characterized by the increased yield in kinetic energy spectra of nucleons emitted near $\theta_{c.m.} = 90^0$ relative to the incident beam axis (z-axis). Details of radial flow is described in Ref. [22].

The non-central collisions lead to directed and elliptical flow, which can be represented by the Fourier coefficients of the expansion given by Voloshin [69].

$$\frac{dN}{d\phi} \propto (1 + 2\sum_{n=1}^{\infty} v_n Cosn\ \phi). \tag{1.3}$$

Where ϕ is the azimuthal angle between the reaction plane and the transverse momentum

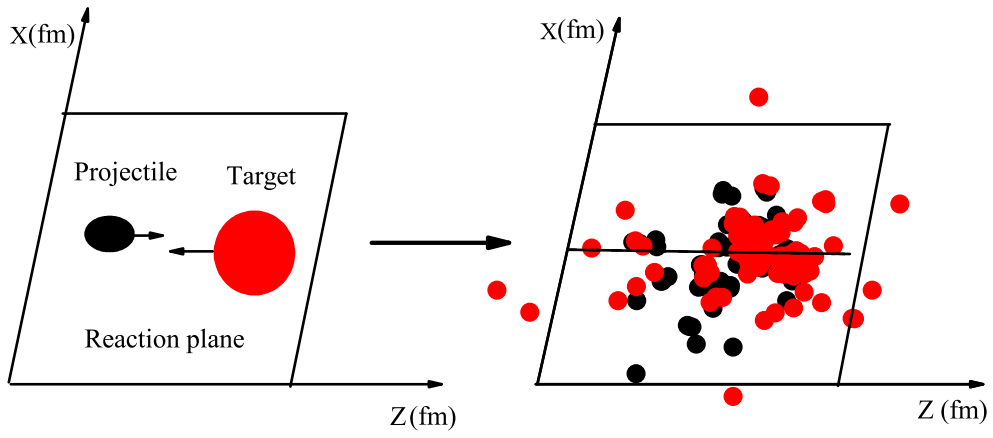

Figure 1.12: *Directed flow for asymmetric collision in the reaction plane.*

of the emitted particle. Fourier coefficient v_n characterized the strength of anisotropic flow.

Directed flow

The directed flow is defined as the transverse component of the particle's momentum with

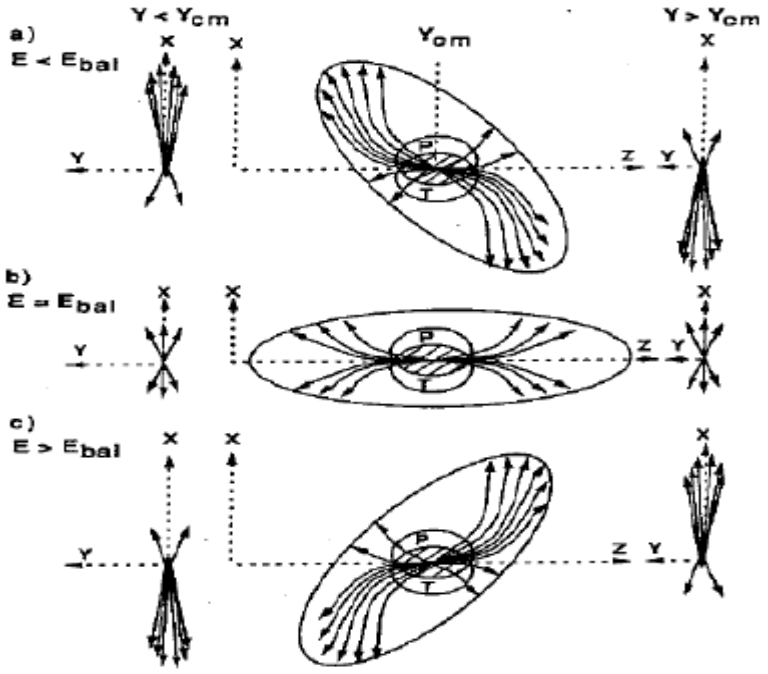

Figure 1.13: *Schematic representation of directed transverse flow in the reaction plane. Figure is taken from Ref. [76].*

in the reaction plane, thus dubbed as directed transverse flow. In literature, it is also known as in-plane or sidewards flow [70]-[75]. The word directed signifies that such flow is observed in a particular direction. Directed flow observed in non-central collisions, the preferential emission of the nucleons to and with in a particular side of reaction plane (the plane that contains both the line joining the centers of colliding nuclei and the incident beam axis). The Fig. 1.12 shows both forward and backward going section of particles flow in reaction plane. In mass asymmetric collisions (with light projectile and heavy target), the nucleons show backward scattering. The directed flow shows sensitivity toward the compressibility of the nuclear matter. It has been experimentally proven that above 100 MeV/nucleon the mean transverse momentum changes sign with collision energy [70, 71, 72]. At low incident energies, the nuclear interactions are governed via attractive nuclear mean field which deflect the nucleons to the negative angles [73]. Moreover, at high energy the NN collisions and the repulsive part of the mean field dominate the dynamics, therefore the nucleons get deflected towards the positive angles [74, 75]. The attractive interactions are balanced by the repulsive interactions on varying incident energy from low to high. The energy, where

directed flow becomes zero is known as the energy of vanishing flow (EVF) or balance energy (E_{bal}) [77, 78, 79]. A schematic illustration is given in Fig. 1.13.

The directed transverse flow in mid-rapidity (highly compressed) region is quite interesting to study the reaction mechanism. The strength of directed transverse flow is measured by calculating the slope in mid-rapidity region ($\left|\frac{Y_{c.m.}}{Y_{beam}}\right| \leq 0.1$, here $Y_{c.m.} = \frac{1}{2} ln \frac{E(i)+p_z(i)c}{E(i)-p_z(i)c}$ where $E(i)$ and $p_z(i)$ are the total energy and the longitudinal momentum of the i^{th} nucleon, respectively) [7]. The detailed analysis of directed transverse flow at different reaction conditions (colliding geometry, incident energies and mass asymmetry) is discussed in chapter 3.

Elliptical flow

In non-central collisions, the anisotropy of the ϕ distribution at mid-rapidity appears

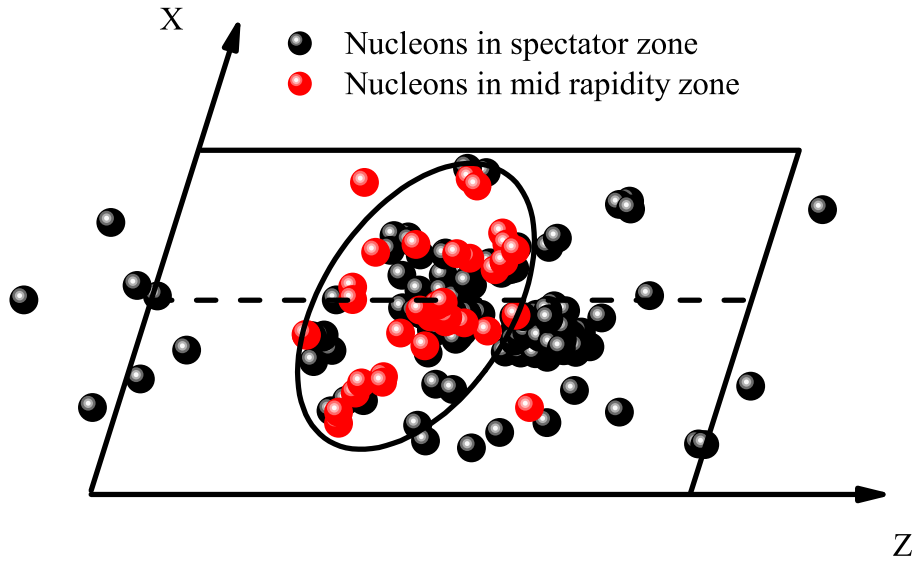

Figure 1.14: *Elliptical flow for asymmetric collision in the reaction plane.*

like an ellipse (as shown in Fig. 1.14) and the corresponding flow of nucleons is known as elliptical flow and generally represented as $\langle v_2 \rangle$. In Fig. 1.14, the red spheres represent the nucleons of mid-rapidity region and one can see that the nucleonic distribution in mid-rapidity region shows a ellipse type behaviour in reaction plane. The value of ϕ distribution

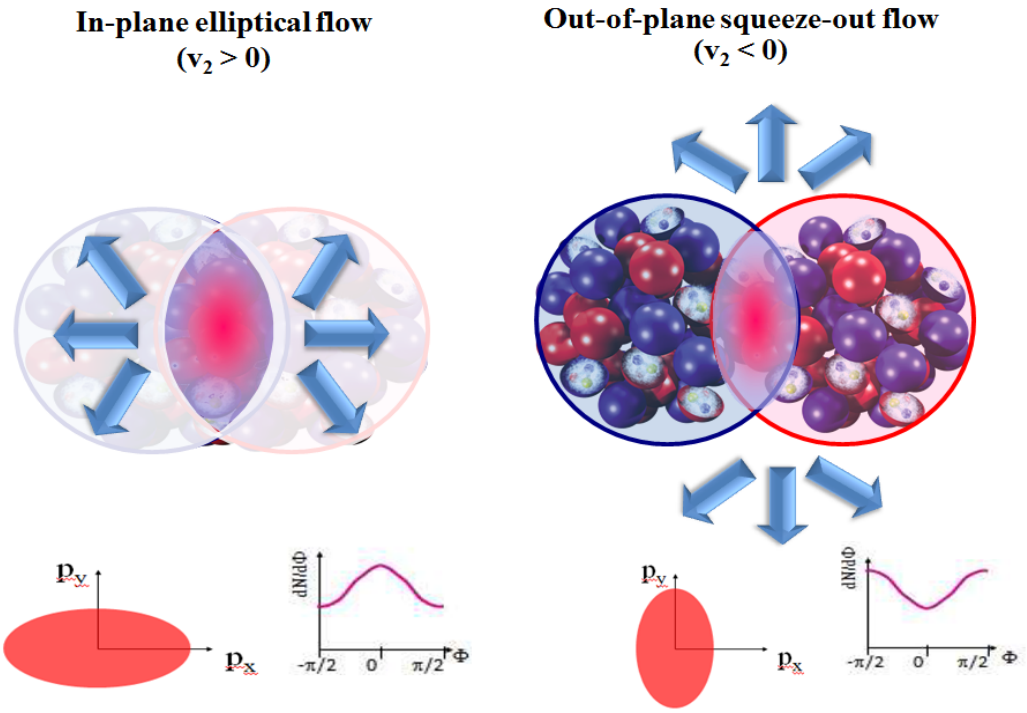

Figure 1.15: *Schematic representation of in-plane flow (left side) and out-of-plane flow (right side) in the reaction plane.*

explains whether the particle emission is out-of-plane ($v_2 < 0$) or in-plane ($v_2 > 0$). A pictorial view of out-of-plane and in-plane is presented in Fig. 1.15. The peak of ϕ distribution at 0^0 and 180^0, indicates the in-plane flow (shown in left side of Fig. 1.15), whereas peak of ϕ distribution at $\pm 90^0$ indicates the out-of-plane flow as shown in right side of Fig. 1.15. The energy, where elliptical flow changes its sign is known as transition energy (E_T) [80]. The effect of mass asymmetry on E_T will be studied in chapter 4.

1.6.3 Nuclear stopping

The theory given by Bohr in 1913 is treated as a precious and active tool in the description of nuclear stopping [81]. Nuclear stopping is defined as the impending force acting on the target nucleons due to the projectile nucleons, results in loss of energy and nucleon set drifted in transverse direction [82]. Due to the breakup of initial correlations among the target and projectile nucleons, there are complete memory loss of incoming momentum, this case is known as full stopping [83].

In literature, several independent parameters (rapidity distribution, anisotropy ratio and

quadrupole moment, variance) have been suggested to describe the nuclear stopping [83, 84, 85]. Other observables of HIC such as multifragmentation and collective flow have been correlated with nuclear stopping [24, 25, 26, 27]. Chapter 4 gives a brief discussion of correlation between nuclear stopping and collective flow (directed and elliptic) for whole range of incident energy and at different mass asymmetries.

1.7 Review of experimental and theoretical attempts to study the collective flow

One of the central goal of experimentalist is to study the nuclear matter under the extreme conditions of density and temperature at intermediate energies. The collective flow is the motion of particles described by the momentum of nucleons [86, 87, 88]. The hot and compressed nuclear matter behave like a compressible fluid and number of experiments have proved that the compressional energy can be studied via collective flow. The collective flow is explained as the azimuthal distribution of nuclear matter. The directed transverse flow is influenced by the cold matter deflected from the participant zone, while elliptical flow is caused by the hot and compressed nuclear matter emitted from the participant zone. Due to their marvel properties, collective flow helps to examine the reaction mechanism from National Superconducting Cyclotron Laboratory (NSCL) energy range to Relativistic Heavy Ion Collider (RHIC) energy range [89]-[94]. The collective flow helps to understand the NEOS of dense and hot nuclear matter. The study of collective flow in HIC has attracted both experimentalist and theoreticians.

Experimental attempts

In 1956, Belenkij and Landau [95], initially proposed the concept of collective flow by using fluid-dynamics model. Later on, in 1984 collective flow has been discovered experimentally at BEVALAC [96, 97, 98]. After that in 1989 Diogene Collaboration at Saturne Synchrotron in Saclay (France) studied the flow of particles at mid-rapidity in Ne-induced reaction at 800 MeV/nucleon [96]. The experiment was carried out at the Bevalac Streamer Chamber facility for highly asymmetric reaction. Their study gave the idea of studying the correlation between nuclear stopping and collective flow. Krofcheck *et al.* [99] in MSU, initially

reported the disappearance of directed flow by using digital streamer chamber photography. Later on, in USA at Michigan State University (MSU), the National Superconducting Cyclotron Laboratory (NSCL) studied the transverse flow for reactions of ^{58}Fe + ^{58}Fe and ^{58}Ni + ^{58}Ni in Fermi energy region and conclude that flow increases with increase in isospin ratio of colliding nuclei [100].

Experimentalists and theorists work together at NSCL to study and advancement in nu-

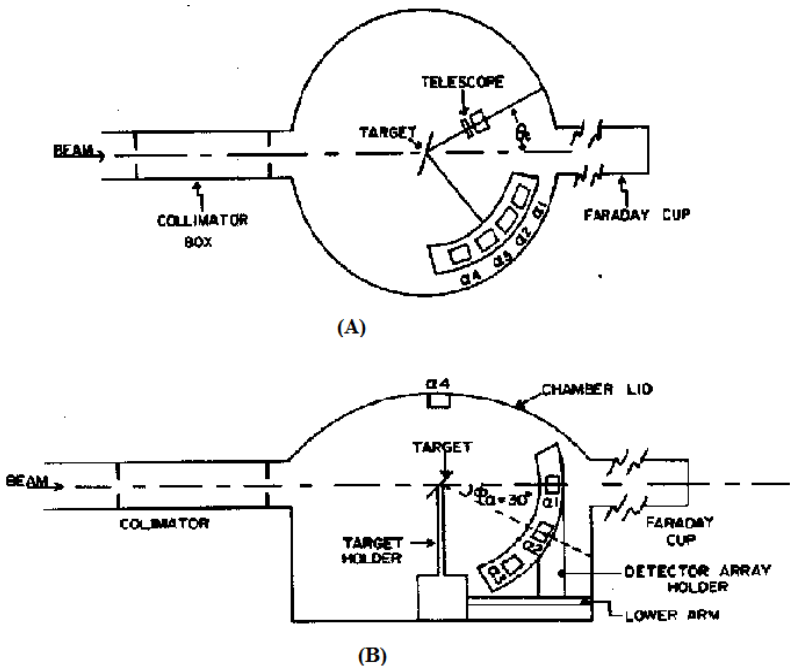

Figure 1.16: *The Scattering chamber set up of in-plane flow (A) and out-of-plane (B) array. Figure is taken from Ref. [101].*

clear physics. The primary goal of NSCL is to disentangle the secrecies of atomic nucleus. In NSCL the High Resolution Array (HiRA) [101] is use to detect the charged particles measuring their energy and identifying their mass & charge in nuclear collisions. The HiRA consists of 20 modules to allow flexibility to configure the arrays in different geometries. Each module has three layers of detector material. The first two layers are made from high purity silicon and third one is made of Cesium iodide. All measurements have been carried out in scattering chamber. The chamber setup for in-plane scattering is shown in Fig. 1.16(A). The scattering chamber is equipped with two moveable arms that can be rotated up to 360^0. The carbon detector was mounted on the upper arm at fixed position while

the alpha detector array was mounted on the lower arm. The out-of-plane (shown in Fig. 1.16(B)) scattering chamber is a simple modified in-plane array . In out-of-plane array, the alpha detector array was mounted on the lower arm perpendicular to the chamber floor. Due to the size of detector it covers only span 60^0 out-of-plane. Three alpha detectors were fixed at $\phi_\alpha = 0^0$, 30^0 and 60^0. The fourth one was mounted in the center of chamber top.

In 2001, FOPI collaboration for the first time studied the directed flow at incident energies from 90 to 400 MeV/nucleon for the reaction of ^{197}Au + ^{197}Au and remarked that differential directed transverse flow increases with fragment charge [68]. In same year, under similar reaction conditions, transition energy of fragments has been studied [102]. Another study discussed the interplay between the spectator shadowing and collective expansion for the reaction of ^{197}Au + ^{197}Au at incident energies from 0.09 to 1.49 GeV/nucleon [103]. Bastid and coworkers [104] reported a new method (Lee-Yang zeros) to analyse the directed and elliptic flow and reported a comparative study based on multi-particle cumulates, on Lee-Yang zeros, and on event-plane reconstruction. The INDRA collaboration [105] studied the elliptic and directed flow of Z $\leq$ 2 particles for the reaction of ^{197}Au on ^{197}Au at different colliding energies (E = 40-150 MeV/nucleon) and showed the similar values of transition and balance energies for $Z \leq 2$ particles as reported by FOPI collaboration [102]. After that, they addressed the effect of system mass and incident energy on radial flow [106]. Recently, FOPI collaboration also studied the directed and elliptic flow for the reactions of ^{40}Ca + ^{40}Ca, ^{58}Ni + ^{58}Ni, ^{96}Ru + ^{96}Ru, ^{96}Zr + ^{96}Zr, ^{129}Xe + CsI and ^{197}Au + ^{197}Au [107] for whole energy range (0.09 to 1.5 GeV/nucleon) and showed that stiff form of NEOS is incompatible with the experimental data.

The K500 Superconducting Cyclotron at the Texas A & M University Cyclotron Institute studied the transverse flow and the mid-rapidity emission of isotopically identical light charged particles for the reactions of ^{70}Zn + ^{70}Zn, ^{64}Zn + ^{64}Zn, and ^{64}Ni + ^{64}Ni at E = 35 MeV/nucleon and showed that the value of flow increases with neutrons content of the colliding nuclei [108]. In addition to intermediate energy region, collective flow is also calculated in high energy region [109, 110]. The theoretical studies give a backbone to experimental data. Thus, it is necessary to take a glance on various theoretical efforts that explain the experimental data of collective flow. However, lot of independent theories also

point the collective flow predictions, that need experimental verifications.

Theoretical attempts

In 1974, Scheid *et al.* [111] showed that the compressed nuclear matter expanded faster in the transverse direction than the longitudinal direction. Later on in 1980, Stöcker [82] used the term "collective sideward flow" and performed the calculations by using non-relativistic fluid dynamics. In hydrodynamical models, for peripheral collisions the shape of ellipsoid was oriented along beam axis, and for central collisions it was nearly perpendicular to the beam axis. Li and Sustich [112], in 1999, first time gave an evidence of the existence of differential transverse flow at balance energy.

By using Isospin-dependent Bolzmann-Uehling-Uhlenbeck (IBUU), Li *et al.* [113] studied the isospin effect on transverse flow and proved that the isospin effect come into the picture in HIC via NN cross-section, symmetry energy and Coulomb interactions. Li *et al.* [114] studied the transverse and elliptic flow of protons for ^{124}Sn + ^{124}Sn at incident energy of E = 50 MeV/nucleon. The study revealed that the differential elliptical flow of protons in mid-rapidity region at high transverse momenta showed large sensitivity to the isospin dependence of NEOS than the directed flow. Chen *et al.* [115] by using Isospin-dependent Quantum Molecular Dynamics (IQMD) model [116], showed that the neutron-rich system has high balance energy. Contrary, one get weaker out-of-plane flow for neutron-rich systems [117]. Russotto *et al.* [118] studied the symmetry energy effect on elliptic flow via studying the free protons and neutrons for ^{197}Au + ^{197}Au reaction. Pan and Danielewicz [119] analysed the momentum dependent interactions on directed flow in terms of p_t-dependence. Recently, Jain *et al.* [23] studied the effect of both momentum dependent interactions (MDI) and isospin dependent NN cross-section on p_t-differential transverse flow. Zheng *et al.* [120] studied the transition energy of ^{48}Ca + ^{48}Ca by using the IBUU model. The study showed that transition energy depends on NN cross-section and EOS. Jain *et al.* [41] studied the influence of isospin dependent NN cross-section on transition energy for charge asymmetric collisions and showed that the transition energy is independent from the N/Z ratio of the colliding nuclei.

1.8 Review of experimental and theoretical attempts to study the nuclear stopping

The HIC, in terrestrial laboratories provides an exclusive possibility to create, ephemeral states of nuclear matter in a broad range of density, temperature, N/Z asymmetry to access the information for basic properties of nuclear matter away form the normal reaction conditions. The information regarding the equilibrium state during the collision of two nuclei is pointed through the nuclear stopping.

Experimental efforts

In 1995, Bass *et al.* [121] introduced the idea to study the phenomena of nuclear stopping via isospin-mixing method. Recently, INDRA collaboration [122] studied the nuclear stopping for different colliding systems in Fermi energy range and proved that above E = 30 MeV/nucleon, nuclear matter is not completely thermalized. The INDRA and ALADIN [123] collaboration also proposed a minimum value of nuclear stopping for the reactions of ^{124,129,136}Xe + ^{112,nat,124}Sn and gave full description about the importance of minimum nuclear stopping in the dynamics of HIC. The FOPI collaboration [124] studied the nuclear stopping for the reaction of ^{197}Au + ^{197}Au in the energy range 90-1930 MeV/nucleon and obtained a plateau of maximal stopping in the interval of 200-800 MeV/nucleon. Ademard *et al.* [125] studied the observable of nuclear stopping for asymmetric collisions in the incident energy range from 5-80 MeV/nucleon. Lehaut *et al.* [126] reported that around 40 to 100 MeV/nucleon, the nuclear stopping become independent from the role of isospin content of colliding systems. Beside the experimental results, nuclear stopping is also pointed out by the various theoretical approaches.

Theoretical efforts

In 1988, Bauer *et al.* [127] by using Boltzmann-Uehling-Uhlenbeck (BUU) approach proved that nuclear stopping can be calculated by in-medium NN cross-section and mean field. Later on, by using IQMD model, Li *et al.,* [128] showed that nuclear stopping show large sensitivity towards the isospin dependent in-medium NN cross-section and weak dependence towards the symmetry energy for energy range from 80-150 MeV/nucleon. However, below E = 80 MeV/nucleon, the nuclear stopping shows sensitivity under both conditions (isospin dependent in-medium NN cross-section and symmetry energy). Yang *et al.* [129]

with same model showed the sensitivity of incident energy, impact parameter and system mass on nuclear stopping. In next year, Li and Li [130] studied the influence of initial N/Z, system size, isospin symmetry potential and in-medium NN cross-section on nuclear stopping. Their study proved that nuclear stopping show weak dependence on the initial N/Z and the symmetry potential, however large sensitivity has been observed toward in-medium NN cross-section. Liu *et al.* [131] studied the isospin effects on nuclear stopping through Coulomb and symmetry potential by using IQMD model. The study concluded that the Coulomb interactions induce the reduction of nuclear stopping and act as an important factor for making the nuclear stopping as a good probe to extract the information about NEOS. Jain *et al.* [40] also studied the effect of charge asymmetry of colliding nuclei and isospin dependent NN cross-section on nuclear stopping. Su and Zhang [132] also proved that full stopping is not achieved even at central collisions. Recently, Kaur and Kumar [133] studied the effect of density dependent symmetry energy and colliding geometry on mass asymmetric collisions over the intermediate energy region.

In 2004, FOPI [123] collaboration performed first attempt to correlate the nuclear stopping with sideward flow at high energies and proved that the correlation between both observables (collective flow and nuclear stopping) has important significance to extract the information of NEOS in non-equilibrium conditions [134]. Lehaut *et al.* [126] performed similar calculations at Fermi energy region. Recently, Bonnet *et al.* [135] studied the correlation between flow and stopping in central collisions for nearly symmetric reactions at incident energy range from 20-50 MeV/nucleon. Their study revealed that for most central collisions in Fermi energy region, one can get the full stopping. Andronic *et al.* [124] addressed a linear correlation between nuclear stopping and flow at high energies. Motivated form above studies effect of incident energy on the correlation between nuclear stopping and flow is shown in chapter 4.

1.9 Organization of thesis

The thesis is organized as follows:

- In **chapter 2**, carries a concise introduction of various theoretical models used to study the HIC. A detailed discussion on isospin dependent primary models such as Isospin-

dependent Boltzmann-Uehling-Uhlenback (IBUU) model and Isospin-dependent Quantum Molecular Dynamics (IQMD) model.

- In **chapter 3**, the role of isospin degree of freedom in HIC through the transverse momentum (p_t), neutron to proton ratio and system mass is studied on p_t-differential transverse flow by using IQMD model. The simulations are carried out for different colliding systems (^{26}Na + ^{26}Na, ^{48}Ca + ^{48}Ca, ^{78}As + ^{78}As, ^{129}Xe + ^{129}Xe). Our study show that p_t-differential transverse flow dependence can act as a sensitive probe to study the density dependent symmetry energy compared to the energy of vanishing flow. Symmetry energy and its density dependence play a dominant role over the isospin dependent NN cross-section in Fermi energy region. Author compared the theoretical results with the experimental data of FOPI collaboration in different rapidity bins for free protons at E = 250 MeV/nucleon and impact parameter in the range of 3-6 fm in different scaled rapidity bins for the reaction of ^{197}Au + ^{197}Au. .

- In **chapter 4**, the effect of mass asymmetry on nuclear stopping by keeping total mass of colliding nuclei fixed and varying the mass asymmetry between 0.0 to 0.5 is studied. To study the system mass effect, we considered three sets of mass asymmetric systems having total mass, A_{tot} = 80, 160 and 240 units. The nuclear stopping of nucleons and fragments phase space is studied. A comparison between theoretical results and experimental data of INDRA collaboration signifies the fragments stopping over the nucleons stopping. The flow created between the colliding nuclei can be connected to the highly thermalized nuclear matter. In **chapter 4**, the correlations between flow (directed transverse and elliptical flow) and nuclear stopping for asymmetric collisions is discussed. The study showed that in Fermi energy region, nuclear stopping show a parabolic dependence with directed transverse flow and above Fermi energy region, exhibit a linear dependence. In addition to it, author has studied the behavior of nuclear stopping in out-of-plane and in-plane emitted particles by studying the nuclear stopping of different fragments mass at and around the transition energy.

- The results are summarized in **chapter 5**, which also contains an outlook of the work.

Bibliography

[1] J. Dalton,"A New System of Chemical Philosophy" (1808).

[2] E. Rutherford, Philos. Mag. **6**, 21 (1911).

[3] A. Bracco, Eur. Phys. News **46**, 26 (2015).

[4] L. A. Booth, Nucl. Eng. and Design **24**, 263 (1973).

[5] M. N. Venkatesan and S. Thanuskodi, Int. Jour. of Library and Inf. studies 4, 65 (2014).

[6] N. Zeraatkar, Iran. Jour. of Nucl. Medicine **21**, 81 (2013).

[7] J. Aichelin, Phys. Rep. **202**, 233 (1991).

[8] A. Shamlath *et al.,* Phys. Rev. C **95**, 034610 (2017).

[9] L. C. Vaz, J. M. Alexander and G. R. Satchler, Phys Rep. **69**, 373 (1981).

[10] B. Borderie amd M. F. Rivet, Prog. Part. Nucl. Phys. Rep. **61**, 551 (2008).

[11] C. A. Ogilvie *et al.,* Phys. Rev. Lett. **67**, 1214 (1991).

[12] R. Donangelo and S. R. Souza, Phys. Rev. C **52**, 326 (1995).

[13] H. M*ü*ller and B. D. Serot, Phys. Rev. C **52**, 2072 (1995).

[14] A. Bonasera, Phys. Rev. C **60**, 065212 (1999).

[15] F. Giacosa, T. Gutsahe and A. Faessler, Phys. Rev. C **71**, 025202 (2005).

[16] P. Czerski *et al.,* Jour. of Phys. G: Nucl. and Part. **36**, 025008 (2009).

[17] P. Braun-Munzinger and J. Stachel, Nucl. Phys. A **606**, 320 (1996).

[18] S. E. Jiri *et al.,* Nucl. Phys. B **119**, 538 (2003).

[19] P. J. Siemens, A. S. Jensen,"Elements of nuclei many body physics with the strong interaction" (1994).

[20] R. Bansal and S. Kumar, Phys. of Part. and Nucl. Lett. **10**, 693 (2013).

[21] K. S. Vinayak and S. Kumar, Phys. Rev. C **83**, 034614 (2011).

[22] W. Reisdorf and H. G. Ritter, Ann. Nucl. Part. Sci., **47**, 663 (1997).

[23] A. Jain, K. S. Vinayak and S. Kumar, Ann. of Phys. **334**, 334 (2013).

[24] S. Kumar, S. Kumar, and R. K. Puri, Phys. Rev. C **81**, 014601 (2010).

[25] T. Gaitanos, M. Colonna, M. Di. Toro and H. H. Wolter Phys. Lett. B **595**, 209 (2004).

[26] K. Zbiri *et al.,* Phys. Rev. C **75**, 034612 (2007).

[27] F. Fu *et al.,* Phys. Lett. B **666**, 359 (2008).

[28] C. Xu, B. A. Li, L. W. Chen, Phys. Rev C **82**, 054607 (2010).

[29] B. A. Li, L. W. Chen, C. M. Ko, Phys. Rep. **464**, 113 (2008).

[30] B. A. Li, C. M. Ko and W. Bauer, Inter. Jour. of Mod. Phys. E, **7**, 147 (1998).

[31] M. B. Tsang, Nucl. Phys. A, **734**, 605 (2004).

[32] K. S. Vinayak and S. Kumar, Jour. of Phys. G: Nucl. Part. Phys. **39**, 095105 (2012).

[33] K. S. Vinayak and S. Kumar, Phys. of Part. and Nuclei Lett. **9(8)**, 583 (2012).

[34] M. Belkacem *et al.,* Phys. Rev. C **58**, 1727 (1998).

[35] A. Ono and H. Horiuchi, Phys. Rev. C **53**, 2958 (1996).

[36] A. Ono, Phys. Rev. C **59**, 853 (1999).

[37] H. Bohr, H. B. Nielsen, Nucl. Phys. B **128**, 275 (1977).

[38] H. Stöcker, J. A. Maruhn and W. Greiner, Phys. Rev. Lett. **44**, 725 (1980).

[39] H. M*ü*ller and B. D. Serat, Phys. Rev. C **72**, 2071 (1995).

[40] A. Jain, S. Kumar and R. K. Puri, Phys. Rev. C **84**, 057602 (2011).

[41] A. Jain, S. Kumar and R. K. Puri, Phys. Rev. C **85**, 064608 (2012).

[42] B. A. Li Phys. Rev. C **69**, 034614 (2004).

[43] B. A. Li, C. M. Ko and W. Bauer, Int. J. Mod. Phys. E **7**, 147 (1998).

[44] G. F. Marranghello *et al.,* Phys. Rev. C **81**, 024307 (2010).

[45] S. Kubis, Phys. Rev. C **76**, 025801 (2007).

[46] B. A. Li *et al.,* Phys. Rev. Lett. **78**, 1644 (1997).

[47] B. A. Li Phys. Rev. Lett. **85**, 421 (2000).

[48] L. W. Chen *et al.,* Phys. Rev. C **68**, 017601 (2003).

[49] T. X. Liu *et al.,* Phys. Rev. C **86**, 024605 (2012).

[50] T. Gaitanos *et al.,* Nucl. Phys. A **732**, 24 (2004).

[51] B. A. Li, G. C. Yong and W. Zuo, Phys. Rev. C **71**, 014608 (2005).

[52] M. Zhang *et al.,* Phys. Rev. C **80**, 034616 (2009).

[53] M. D. Toro *et al.,* Nucl. Phys. A **782**, 267 (2007).

[54] Q. Li *et al.,* J. Phys. G: Nucl. Part. Phys. **31**, 1359 (2005).

[55] B. A. Li, L. W. Chen and C. M. Ko, Phys. Rep. **464**, 113 (2008).

[56] Heiselberg and H. Jensen, Phys. Rep. **328**, 237 (2000).

[57] D. V. Shetty, S. J. Yenello, G. A. Souliotis, Phys. Rev. C **75**, 034602 (2007).

[58] D. V. Shetty *et al.,* Nucl. Instr. and Meth. in Phys. Res. B **261**, 990 (2007).

[59] Z. Q. Feng, Phy. Rev. C **84**, 024610 (2011).

[60] L. W. Chen, C. M. Ko and B. A. Li, Phys. Rev. Lett. **94,** 032701 (2005).

[61] D. V. Shetty, S. J. Yennello and G. A. Souliotis, Phys. Rev. C **75**, 034602 (2005).

[62] J. Cugnon, T. Mizutani, and J. Vandermeulen, Nucl. Phys. A **352**, 505 (1981).

[63] A. Faessler, W. H. Dickhoff and M. Trefz, Nucl. Phys. A **428**, 271c (1981).

[64] M. Trefz, A. Faessler and W. H. Dickhoff, Nucl. Phys. A **443**, 499 (1985).

[65] G. Q. Li and R. Machleidt, Phys. Rev. C **48**, 1702 (1993).

[66] W. Cassing and U. Mosel, Prog. Part. Nucl. Phys. **25**, 235 (1990).

[67] L. P. Csernai, "Introduction to the relativistic heavy-ion collision" (2008).

[68] A. Andronic *et al.,* Phys. Rev. C **64**, 041604(R) (2001).

[69] S. A. Voloshin, Phys. Rev. C **55**, 1630(R) (1997).

[70] B. A. Li, Phys. Rev. C **48**, 2415 (1993).

[71] W. M. Zhang *et al.,* Phys. Rev. C **42**, 491(R) (1990).

[72] G. F. Bertsch, W. G. Lynch and M. B. Tsang, Phys. Lett. B **189**, 384 (1987).

[73] M. B. Tsang *et al.,* Phys. Rev. Lett. **57**, 559 (1986).

[74] P. Danielewicz and G. Odyniec, Phys. Lett. B **157**, 146 (1985).

[75] J. W. Harris, Nucl. Phys. A **471**, 241 (1987).

[76] R. Pak, PhD. thesis, Michigan State University (1996).

[77] J. J. Molitoris and H. Stöcker, Phys. Lett. B 162, 47 (1985).

[78] D. Krofcheck *et al.,* Phys. Rev. Lett. **63**, 2028 (1989).

[79] J. Peter, Nucl. Phys. A **545**, 173 (1992).

[80] Sangeeta and V. Kaur, Nucl. Phys. A **966**, 20 (2017).

[81] N. Bohr, Nature, **37**, 344 (1936).

[82] H. Stöcker, J. A. Maruhn and W. Greiner, Phys. Rev. Lett. **44**, 725 (1980).

[83] W. Reisdorf *et al.,* Phys. Rev. Lett. **92**, 232301 (2004).

[84] J. Y. Liu, W. J. Guo, S. J. Wang, W. Zuo, Q. Zhao and Y. F. Yang, Phys. Rev. Lett. **86**, 975 (2001).

[85] V. Kaur, S. Kumar and R. K. Puri, Nucl. Phys. A **861**, 37 (2011).

[86] A. D. Sood and R. K. Puri, Phys. Rev., Ser. C **73**, 067602 (2006).

[87] D. J. Majestro *et al.,* Phys. Rev., Ser. C **61**, 021602(R) (2000).

[88] R. Kumar, K. S. Vinayak and R. Chugh, Int. Jour. of Pure and App. Phys. **13**, 44 (2017).

[89] J. Barrette *et al.,* Phys. Rev. C **55**, 1420 (1997).

[90] L. Ahle *et al.,* Phys. Rev. C **57**, 1416 (1998).

[91] T. Wienold *et al.,* Nucl. Phys. A **610**, 76 (1996).

[92] Y. G. Ma *et al.,* Phys. Rev. **69**, 065610 (2005).

[93] D. Q. Fang *et al.,* J. Phys. **34**, 2173 (2007).

[94] W. D. Tian, *et al.,* Phys. Rev. **76**, 024607 (2007).

[95] S. Z. Belenkij and L. D. Landau, Nuovo Cimento Suppl. **3**, 15 (1956).

[96] M. Demoulins, *et al.,* Phys. Lett. B **241**, 476 (1990).

[97] H. H. Gutbroad *et al.,* Phys. Lett. B **216**, 267 (1989).

[98] H. H. Gutbroad *et al.,* Phys. Rev. C **42**, 640 (1990).

[99] D. Krofcheck, *et al.,* Phys. Rev. Lett. **63**, 2028 (1989).

[100] R. Pak, *et al.,* Phys. Rev. Lett. **78**, 1022 (1997).

[101] B. Tsang, Ph. D. Thesis, Washington University (1980).

[102] A. Andronic, *et al.,* Nucl. Phys. A **679**, 765 (2001).

[103] A. Andronic, *et al.,* Phys. Lett. B **612**, 173 (2005).

[104] N. Bastid, *et al.,* Phys. Rev. C **72**, 011901(R) (2005).

[105] J. Lukasik, *et al.,* Phys. Lett. B **608**, 233 (2005).

[106] W. Reisdorf, *et al.,* Nucl. Phys. A **848**, 366 (2010).

[107] W. Reisdorf, *et al.,* Nucl. Phys. A **876**, 1 (2012).

[108] Z. Kohley, *et al.,* Phys. Rev. C **83**, 044601 (2011).

[109] B. Hong, *et al.,* Phys. Rev. C **57**, 244 (1989).

[110] H. Liu *et al.,* Nucl. Phys. A **638**, 451 (1998).

[111] W. Scheid, H. M*ü*ller and W. Greiner, Phys. Rev. Lett. **32**, 741 (1974).

[112] B. A. Li and T. Sustich, Phys. Rev. Lett. **82**, 5004 (1999).

[113] B. A. Li, Z. Z. Ren, C. M. Ko and S. J. Yennello, Phys. Rev. Lett. **76**, 4492 (1996).

[114] B. A. Li, A. T. Sustich and B. Zhang, Phys. Rev. C **64**, 054604 (2001).

[115] L. W. Chen, F. S. Zhang and G. M. Jin, Phys. Rev. C **58**, 2283 (1998).

[116] C. Hartnack *et al.,* Eur. Phys. J. A **1**, 151 (1998).

[117] S. Kumar, S. Kumar and R. K. Puri, Phys. Rev. C **81**, 014611 (2010).

[118] P. Russotto *et al.,* Phys. Lett. B **697**, 471 (2011).

[119] Q. Pan and P. Danielewicz, Phys. Rev. Lett. **70**, 2062 (1993).

[120] Y. M. Zheng, C. M. Ko, B. A. Li and B. Zhang, Phys. Rev. C **83**, 2534 (1999).

[121] S. A. Bass *et al.*,, GSI Scientific Rep., **94**, 66 (1995).

[122] O. Lopez *et al.,* Phys. Rev. C **90**, 064602 (2014).

[123] W. Reisdorf *et al.,* Phys. Rev. Lett. **92**, 232301 (2004).

[124] A. Andronic *et al.,* Eur. Phys. J. A **30**, 31 (2006).

[125] G. Ademard *et al.,* Eur. Phy. J. A **50**, 33 (2014).

[126] G. Lehaut *et al.,* Phys. Rev. Lett. **104**, 232701 (2010).

[127] W. Bauer, Phys. Rev. Lett. **61**, 2534 (1988).

[128] J. Y. Li, W. J. Guo, S. J. Wang, W. Zuo, Q. Zhao and Y. F. Yang, Phys. Rev. Lett. **86**, 475 (2001).

[129] Y. F. Yang, J. Y. liu and W. Zuo, Chin. Phys. Lett. **18**, 1040 (2001).

[130] Q. F. Li and Z. X. Li, Chin. Phys. Lett. **19**, 321 (2002).

[131] J. Y. Liu, W. J. Guo, Y. Z. Xing and X. G. Li, Chin. Phys. Lett. **21**, 1914 (2004).

[132] J. Su and F. S. Zhang, Phys. Rev. C **87**, 017602 (2013).

[133] A. Kaur and S. Kumar, Ind. Jour. Phys. DOI 10.1007/s12648-017-1002-6(2017).

[134] C. Fuchs and T. Gaitanos, Nucl. Phys. A **714**, 643 (2003).

[135] E. Bonnet, M. Colonna, A. Chbihi, J. D. Frankland, D. Gruyer, and J. P. Wieleczko, Phys. Rev. C **89**, 034608 (2014).

Chapter 2

Methodology

2.1 Introduction

One needs a suitable methodology to explain the reaction mechanism at intermediate energies. A complicated non-equilibrium physics involved in HIC, that cannot be explained via simple numerical modelling. There are many factors, which affect the theoretical out comes of HIC, such as the initialization of colliding nuclei (target and projectile), nucleon-nucleon (NN) cross-section. To explain the reaction mechanism, one need specific theories and models, those are based on the initial conditions (e.g. type of target, projectile, colliding geometry and incident energies) [1]-[8] The energy dependent reaction mechanism is involved to explain the complex reaction dynamics of HIC. At low incident energy, attractive mean field governs the reaction mechanism, whereas at high incident energies, the reaction dynamics is mainly governed by the NN collisions. However, at intermediate energies, the reaction mechanism is very complex and is governed by the combined effect of mean field and NN collisions.

To extract information about NEOS of stable and/or radioactive nucleus-nucleus collisions, one must consider unambiguously the isospin degree of freedom [9]. The HIC at intermediate energies involves convoluted non-equilibrium physics. In order to extract information about NEOS as well as reaction dynamics (which involves affects of Pauli blocking, mean field and two body collisions) at intermediate energies, one need proper transport model. On the basis of fundamental theories and approaches, theoretical models have been divided into two categories: Statistical models and Dynamical models.

Statistical models

In 1936, Niels Bohr introduced the concept of compound nucleus [10]. To explain the concept of compound nucleus, the statistical models are highly appreciable. On the basis of statistical approach, the statistical models consider the nuclear level density [11, 12]. Due to the improvement and advancement in theories, statistical models are also used to explain the phenomena of intermediate and high energy physics [11, 12]. The process of statistical models is divided into three stages:

i) The equilibrated nuclear system (compound nucleus) is formed from a dynamics stage.

ii) The disassembly of compound nucleus into hot and excited fragments (primary fragments).

iii) The de-excitation of primary fragments.

The Statistical Multifragmentation Model (SMM) [13], is based on the theory of simultaneous break-up of a thermalized nuclear system. In SMM model, the surface energy of participant zone is parameterized in such a way that at certain temperature, the effect of surface energy vanishes [13]. Similar to SMM model, Berlin Multifragmentation Model (BMM) [14] also has as a feature to explain the nuclear effects such as Coulomb and nuclear interactions, finite size of colliding nuclei, de-excitation of primary fragments etc. The Statistical models also include the study of weakly bound nuclei via Participant-Spectator Model [15]. In addition to this, Expanding Emitting Source (EES) model also come into the picture which consider the emission of light fragments only [16]. The demerits of statistical models are that it does not explain the experimental data, until the energy is comparable or higher than the thermal energy and it explains only the final stage of the reaction mechanism. It is essential to have the knowledge of NEOS, NN cross-section, Pauli blocking [17] from the initial (where nuclear matter is non-equilibrate) to the final state (where nuclear matter is cold and fragmented into small pieces). Thus, one needs a different approach to explain the whole reaction mechanism. Thus, curiosity to expand the knowledge regarding nuclear physics in wider range, one needs a new approach to understand the rare phenomena, which is highlighted through the dynamics models.

Dynamical models

The statistical models give explanation of the final state. Since no dynamical information can be extracted from Statistical models. The study of dynamics of a reaction includes cor-

relations and fluctuations, which can be studied by dynamical models only. The theoretical models that explain the time evolution of hot and compressed nuclear matter are named as dynamical models. In late 1980's, Yariv, [18] firstly studied the whole reaction dynamic of HIC, starting from initial stage to final stage by using intra nuclear cascade calculations. The model studied the two-body scattering with free cross-section, but did not include the influence of mean field and Pauli blocking. Moreover, the initialization of nucleus did not include the effect of Fermi momentum. On the other side, Time dependent Hartree Fock (TDHF) approach [19] at low energy considered only attractive mean field and Pauli blocking and was silent regarding the role of repulsive NN collisions. Later on, TDHF was improved by inclusion of repulsive NN collisions at low energies and named it as Extended Time dependent Hartree Fock (ETDHF) [20] theory, but still the numerical implementation was not valid to explain whole picture of HIC. To complete the picture ETDHF theory was further refined to study the NN collision for whole energy range and named as Boltzmann-Uehling-Uhlenback (BUU) model [21, 22]. In addition to BUU model, Landau-Vlasov (LV) [23] also came into picture, which are also solve by the Bolzmann-Nordheim equation.

All BUU-type models [24, 25, 26] study the evolution of one-body phase space distribution by using test particle method. However, all the possible interactions between the test particles are considered. The BUU model gave a good estimate for early stage of NN collisions, while in final stage, the particles are separated from each other and dynamics follow for the individual particle, thus n-body correlations are suppressed in BUU-type models. Due to large number of test particles per nucleon, the collision induced fluctuations are less in BUU-type models, which suppress the rate of fragments formation. Thus, BUU-type models are suitable to study only one-body observables, such as fragments production, collective flow and nuclear stopping. The mechanism behind BUU-type model is discussed in following sections. In n-body system, both correlation as well as fluctuations play important role and mean field approximations are insufficient to explain the dynamical evolution of n-body system, then molecular dynamics methods are normally used. In molecular dynamics models equations of motion are solved numerically. To explain the correlations between the n-body system Classical Molecular Dynamics (CMD) [27, 28] model come into picture. It carried complete information about the n-body correlations, those are essential to explain

the fragments formation. In CMD approach, classical nucleons interact through classical potential, but failed to explain the NN collisions.

The two main ingredients (mean field and NN cross-section) of transport models are treated in different manner in different transport models. Thus, different approximations give different predictions. With different approximations, another transport model given by Aichelin and Stöcker [29]-citeqmd5 came into picture, named as Quantum Molecular Dynamics (QMD) model. The QMD model is an extended version of CMD model by inclusion of quantum features. In QMD model, particles propagate classically under the influence of NN collisions and mean field, similarly like BUU model. The role of Pauli blocking is introduced by Pauli blocking factor. Moreover, due to the single test particle per nucleon, n-body correlation and fluctuations are preserved in QMD approach. The classically induced fluctuations are large in QMD model compared to the BUU model, thus rate of fragments formation is large in QMD approach. The QMD model explains most of the observables of intermediate energy HIC such as fragment formation, collective flow, nuclear stopping, etc.

With the time, several improvements have been made in original QMD model. In all the revised versions of QMD model the basic principal structure remain same. The revised versions are differing only in the initialization of colliding nuclei. The new versions of QMD model were named as BQMD [34], HQMD [35], RQMD [36], FMD [37, 38], AMD [39], ImQMD [40], etc. To study the low energy fragments formation Bohnet *et al.* [34] rewrite the original QMD with the inclusion of proper binding of the nucleus in fragmentation process and named it BQMD model. The coupling constant of Skyrme-type interactions is also modified in order to keep the binding energy and NEOS independent from the Yukawa interactions. The drawback of this version is that it used only nucleons and deltas and all other nucleonic interactions considered at same average cross-section without taking into account of isospin effects. In addition, to concerning the meson production, the Huber and Aichelin [35] upgraded the QMD model, and dubbed it HQMD model. It has been extensively used to study the kaons production. The HQMD model included free pions, deltas and isospin couplings. But, HQMD model is unable to give details of experimental data in AGS and CERN/SPS energy domain.

The relativistic version of QMD or BUU models come into picture in recent years. The

Relativistic Quantum Molecular Dynamics (RQMD) [36] is an extending form of QMD model up to relativistic energies. The RQMD model used classical co-variant equation of motion to describe the time evolution of many body systems. The RQMD model considered the covariant dynamics with total collision term with strange particles, string excitation for high energy NN interactions and heavy baryon resonances. This model successfully explains the final state, but fails to generate the nuclei in their ground state. The Feldmeier improved the QMD model by considering the fermionic properties of nucleons through antisymmeterization of the wave function of the nucleus and named it Fermionic Molecular Dynamics (FMD) [37, 38] model. This model combines to the Fermi-Dirac statistics with a semi-quantal trajectory picture. The classical molecular dynamics is limited in dilute phase space i.e. for low density and high temperature. The isospin degree of freedom of the nucleons is also incorporated and they are assumed to move under the affect of attractive mean field. Because of the Slater determinant, the Pauli principle is also incorporated correctly. For many-body problems the Fermi-Dirac statistics is included. The main drawback of this model is that it does not consider the total wave mechanical interference. Due to this, the FMD model is not considered as fully quantum mechanical model.

It was demonstrated that the frictional cooling method [43] combined with the antisymmetrized version of the molecular dynamics helps to study the nuclear structure. Moreover, this method is independent from model assumptions. Based on it, Ono *et al.* [44, 45] have been succeeded in incorporating two nucleon collisions in a antisymmetrized version of molecular dynamics and named it as Antisymmetrized Molecular Dynamics (AMD) model. The main drawback of AMD model is that it considered the constant width parameter, which is a dynamical variable and it does not conserve the total angular momentum. However, it considered light systems only. To study the massive nucleus-nucleus collisions Improved Quantum Molecular Dynamics (ImQMD) [40] is come into the picture. The ImQMD model explained the time evolution of configuration and lifetime of the composite system in whole energy range. ImQMD successfully explained the angular distribution of fragments. In ImQMD the effective interaction potential energy considers both potential and Coulomb interaction energy.

Beside all the features, the various versions of QMD model do not consider the isospin

effects of nucleons. Thus, in order to describe the NEOS of neutron-rich matter, one has to introduce the isospin effects in calculations. Moreover, the isospin effects come into picture via symmetry potential, Coulomb potential, Pauli blocking and NN cross-section. Thus, one needs more reliable theoretical model to understand the isospin dependence of nucleons. With the inclusion of isospin effects, the modified form of BUU and QMD models come into literature, which are named as Isospin-dependent Boltzmann-Uehling-Uhlenback (IBUU) model [46] and Isospin-dependent Quantum Molecular Dynamics (IQMD) model [47].

The following sections contain a detailed prefaces of isospin-dependent (IBUU and IQMD) models used to study the HIC at intermediate energies.

2.2 Isospin-dependent models

2.2.1 Isospin-dependent Boltzmann-Uehling-Uhlenbeck (IBUU) model

To obtain space and momentum distributions of nucleons at freeze out in intermediate energy HIC, one can opt the isospin-dependent Boltzmann-Uehling-Uhlenbeck (IBUU) transport model based on BUU model [21, 22]. The test particle method [46] is used to solve the IBUU equation. The test particles are used to evaluate the mean field potential, thus, at each event single collision among the nucleons are allowed. Similar to BUU [21, 22] model, the IBUU model [46] has been extensively use to simulate the HIC and extracting important information of nuclear matter. The transport equation in IBUU model is solved for one-body Wigner density $f(r, p, t)$ in the limit $\hbar \to 0$:

$$\begin{aligned} \frac{\partial f}{\partial t} \; + \; v \cdot \nabla_r f - \nabla_r U \cdot \nabla_p f \;\; &= \;\; -\frac{4\pi^3(\hbar c)^4}{\hbar (mc^2)^2} \int \frac{d^3p_2}{(2\pi\hbar)^3} \; \frac{d^3p_3}{(2\pi\hbar)^3} \; d\Omega \; \frac{d\sigma_{NN}}{d\Omega} v_{12} \\ &\times [f_3 \; f_4(1-f)(1-f_2) \; - \; f \; f_2(1-f)(1-f_2)] \\ &\times \delta^3(p \; + p_2 \; - p_3 - p_4), \end{aligned} \tag{2.1}$$

where $\frac{d\sigma_{NN}}{d\Omega}$ is in-medium NN scattering cross-section and v_{12} is relative velocity of colliding nucleons, respectively.

The isospin dependent part is incorporated in model via NN cross-section (σ_{12}) and the nuclear mean field potential U. In IBUU model, isospin dependent NN cross-section is

taken from the experimental fit of free-space cross-section. In experimental free-space cross-sections, the np cross-section is about three times larger than the nn and pp cross-section. In IBUU model, U is a function of local density and can be parameterized as an arbitrary function of density. The term U can be expressed as sum of three terms:

$$U(\rho, \tau_z) \;=\; \alpha\left(\frac{\rho}{\rho_0}\right) + \beta\left(\frac{\rho}{\rho_0}\right)^{\gamma} + (1-\rho_0)V_{Coulomb} + V_{asy}^{n(p)}(\rho,\delta). \tag{2.2}$$

Here ρ_0 is the normal nuclear matter density and ρ, ρ_n and ρ_p are the densities of nucleons, neutrons and protons, respectively. τ_z equals to +1(-1) for neutrons(protons). The α, β and γ are parameters for the isoscalar NEOS. The term $V_{Coulomb}$ corresponds to the Coulomb potential. The single particle symmetry potential V_{asy} has the form of:

$$\begin{aligned} V_{asy}^{n(p)}(\rho,\delta) &= \frac{\partial}{\partial\rho}\left[\frac{C_{sym}}{2}\left(\frac{\rho}{\rho_0}\right)^{\gamma}\rho\delta^2\right] \\ &= \frac{C_{sym}}{2}\left[(\gamma-1)\left(\frac{\rho}{\rho_0}\right)^{\gamma}\delta^2 \pm 2\,\left(\frac{\rho}{\rho_0}\right)^{\gamma}\delta\right], \end{aligned} \tag{2.3}$$

where C_{sym} is the symmetry energy coefficient.

The IBUU model can predict the pre-equilibrium n/p ratio [48], the isospin fractionation [49, 50], the isoscaling in multifragmentation [51], the n-p differential transverse flow [52], the proton differential elliptic flow [53] and the π^- to π^+ ratio [54]. The IBUU model gave explanation about the time dependent one-body distribution function. The density fluctuations are suppressed in the BUU equation, so the calculation of fragments yield is not feasible directly from BUU-type model. Therefore, one needs an alternate model such as, Isospin-dependent Quantum Molecular Dynamics (IQMD) model [47] to overcome this limitation.

2.2.2 Isospin-dependent Quantum Molecular Dynamics (IQMD) model

The IQMD model is a revised form of QMD model which incorporates the isospin degree of freedom, developed by the Hartnack and coworkers [47]. In IQMD model, the isospin degree of freedom is considered unambiguously by incorporating the symmetry potential (to calculate the particles distribution in the nucleus) and the Coulomb forces between charge particles (protons) of projectile and target. The IQMD model assigns different charge states of pions, deltas and nucleons, [47] like VUU model. In IQMD model each nucleon crossponds

to a Gaussian wave packet. This model is based on three steps:

1. In first step, one has to generate the nuclei (target and projectile nucleus). This step is named as initialization.

2. In second step, two successfully generated nuclei propagate toward each other. This step is named as propagation.

3. In last step, two nucleons are considered to collide with each other, if they come closer to a specific distance. This step is named as nucleon-nucleon (NN) collision.

Initialization

IQMD model is an revised form of QMD model. Similar to QMD model, in IQMD model baryons are also assigned to follow Gaussian-shaped density distribution function. As the model is semi-classical, it is better to explain the formulation in classical transport theory rather than wave function. Thus, Wigner densities are used. The phase space density obtained by the Wigner transformation of the wave function is

$$\Phi(r,p) = \sum_i \ f_i(r,p), \tag{2.4}$$

where $f_i(r,p)$ is given by

$$\begin{aligned} f_i(r,\ p) &= \frac{1}{(2\pi\hbar)^3} \int e^{-\frac{i}{\hbar}p\cdot r_{12}} \psi_i(r+\frac{r_{12}}{2},\ t)\ \psi_i^*(r-\frac{r_{12}}{2},\ t) d^3r_{12} \\ &= \frac{1}{(\pi\hbar)^3} e^{-(r\ -r_i(t))^2/2L}\ e^{-(p\ -p_i(t))^2 2L/\hbar^2}. \end{aligned} \tag{2.5}$$

Where $p_i(t)$ and $r_i(t)$ are defined as momentum and position of the i^{th} particle. To obtain maximum stability, system dependent L values are introduced in IQMD model. The value of Gaussian width L is confined 8.66 fm^2 for heavier systems like Au, whereas L is confined to 4.33 fm^2 for lighter systems like Ca. Based on Liquid drop model, in IQMD model, nucleons are located in a sphere of radius $R = 1.12A^{\frac{1}{3}}$, where A is nucleus mass number.

To initialize a nucleus, each nucleon have to assign in three dimensional momentum and coordinate phase space inside a sphere. The classical orbit (r_i) explained via polar coordinates:

$$\begin{aligned} r &= R\ x_1^{1/3}, \\ cos\theta &= 1\ -\ 2x_2, \end{aligned}$$

$$\phi \;=\; 2\pi\; x_3, \tag{2.6}$$

where x_1, x_2 and x_3 are the random numbers. The local Fermi momentum is obtained from:

$$p_F(r_i) \;=\; \sqrt{-2mU(r_i)}, \tag{2.7}$$

where $U(r_i)$ is the local potential. The classical orbit (p_i) explained in polar coordinates by:

$$\begin{aligned} p_i &= p_F(r_i)x_4^{1/3}, \\ cos\theta &= 1 \;-\; 2x_5, \\ \phi &= 2\pi x_6. \end{aligned}$$

where, x_4, x_5 and x_6 are again the random numbers. In calculations those distributions are rejected in which two particles come closer beyond certain distance, which is dubbed as d_{min}. The relation between d_{min} and co-ordinate phase-space of two nucleons is

$$(r_i - r_j)^2(p_i - p_j)^2 \geq d_{min}. \tag{2.8}$$

From thousands initialization, only one is fulfied the selected criteria. For uniformly distribution of phase space each nucleon occupies a volume of h^3. A randamly selected initial momenta is chosen between 0 and Fermi momentum(p_F), without any further local constraints same as in QMD model [29].

Propagation

After successfully initialization, by using relativistic kinematics the two colliding nucleus boosted toward each other with appropriate center of mass velocity. For many body system the equation of motion is estimated by Ritz variational principle [19], which determine the time evolution of colliding system. Starting from the action

$$S = \int_{t_1}^{t_2} \mathcal{L}[\Phi, \Phi^*]d\tau, \tag{2.9}$$

where Lagrange function is defined as

$$\mathcal{L} = \langle\Phi|i\hbar\frac{d}{dt} - H|\Phi\rangle, \tag{2.10}$$

The neccesary and sufficient condition for time evolution of the action (define in Eqn. 2.9) is that for all possible variations of the wave function, it remains stationary.

$$\delta S = \delta \int_{t_1}^{t_2} \mathcal{L}[\Phi, \Phi^*] dt = 0. \tag{2.11}$$

Which genrates an distinct Euler Lagrange equation for different parameters. The Euler-Lagrange equation for each parameter λ is define as:

$$\frac{d}{dt}\frac{\partial \mathcal{L}}{\partial \dot{\lambda}} - \frac{\partial \mathcal{L}}{\partial \lambda} = 0. \tag{2.12}$$

The variation of action gives an exact solution of the Schrödinger equation if the true solution of the Schrödinger equation is limited for particular set of wave function i.e. $\psi(r, p_i(t), r_i(t))$. For coherent states, the Hamiltonian is defined as,

$$H = \sum_i T_i + \frac{1}{2} \sum_{i,j;i\neq j} V(r_i(t) - r_j(t)) \quad (i = 1, N), \tag{2.13}$$

Where T_i is kinetic energy and V_{ij} is potential energy equivalent to $V(r_i(t) - r_j(t))$. Using classical Liouville equation, one finds that the equation of motion of r_i and p_i shows similar structure like classical Hamilton equation (provided the Hamiltonian can be written in the form of Eq. 2.13). After solving the Lagrangian and the variation, one gets the time dependent equation, which diminishes the n-body Schrödinger equation to $6\cdot(A_T + A_P)$. Thus the equations of motion in the form of classical Hamiltonian equation are represent as:

$$\dot{r}_i = \frac{\partial H}{\partial p_i}; \quad \dot{p}_i = \frac{-\partial H}{\partial r_i}. \tag{2.14}$$

The numerical solution calculated in the form of classical molecular dynamics [55]. The total Hamiltonian is represented in the form of kinetic energy and potentials as:

$$\begin{aligned} H_i &= T_i + V_i \\ &= \sum_i \frac{p_i^2(t)}{2m} + V^{ij}_{Skyrme} + V^{ij}_{Yukawa} + V^{ij}_{Coulomb} + V^{ij}_{MDI} + V^{ij}_{Sym} \end{aligned} \tag{2.15}$$

$$\tag{2.16}$$

where V^{ij}_{Skyrme}, V^{ij}_{Yukawa}, $V^{ij}_{Coulomb}$, V^{ij}_{MDI} and V^{ij}_{sym} are, Skyrme, Yukawa, Coulomb, momentum dependent and symmetry potentials, respectively between two colliding nucleons. These are local two- and three- body interactions. Due to this Hamiltonian become:

$$H_i = T_i + \frac{1}{2!} \sum_{j;i\neq j} V^{(2)}_{ij} + \frac{1}{3!} \sum_{j,k;i\neq j\neq k} V^{(3)}_{ijk} \tag{2.17}$$

Here, $V_{ij}^{(2)}$ and $V_{ijk}^{(3)}$ are the two- and three-body interactions and represent in the form of densities of both colliding nucleons.

The two-body interactions can be calculated as follows:

$$\begin{aligned}
\frac{1}{2}\sum_{j;i\neq j} V_{ij} &= \frac{1}{2}\sum_{j;i\neq j}\int f_i(r_i,p_i;t)\ f_j(r_j,p_j;t)\ V(r_i,r_j) \\
&\quad \times\ d^3r_i\ d^3r_j\ d^3p_i\ d^3p_j, \\
&= \frac{1}{2}\sum_{j;i\neq j}\int f_i(r_i,p_i;t)\ f_j(r_j,p_j;t)\ t_1 \\
&\quad \times\delta(r_i-r_j) d^3r_i\ d^3r_j\ d^3p_i\ d^3p_j, \\
&= \frac{1}{2}\sum_{j;i\neq j}\ t_1\int f_i(r_i,p_i;t)\ f_j(r_j,p_j;t) \\
&\quad \times\ d^3r_i\ d^3p_i\ d^3p_j, \\
&= \frac{1}{2}\sum_{j;i\neq j}\ t_1\int \frac{1}{(\pi\hbar)^3} e^{-(r-r_i(t))^2 2/L} e^{-(p-p_i(t))^2 L/2\hbar^2} \\
&\quad \times\frac{1}{(\pi\hbar)^3} e^{-(r-r_j(t))^2 2/L}\ e^{-(p-p_j(t))^2 L/2\hbar^2}\ d^3r_i\ d^3p_i\ d^3p_j, \\
&= \frac{1}{2}\sum_{j}\ t_1 \frac{1}{(4\pi L)^{3/2}} e^{-(r_i-r_j)^2/4L}, \\
&= \frac{t_1}{2}\sum_{j;i\neq j}\rho_{ij}. \qquad (2.19)
\end{aligned}$$

where, the interaction density ρ_{ij} is given by:

$$\rho_{ij} = \int d^3r\ \rho_i(r)\ \rho_j(r) = \frac{1}{(4\pi L)^{3/2}} e^{-(r_i-r_j)^2/4L}. \qquad (2.20)$$

The three-body interactions can be calculated as follows:

$$\begin{aligned}
\frac{1}{3!}\sum_{j,k;i\neq j\neq k} V_{ijk} &= \frac{1}{3!}\sum_{j,k;i\neq j\neq k}\int f_i(r_i,p_i,t)\ f_j(r_j,p_j,t)\ f_k(r_k,p_k,t)\ V(r_i,r_j,r_k) \\
&\quad \times\ d^3r_i\ d^3r_j\ d^3r_k\ d^3p_i\ d^3p_j\ d^3p_k, \\
&= \frac{1}{3!}\sum_{j,k;i\neq j\neq k}\int f_i(r_i,p_i,t)\ f_j(r_j,p_j,t)\ f_k(r_k,p_k,t)\ t_2 \\
&\quad \times\delta(r_i-r_j)\ \delta(r_i-r_k) d^3r_i\ d^3r_j\ d^3r_k\ d^3p_i\ d^3p_j\ d^3p_k, \\
&= \frac{1}{3!}\frac{t_2}{(2\pi L)^3\cdot 3^{3/2}}\sum_{j,k;i\neq j\neq k} e^{-\left[(r_i-r_j)^2+(r_i-r_k)^2+(r_k-r_j)^2\right]/6L}, \\
&= \frac{1}{3!}\frac{t_2}{(2\pi L)^3 3^{3/2}}\sum_{j,k;i\neq j\neq k} e^{-\left[(r_i-r_j)^2+(r_i-r_k)^2\right]/6L\times\frac{3}{2}}, \\
&= \frac{1}{3!}\frac{t_2\ (4\pi L)^{3/2\times 2}}{(2\pi L)^3\cdot 3^{3/2}}\left[\sum_{j\neq i}\frac{1}{(4\pi L)^{3/2}} e^{-(r_i-r_j)^2/4L}\right]^2, \\
&= \frac{1}{3!}\frac{t_2\ 2^3}{3^{3/2}}\left[\sum_{j\neq i}\rho_{ij}\right]^2. \qquad (2.21)
\end{aligned}$$

In above derivation, the three-body term can be reduced into two-body term. To probe the NEOS, the value of parameters t_1 and t_2 in above equations (2.19 and 2.21) are determined in such a condition that the Hamiltonian of Eqns 2.19 and 2.21 can genrates the NEOS in infinite limits.

Further the short range Yukawa potential expressed as:

$$V_{Yukawa} \;=\; t_3 \frac{exp\{-|r_i - r_j|\}/\mu}{|r_i - r_j|/\mu}, \tag{2.22}$$

here t_3= -6.66 MeV and μ = 0.4 fm. The Yukawa potential (V_{Yukawa}) improves the interactions of surface properties, which plays a significant role in study of multifragmentation. The next Coulomb potential $V_{Coulomb}$ is express as:

$$V_{Coulomb} \;=\; \frac{Z_i Z_j \; e^2}{|r_i - r_j|}, \tag{2.23}$$

here Z_i and Z_j denote the charges of i^{th} and j^{th} baryon.

Due to the constant density value in nucleus the interaction density agrees the single particle density, and the two-body part of V_{loc} (local potential), and V_{Yukawa}, are directly proportional to $(\frac{\rho}{\rho_o})$. Moreover, the three-body part V_{loc} is directly related to $(\frac{\rho}{\rho_o})^2$. For nuclear matter, local potential is defined as:

$$V_{loc} \;=\; \frac{\alpha}{2}\left(\frac{\rho}{\rho_o}\right) \;+\; \frac{\beta}{\zeta+1}\left(\frac{\rho}{\rho_o}\right)^2. \tag{2.24}$$

The free parameters α and β of above potential fixed by the requirement. At normal nuclear matter density the total density approches to ρ_o and the average binding energy is consider to be -16 MeV. The parameter ζ is known as compressibility factor. The Skyrme parameterization of NEOS, contains two different forms of parameter that give same values of saturation density and binding energy, but give two different incompressibility K factor value. The factor K at small value of ζ is 200 MeV, corresponds to soft EOS, while at larger value of ζ corresponds to hard EOS with K = 380 MeV. To calculate the affect of different compressibilities, the above potential energy (eq. 2.24) can be generalize from

$$V_{loc} \;=\; \frac{\alpha}{2}\left(\frac{\rho}{\rho_o}\right) \;+\; \frac{\beta}{\zeta+1}\left(\frac{\rho}{\rho_o}\right)^{\zeta}. \tag{2.25}$$

Then the total Skyrme potential is repsesented as:

$$V^{Skyrme} = \sum_{j;i\neq j} t_4\delta(r_i - r_j) + t_2\delta(r_i - r_j)\rho^{\acute{\gamma}-1}((r_i + r_j)/2). \tag{2.26}$$

The momentum dependent part came naturally in calculations via framework of G-matrix. However, the numerical utility of G-matrix is very time consuming, thus one uses the parameterized form of momentum-dependent potential (V_{MDI}).

$$V_{MDI} = \sum_{j;i\neq j} t_4 ln^2(t_5(p_i - p_j)^2 + 1)\delta(r_i - r_j), \tag{2.27}$$

where $t_4 = 1.57$ MeV and $t_5 = 5 \times 10^{-4}\ MeV^{-2}$. The parameterized form of V_{MDI} used in IQMD model can be obtained by fitting the real part of optical potential of nucleon coming from the experimental data [56, 57]. In Table2.1 containes different parameters and their incompressibilities.

Table 2.1: Sets of IQMD model parameters [58, 59, 60, 61].

EOS	α(MeV)	β(MeV)	ζ	K(MeV)
S	-356	303	1.17	200
H	-124	71	2.00	380

$$V_{sym} = t_6 \frac{1}{\varrho_0} T_3^i T_3^j \delta(r_i - r_j), \tag{2.28}$$

Here $t_6 = 100$ MeV and T_3^i, T_3^j known as isospin projection of nucleons i.e. T_3 components of baryon (i.e. -1/2 for neutrons and 1/2 for protons). The total potential among the baryons in IQMD model is written as:

$$\begin{aligned} H &= \sum_i \frac{p_i^2(t)}{2m} + V_{Skyrme}^{ij} + V_{Yukawa}^{ij} + V_{Coulomb}^{ij} + V_{MDI}^{ij} + V_{Sym}^{ij} \\ &= t_1\delta(r_i - r_j) + t_2\delta(r_i - r_j)\rho^{\gamma-1}\left(\frac{r_i + r_j}{2}\right) \\ &\quad + t_3 \frac{exp(|r_i - r_j|/\mu)}{(|r_i - r_j|/\mu)} + \frac{Z_i Z_j e^2}{|r_i - r_j|} \\ &\quad + t_4 \ln^2[t_5(p_i - p_j)^2 + 1]\delta(r_i - r_j) \\ &\quad + t_6 \frac{1}{\varrho_0} T_3^i T_3^j \delta(r_i - r_j). \end{aligned} \tag{2.29}$$

Nucleon-Nucleon (NN) collisions

In IQMD model, the binary NN collisions are included on the basis of VUU-BUU equation [59, 60, 61] like in CASCADE model [18]. In propagation, a binary collision is considered to occur, if their centroid are following the below conditions:

$$|r_i - r_j| \leq \sqrt{\frac{\sigma_{NN}}{\pi}}, \sigma_{NN} = \sigma(\sqrt{s}, type). \tag{2.30}$$

Here $\sigma_{NN}(\sqrt{s})$ stands for total NN cross-section and '$\sqrt{s}$' stands for center-of-mass energy in GeV. "type" denotes the patners of ingoing collision (N-N, N-Δ, N-π,..). During collision, phase-space is checked in the region of scattering partners. Moreover, the phase-space density in final state is checked through the Pauli-blocking. The Pauli-blocking also played a significant role in NN collision. In IQMD model, the overlap phase space density f_i^{ovp} as well as particle density ρ_i^{ovp} of i^{th} particle with other particles (j^{th}) is given by

$$\begin{aligned} f_i^{ovp} &= \sum_{j\neq i} \int dr dp f_i(r,p) f_j(r,p) \\ &= \frac{1}{8(\pi\hbar)^3} \sum_{j\neq i} e^{\left[-\alpha(r_i-r_j)^2 - \frac{1}{4\alpha\hbar^2}(p_i-p_j)^2\right]} \end{aligned} \tag{2.31}$$

and

$$\begin{aligned} \rho_i^{ovp} &= \sum_{j\neq i} \int dr \rho_i(r) \rho_j(r) \\ &= \sum_{j\neq i} \left(\frac{\pi}{\alpha}\right)^{-3/2} e^{\left[-\alpha(r_i-r_j)^2\right]} \end{aligned} \tag{2.32}$$

where $\alpha = 0.25 fm^{-2}$ is a model parameter. Therefore, the phase space Fermion overlapping densities f_i^{ovp} at the final states can be directly calculated and used for simulation of Pauli blocking. For two indistinguishable nucleons i and j, the function F_i^{block} can be interpreted as the Pauli blocking probability and is given by

$$\begin{aligned} F_i^{block} &= \sum_{j\neq i} 8(\pi\hbar)^3 \delta_{\sigma_i\sigma_j} \delta_{T_iT_j} \int dr dp f_i(r,p) f_j(r,p) \\ &= \delta_{\sigma_i\sigma_j} \delta_{T_iT_j} e^{\left[-\alpha(r_i-r_j)^2 - \frac{1}{4\alpha\hbar^2}(p_i-p_j)^2\right]}, \end{aligned} \tag{2.33}$$

where $\sigma_{i,j} = \pm 1$ and $T_{i,j} = \pm 1$ stand for spin and isospin indices of nucleons, respectively. The Pauli blocking of the two-body collisions can be checked by the blocking probability P_{block} given by

$$P_{block} = 1 - (1 - F_i^{block})(1 - F_j^{block}) \tag{2.34}$$

and the correspondingly allowed probability by $1 - P_{block}$. The Pauli factor become 0(1), if phase-space is occupied(unoccupied). Souza *et al.* [62] proposed another method to implement the Pauli principle via two situations. Firstly, in formation of initial pattern of a nucleus. Secondly, during the NN collisions. In this approach, the role of Pauli blocking is noticeable via the significantly overlapping of the nucleons Gaussians. The Gaussians

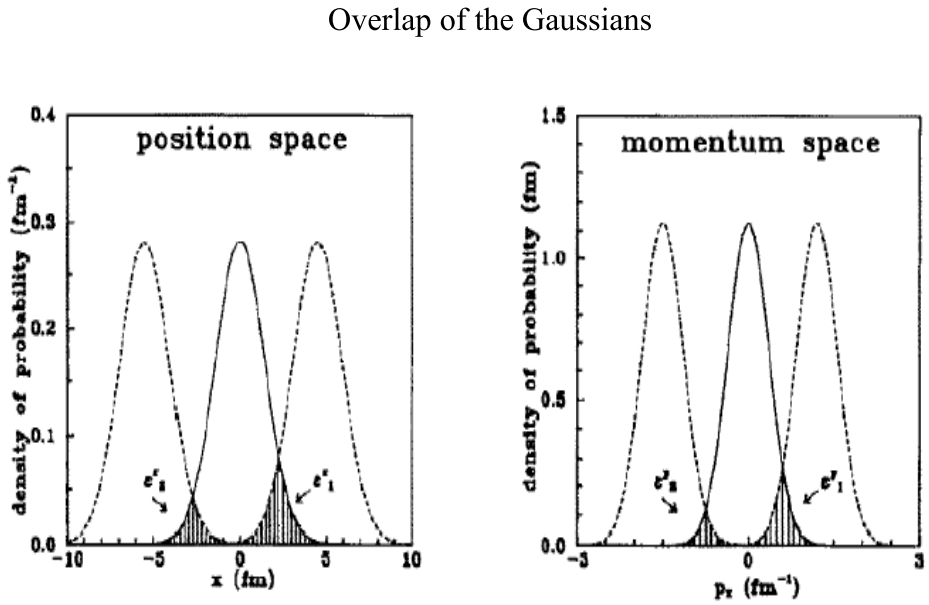

Figure 2.1: *The two dimensional phase space of the overlap of Gaussian wave packet. The figure is taken from Ref.[62].*

pattern appear as a good tool to measure the phase-space density as shown in 2.1. In Fig. 2.1, the solid lines represent for the Gaussians of a nucleon situated at $p_x = 0\ fm^{-1}$ and x = 0 fm, whereas dashed lines represent the Gaussians in phase-space of surrounding nucleons. The phase space, mean position r_i and mean momentum p_i of allowed collisions is calculated with respect to the overlapping of Gaussians connected with other nucleons to a particular nucleon. The blocked collision with probability P_{block} depends on total overlap ϵ is assumed to be 'ϵ' for $0 \leq \epsilon \leq$ '1' and 1 for $\epsilon \geq 1$. In condition of two nucleons (1 and 2) surrounding a given nucleon. Then, the total overlap function (ϵ) is define as:

$$\epsilon = \epsilon_1^r \epsilon_1^p + \epsilon_2^r \epsilon_2^p, \tag{2.35}$$

where ϵ_z^r and ϵ_z^p (Z = 1, 2) stands for overlapping in coordinate and momentum phase-space, respectively. This method makes sure to occupy a reasonable phase-space of the colliding system during the collision and the value of Pauli blocking factor depends on whether the final phase-space is occupied or not.

In order to further understand the concept of rate of change for total collisions, Pauli

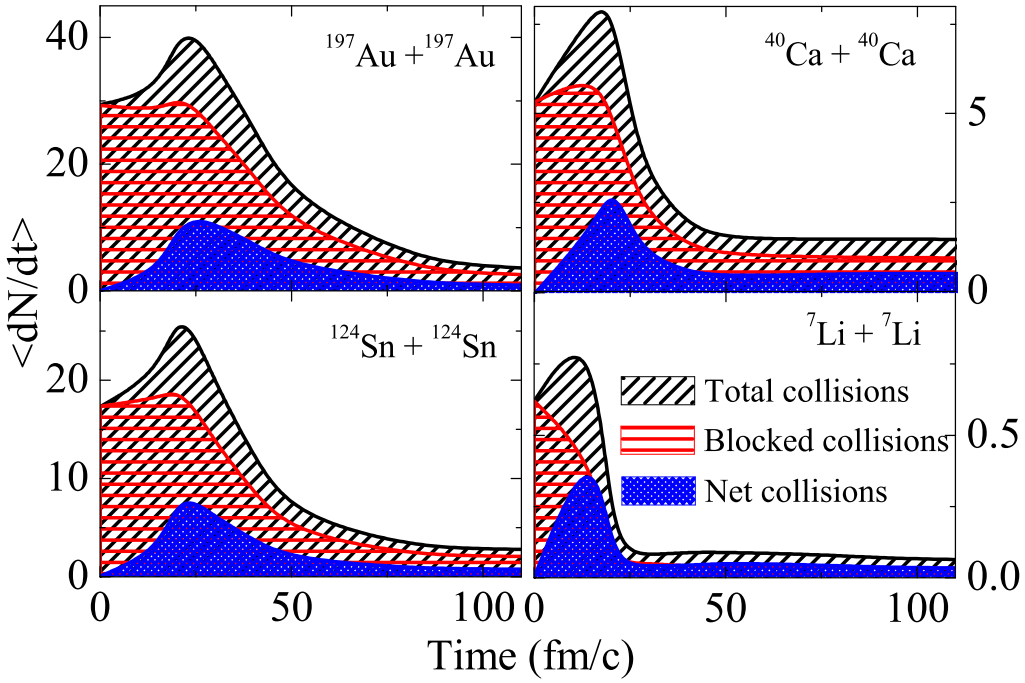

Figure 2.2: *Time evolution of the total collisions, blocked collisions and net collisions for the reactions of* ^{197}Au + ^{197}Au, ^{124}Sn + ^{124}Sn, ^{40}Ca + ^{40}Ca *and* ^{7}Li + ^{7}Li *at E = 50 MeV/nucleon.*

blocking, blocked collisions and net collisions for reactions of ^{197}Au + ^{197}Au, ^{124}Sn + ^{124}Sn, ^{40}Ca + ^{40}Ca and ^{7}Li + ^{7}Li are shown in Fig. 2.2. From the figure one can see that the collision rate shows a rise and fall behavior. It shows a peak around t = 30 fm/c (region of high density phase achieved during the reaction). After this around t = 80 fm/c the collisions rate becomes constant. One can also notice that the collision rate increases with colliding system masses. This happens due to the large colliding volume in heavy colliding nuclei, which leads to increase the interaction time among the colliding nucleons. Fig. 2.3, displays the energy dependence of allowed collisions for same set of reactions as taken in Fig. 2.2. From Fig. 2.3, one can see a linear dependence between NN collisions and incident energy. This shows that the role of Pauli blocking diminish as one move high energy region, which is more prominent in case of heavier systems than the lighter systems. This happens because the total excitation energy counted in lighter system is lower compared to the heavier system.

In mass asymmetric reactions, the collision profile behave differently. The Fig. 2.4 shows

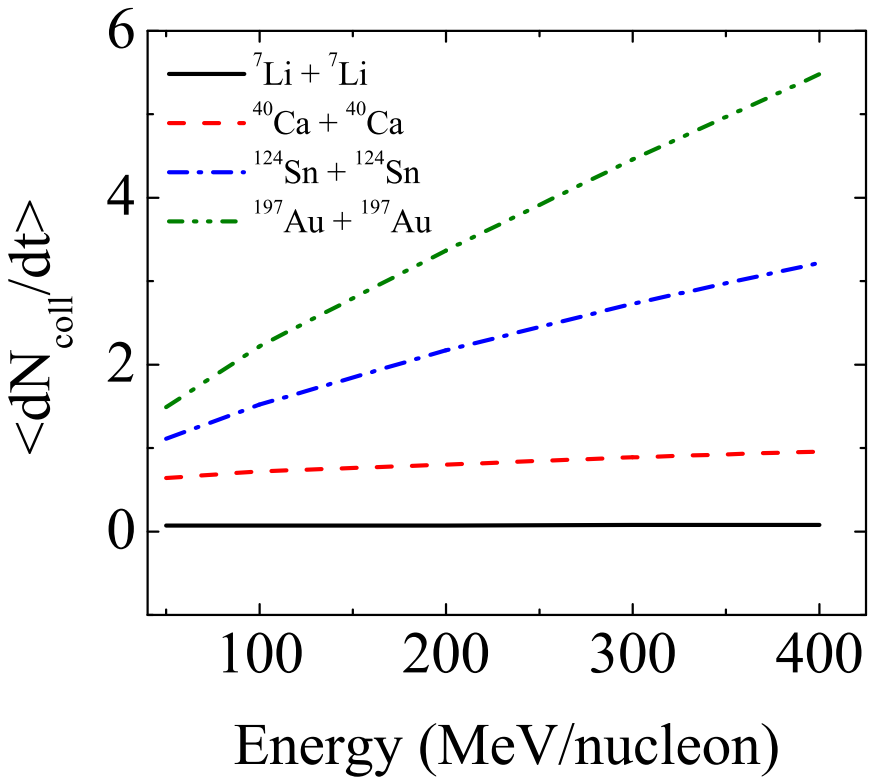

Figure 2.3: *The energy dependence of allowed collisions for the reactions of* ^{197}Au + ^{197}Au, ^{124}Sn + ^{124}Sn, ^{40}Ca + ^{40}Ca *and* ^{7}Li + ^{7}Li.

the effect of Pauli blocking on mass asymmetric collisions in Fermi energy region. From figure, one can see that the number of maximum allowed collisions increase with incident energy, which signifies that the role of Pauli blocking decreases with increase in incident energy. The rate of change of bar length is more in highly mass asymmetric collisions compared to the other one. It signifies that mass asymmetric collisions in Fermi energy region considered as a useful probe to hit the pauli blocking.

The QMD and IQMD models also differ in terms of parametreization of NN cross-section. In IQMD model, parameterized form of free nn, pp and np cross-sections are used instead of the average NN cross-section. The total cross-section contains both elastic and inelastic cross-section.

$$\sigma_{NN} = \sigma_{el} + \sigma_{inel} = \sigma_{el} + \Sigma_{channels}\sigma_i. \tag{2.36}$$

The following inelastic reactions are taken explicitly in calculations and might influence the collision dynamics:

$$N + N \rightarrow \Delta + N \ (hard - delta\ production) \ \ (a),$$

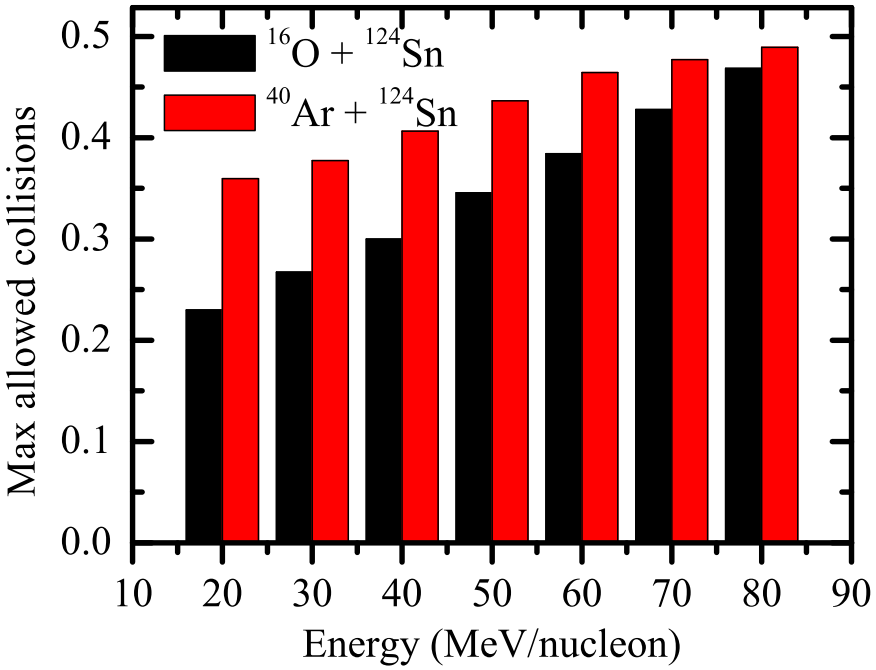

Figure 2.4: *Energy dependence of maximum allowed NN collisions for mass asymmetric collisions.*

$$\begin{aligned} \Delta \rightarrow\ & N + \pi\ (delta\ decay) && (b), \\ \Delta + N \rightarrow\ & N + N\ (delta\ absorption) && (c), \\ N + \pi \rightarrow\ & \Delta\ (soft - delta\ production) && (d). \end{aligned} \tag{2.37}$$

Experimental cross-sections are taken in consideration for the processes of elastic and inelastic cross-section. By using model detailed balance formula, the reverse reaction, which are not physically accessible are also considered in IQMD model.

The elastic angular distribution of NN scattering is consider as:

$$\frac{d\sigma_{el}}{d\Omega} \approx exp\left[A(s), t\right], \tag{2.38}$$

where t is $-q^2$, the transverse momentum transfer and

$$A(s) = 6\frac{\left[3.65\left(\sqrt{s} - 1.8766\right)\right]^6}{1 + \left[3.65\left(\sqrt{s} - 1.8766\right)\right]^6}, \tag{2.39}$$

A is given in $(GeV/c)^{-2}$.

The inelastic NN scattering angular distribution is defined as:

$$\frac{d\sigma_{in}}{d\Omega} \approx a(s)exp\left[b(s)cos\theta\right]. \tag{2.40}$$

The $a(s)$ and $b(s)$ depend on $\sqrt{s}$ and attain different values at different intervals of $\sqrt{s}$. θ is a polar angle.

The inclusion of isospin effects in QMD model improve the theoretical calculations, which can better explain the experimental data.

Numerical Tests

A nucleus is made up of several nucleons. A nucleon remains confined in a nucleus by the influence of the mean field of its neighbors. During the motion, when a nucleon comes closer to the surface of the nucleus, it will pull backside by other nucleons to keep confined in spherical distribution of radius R. After checking the destabilization of cold nuclei in initialization. In transport models after some lapse of hundred fm/c the nucleus start emitting the particles. A large number of tests were conducted to confirm the stability of nuclei [63, 64]. In this work the time evolution of r.m.s radius ($\langle r\rangle$) and momentum ($\langle p\rangle$) for single nucleus of ^{40}Ca and ^{197}Au is studied to understand the ground state properties. Fig. 2.5 shows the time dependence of the r.m.s. radius and momentum. One can observe the oscillations in values of r.m.s. radius and momentum about their mean value. On the other hand light nucleus is little less stable. This happens due to the poor density approximation in light nuclei.

2.3 Secondary models

The dynamics models can also be termed as "primary models" because they can explain the time span of the each nucleon and generate their phase-space. The correlations among the nucleons in final stage is mapped by a specific algorithm which are named as "secondary models". Now days, Minimum Spanning Tree (MST) [65, 66] method is considered to be generally critical. The MST approach clusterize the nucleons in terms of the spatial relationship among them.

Minimum Spanning Tree (MST) method

The easiest and more instinctive fragment definition depends on correlations in configuration space i.e. a nucleon $'i'$ fits with in a fragment, if there is another nucleon $'j'$ that has a place

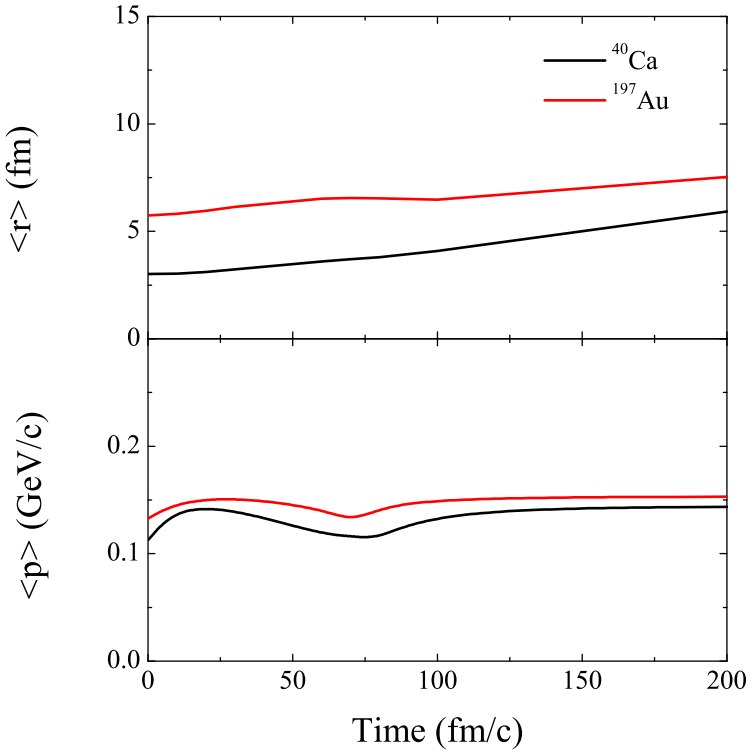

Figure 2.5: *Time evolution of the r.m.s. values of the radius and the momentum for single nucleus of* ^{40}Ca *and* ^{197}Au *in ground state.*

with same cluster with the condition:

$$\mid r_i - r_j \mid \leq d_{min}, \tag{2.41}$$

where r_i and r_j are the spatial positions of i^{th} and j^{th} nucleon and d_{min} is considered as a free-parameter, fluctuates from 2-4 fm. The fragments production with $d_{min} \leq 4$ fm is shown in Fig. 2.6. The main problem with MST method is that it is applicable to the dilute systems only. Since it depends on the proximity in space, the nucleons with different velocities can end up in the same fragment, though will leave the fragment at later stage.

It is well clear that, there are several theoretical models to explain the various observables of intermediate energy HIC. We have planned to study the phenomena of collective flow and nuclear stopping using primary model namely IQMD and then clustrize the nucleons in a fragment by using secondary model named MST.

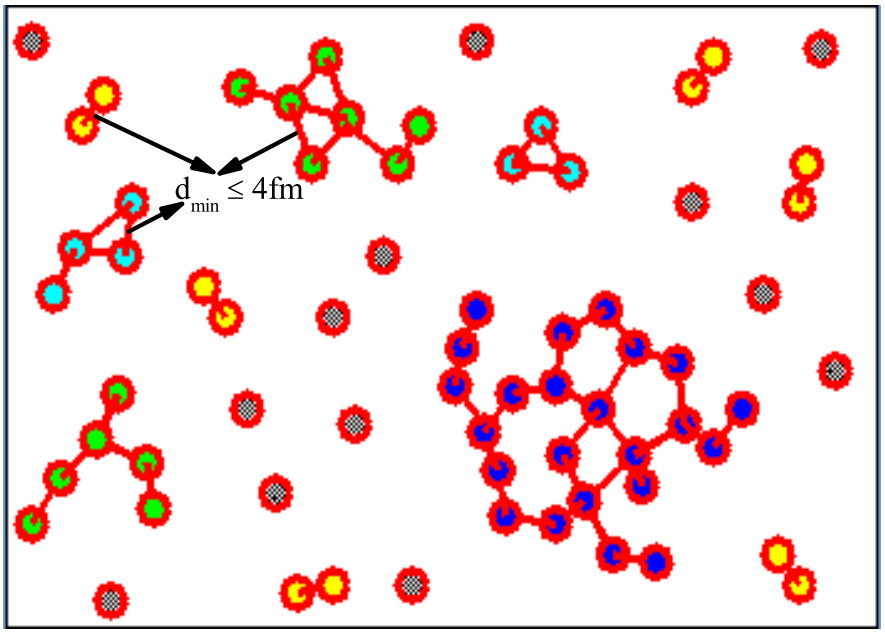

Figure 2.6: *The pictorial view of fragment formation with MST method with* $d_{min} \leq 4$ *fm.*

Bibliography

[1] R. Bansal and S. Kumar, Phys. of Part. and Nucl. Lett. **10**, 693 (2013).

[2] K. S. Vinayak and S. Kumar, Phys. Rev. C **83**, 034614 (2011).

[3] W. Reisdorf and H. G. Ritter, Ann. Nucl. Part. Sci., **47**, 663 (1997).

[4] A. Jain, K. S. Vinayak and S. Kumar, Ann. of Phys. **334**, 334 (2013).

[5] S. Kumar, S. Kumar, and R. K. Puri, Phys. Rev. C **81**, 014601 (2010).

[6] T. Gaitanos, M. Colonna, M. Di. Toro and H. H. Wolter Phys. Lett. B **595**, 209 (2004).

[7] K. Zbiri *et al.,* Phys. Rev. C **75**, 034612 (2007).

[8] F. Fu *et al.,* Phys. Lett. B **666**, 359 (2008).

[9] H. M*ü*ller and B. D. Serat, Phys. Rev. C **72**, 2071 (1995).

[10] N. Bohr, Nature, **37**, 344 (1936).

[11] S. E. Koohin and J. Randrup, Nucl. Phys. A **474**, 173 (1987).

[12] D. H. E. Gross, Rep. Progs. Phys. **53**, 605 (1999).

[13] J. P. Bondorf *et al.,* Phys. Rep. **257**, 133 (1995).

[14] G. A. Souliotis *et al.,* Phys. Rev. C **75**, 011601 (2007).

[15] D. V. Fedorov, A. S. Jensen and E. Garrido, Heavy Ion Phys. **18**, 203 (2003).

[16] W. A. Friedman, Phys. Rev. C **42**, 667 (1990).

[17] Q. Li, C. Shen, C. Guo, Y. Wang, Z. Li, J. Lukasik, W. Trautmann, Phys. Rev. C **83**, 044617 (2011).

[18] Y. Yariv and Z. Fraenkel, Phys. Rev. C **20**, 2227 (1979).

[19] A. K. Kerman and S. E. Koonin, Anns. of Phys. **100**, 332 (1976).

[20] E. Suraud, C. Gregoire and B. Tamain, Prog. Part. Nucl. Phys. **23**, 357 (1989).

[21] H. M. Xu, Phys. Rev. Lett. **67**, 2769 (1991).

[22] H. M. Xu, Phys. Rev. C **46**, 389(R) (1992).

[23] C. Gregoire, B. Remaud, F. Sebille, L. Vinet, and Y. Raffray, Nucl. Phys. A **465**, 317 (1987).

[24] G. F. Bertsch, H. Kruse and S. D. Gupta, Phys. Rev. C **29**, 673(R) (1984).

[25] J. J. Molitoris, H. Stocker, and B. L. Winer, Phys. Rev. C **36**, 220 (1987).

[26] C. Gale *et al.,* Phys. Rev. C **41**, 1545 (1990).

[27] L. Wilets, Y. Yariv, and R. Chestnut, Nucl. Phys. A **301**, 359 (1978).

[28] A. R. Bodmer, C. N. Panas and A. D. Mackellar, Phys. Rev. C **22**, 1025 (1980).

[29] J. Aichelin, Phys. Report **202**, 233 (1991).

[30] G. Peilert, H. Stocker, W. Greiner, A. Rosenhauer, A. Bohnet, and J. Aichelin, Phys. Rev. C **39**, 1402 (1989).

[31] A. Bohnet, N. Ohtsuka, J. Aichelin, R. Linden, and A. Faessler, Nucl. Phys. A **494**, 349 (1989).

[32] L. Neise, M. Berenguer, C. Hartnack, G. Peilert, H. Stocker and W. Greiner, Nucl. Phys. A **519**, 375 (1990).

[33] M. Berenguer, C. Hartnack, G. Peilert, H. Stocker, and W. Greiner, J. Phys. G **18**, 655 (1992).

[34] A. Bohnet *et al.,* Phys. Rev. C **44**, 2111 (1991).

[35] S. Huber and J. Aichelin, Nucl. Phys. A **573**, 587 (1994).

[36] H. Sorge, H. Stöcker, and W. Greiner, Ann. Phys. **192**, 266 (1989).

[37] H. Feldmeier, Nucl. Phys. A **515**, 147 (1990).

[38] H. Feldmeier and J. Schnack, Prog. Part. Nucl. Phys. **39**, 393 (1997).

[39] L. Wilet, E. M. Henley, M. Kraft and A. D. MacKellar, Nucl. Phys. A **282**, 341 (1977).

[40] N. Wang *et al.,* Phys. Rev. C **69**, 034608 (2004).

[41] M. Begemann-Blaich *et al.,* Phys. Rev. C **48**, 610 (1993).

[42] W. F. J. Müller *et al.,* Phys. Lett. B **298**, 27 (1993).

[43] L. Wilet, E. M. Henley, M. Kraft and A. D. MacKellar, Nucl. Phys. A 282, 341 (1977).

[44] A. Ono, H. Horiuchi, T. Maruyama, and A. Ohnishi, Phys. Rev. Lett. 68, 2898 (1992).

[45] A. Ono, H. Horiuchi, T. Maruyama, and A. Ohnishi, Prog. Theo. Phys. 87, 1185 (1992).

[46] G. F. Bertsch and S. Das Gupta, Phys. Rep. **160**, 189 (1988).

[47] C. Hartnack *et al.,* Eur. Phys. J. A **1**, 151 (1998).

[48] B. A. Li, C.M. Ko, and Z.Z. Ren, Phys. Rev. Lett. **78**, 1644 (1997).

[49] B. A. Li and C.M. Ko, Nucl. Phys. A **618**, 498 (1997).

[50] W. P. Tan *et al.,* Phys. Rev. C **64**, 051901(R) (2001).

[51] M. B. Tsang *et al.,* Phys. Rev. Lett. **86**, 5023 (2001).

[52] B. A. Li, Phys. Rev. Lett. **85**, 4221 (2000).

[53] B. A. Li, A.T. Sustich, and B. Zhang, Phys. Rev. C **64**, 054604 (2001).

[54] B. A. Li, Phys. Rev. Lett. **88**, 192701 (2002).

[55] J. Molitoris, J. B. Hoffer, H. Kruse, and H. Stocker, Phys. Rev. Lett. **53**, 899 (1984).

[56] G. F. Arnold *et al.,* Phys. Rev. C **25**, 936 (1982).

[57] G. Passatore, Nucl. Phys. A **95**, 694 (1967).

[58] S. A. Bass, C. Hartnack, H. Stöcker, and W. Greiner, Phys. Rev. C **51**, 3343 (1995).

[59] B. J. VerWest and R. A. Arndt, Phys. Rev. C **25**, 1979 (1982).

[60] H. Kruse, B. V. Jacak, and H. Stöcker. Phys. Rev. Lett. **54**, 289 (1985).

[61] J. J Molitoris and H. Stöcker, Phys. Rev C **32**, R346 (1985).

[62] S. R. Souza, L. de Paula, S. Leray, J. Nemeth, C. Ngô and H. Ngô, Nucl. Phys. A **571**, 159 (1994).

[63] G. Peilert *et al.,* Phys. Lett. B **260**, 271 (1991).

[64] G. Peilert *et al.,* Phys. Rev. C **46**, 1457 (1992).

[65] J. Aichelin, Phys. Rep. **202**, 223 (1991).

[66] R. K. Puri *et al.,* Phys. Rev. C **45**, 1837 (1997).

Chapter 3

Isospin effects on directed transverse flow

3.1 Introduction

The advancement of radioactive ion beam facilities has opened up new doors for the community of nuclear physics to understand the isospin asymmetries nuclear matter [1, 2, 3]. The influence of isospin degree of freedom on various physical phenomena, like collective flow [4, 5], multifragmentation [6, 7], nuclear stopping [8, 9], pre-equilibrium nucleon emission [10, 11], etc., have extensively been reported in the literature. Among the various observables, collective flow has a special state in HIC, as it shows high sensitivity towards the model ingredients, which are important to explain the NEOS. The isospin effects enter into the calculations via the Coulomb potential, the symmetry energy as well as through the isospin dependent NN cross-section. Till now, various attempts have been done to understand the importance of collective flow at and above the Fermi energy region. Recently, Puri and collaborators [12] studied the relative contributions of symmetry energy and Coulomb potential on transverse flow and also studied the disappearance of transverse flow for isobaric and isotonic systems throughout the mass range. The results clearly indicate that the density dependent symmetry energy shows a remarkable effect on directed transverse flow in intermediate energy region. Jain *et al.* [13] studied the effect of momentum dependent interactions (MDIs) and isospin dependent NN cross-section on n/p p_t-differential transverse flow. The study reported that neutrons and protons directed transverse flow is influenced by the momentum dependent interactions and the isospin dependent NN cross-section. FOPI collaboration [14] studied the p_t-differential transverse flow for different charged fragments

of ^{197}Au + ^{197}Au reaction in non-central collision and reported that the p_t-differential transverse flow increases with increase in fragment charge. INDRA collaboration [15] reported a significant contribution of Coulomb potential towards the directed flow. Kohley *et al.* [16] reported that the flow of intermediate mass fragments depend on both mass as well as charge of colliding systems. Transverse flow of intermediate mass fragments showed a remarkable affect towards the density dependent symmetry energy [16]. Li and Sustich [17] reported that even at balance energy, one gets a measurable value of differential transverse flow, which signifies that the differential transverse flow can act as a sensitive probe to study the NEOS. Moreover, differential transverse flow shows larger sensitivity toward the parameters that are come into calculations by the assimilation of other parameters. The ultimate goal of this chapter is to extract the information about the isospin dependent NEOS via density dependent symmetry energy and isospin dependent NN cross-section. The results are elaborated as follow [18].

3.2 Results and discussion

3.2.1 Density profile of various form of symmetry energy

During the collision, two nuclei (target and projectile) approach to each other and form a highly dense and compressed state. At this state, the symmetry energy plays a crucial role. In such situations, one tends to study the various form of density dependent symmetry energy. To study the influence of density dependent symmetry energy, author started with the study of density profile. Fig. 3.1, shows the time evolution of average density for ^{48}Ca + ^{48}Ca at E = 80 MeV/nucleon (in Fermi energy region), for the various form of symmetry energy having $\gamma = 0.66$, 1 and 2. The density is defined as [19]:

$$\rho_{ij}(r,t) = \sum_{i,j=1}^{A_T+A_P} \frac{1}{(2\pi L)^{\frac{3}{2}}}\ exp^{[\frac{-(r_i-r_j)^2}{2L}]}, \tag{3.1}$$

where r_i and r_j are the positions in coordinate space corresponding to the i^{th} and j^{th} nucleons, respectively. L stands for the Gaussian width of wave packet. A_T and A_P are the masses of target and projectile nucleus, respectively. Here, author calculated the average density over whole volume, represented by a single point at various time steps. The density dependent symmetry energy influence the reaction dynamics. Moreover, the peak value of

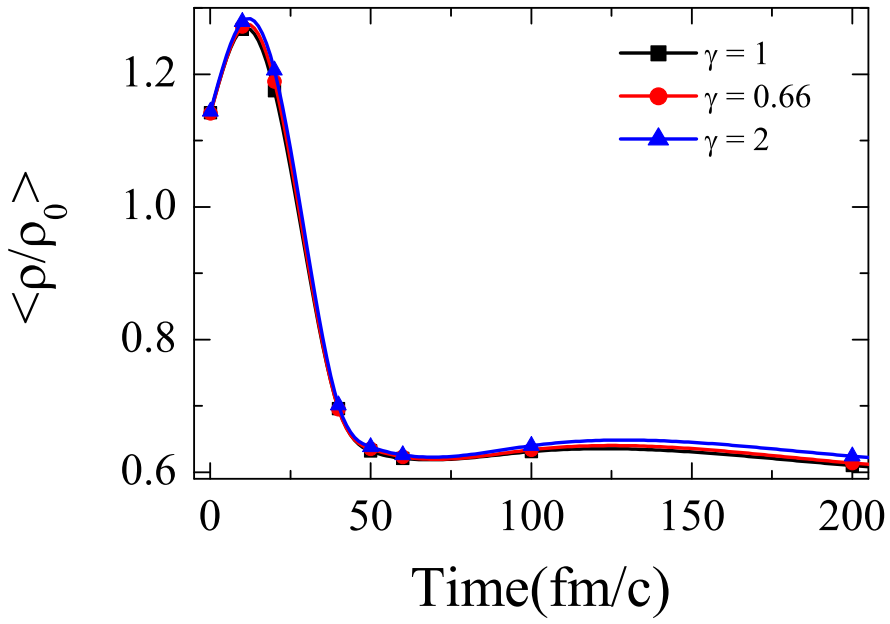

Figure 3.1: *Density profile for the reaction of* ^{48}Ca + ^{48}Ca *at E = 80 MeV/nucleon, for various form of density dependent symmetry energy having* γ = *0.66, 1 and 2.*

density dependent symmetry energy having $\gamma = 1$ is low compared to other forms of density dependent symmetry energy. As the NEOS is related to the density, therefore, one can say that density dependent symmetry energy affects the NEOS. The density dependent symmetry energy does not show a huge variation in fragment production [20]. However the effect of density dependent symmetry energy on elliptical flow has already reported in literature [21].

3.2.2 Directed transverse flow

In this chapter [18], influence of different forms of symmetry energy on p_t-differential transverse flow is studied. The mathematical formulation of directed transverse flow taken from the anisotropic distribution of nucleons reported by first-order Fourier coefficient given by Voloshin [22] as:

$$\frac{dN}{d\phi} \propto (1 + 2\sum_{n=1}^{\infty} v_n cos\ n\phi). \tag{3.2}$$

Where ϕ is azimuthal angle between the reaction plane and the transverse momentum of emitted particles. v_n characterized the strength of anisotropic flow. The first-order

anisotropic flow (v_1) is known as directed transverse flow. It can be defined as :

$$\langle v_1 \rangle = \langle cos\phi \rangle = \langle \frac{p_x}{p_t} \rangle, \tag{3.3}$$

here $p_t = \sqrt{(p_x)^2 + (p_y)^2}$, with p_x and p_y are parallel and perpendicular projections of particles transverse momentum. The directed flow signifies the pressure created between the colliding nuclear matter, which is connected to the highly thermalized. Thus, one can connect both observables (collective flow and nuclear stopping) of HIC with each other, which will be discussed in next chapter [23] under different reaction conditions. The magnitude and shape of directed flow has special feature in HIC. The rapidity dependence with directed flow under different reaction conditions (incident energy) can explain the phenomena of one- and two-body NN collisions.

It has been proved that the directed flow as a function of rapidity distribution shows a typical 'S-like' behavior. However, the shape of directed flow varies with incident energy. As presented in Fig. 3.2, directed transverse flow changes its sign as one increases the incident energy above 100 MeV/nucleon [24]. This happens because at low energy (E < E_{bal}, where balance energy (E_{bal}) is an energy where directed flow turn into zero) NN interactions are dominated by attractive mean field, which deflect the nucleons toward negative angle [25]. However, at high energies (few hundred MeV/nucleon to 1 GeV/nucleon) i.e. when E > E_{bal}, the individual NN scattering and repulsive mean field dominate, which deflect the emitted nucleons toward the positive angle [26]. As one move from low incident energy to higher one, the attractive interactions between the nucleons are balanced through repulsive NN interactions and result in zero directed transverse flow (E = E_{bal}). In Fermi energy region, very small values of higher order anisotropic flow is obtained. But, first-order anisotropic flow (v_1) gives a measurable value at low as well as at high incident energy.

3.2.3 Rapidity dependence of transverse directed flow

The directed transverse flow depends on region of rapidity distribution [27, 28]. Fig. 3.3 represents the dependence of directed transverse flow with scaled rapidity $\left(\frac{Y_{c.m}}{Y_{beam}}\right)$. Different lines represent the different colliding systems (^{26}Na + ^{26}Na, ^{48}Ca + ^{48}Ca, ^{78}As + ^{78}As, ^{129}Xe + ^{129}Xe) at scaled impact parameter $\hat{b} = 0.3$, where $\hat{b} = \frac{b}{b_{max}}$, here b is impact parameter

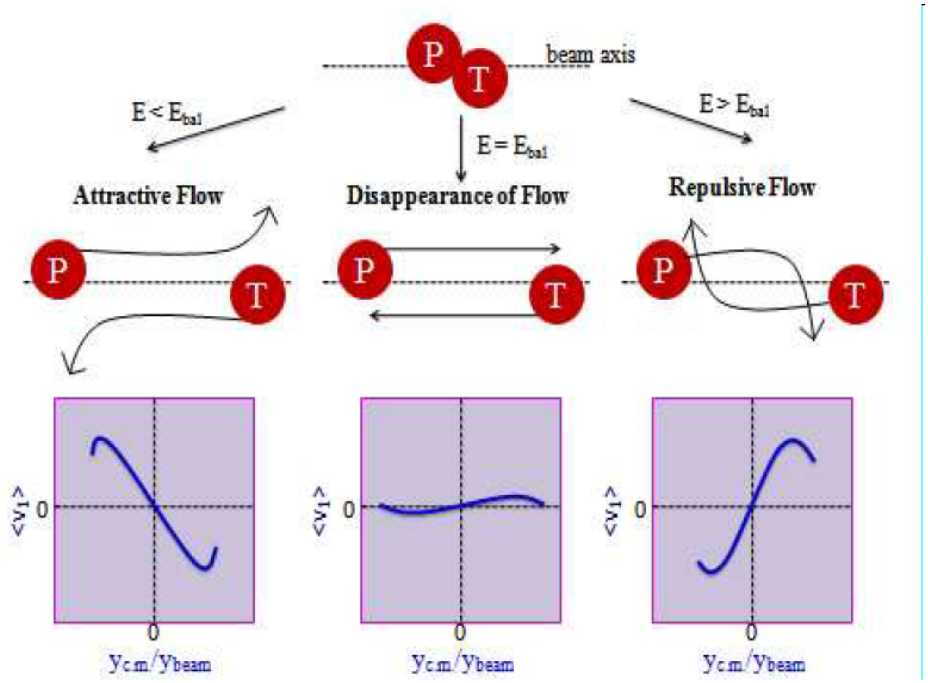

Figure 3.2: *Pictorial view of the energy dependence of directed flow.*

between the colliding nuclei and $b_{max} = 1.12(A_T^{\frac{1}{3}} + A_P^{\frac{1}{3}})$. The results are calculated at two different energies E = 80 (upper panel) and 400 (lower panel) MeV/nucleon. The flow parameter shows typical "S-like" curve for all colliding systems. At low incident energies, the nuclear interactions are dominated by attractive nuclear mean field, which deflect the nucleons toward the negative angles. Moreover, the slope become more negative with increase in system mass [28]. At high energy, the NN collisions drift the nucleons toward the positive angles corresponding to positive slope. The directed transverse flow shows large sensitivity toward the system mass through out the rapidity range $\left(|\ \frac{Y_{c.m.}}{Y_{beam}}\ | \leq 1.75\right)$. The sideward deflection of nucleons in directed transverse flow, vanishes at mid-rapidity region $\left(|\ \frac{Y_{c.m.}}{Y_{beam}}\ | \leq 0.1\right)$ and give a measurable value of flow in target-like (TL) $\left(\frac{Y_{c.m.}}{Y_{beam}} \leq -0.1\right)$ as well as projectile-like (PL) $\left(\frac{Y_{c.m.}}{Y_{beam}} \geq 0.1\right)$ region.

Jain *et al* [13] studied the influence of NN cross-section and momentum dependent interactions (MDIs) on directed transverse flow of protons and neutrons at E = 400 MeV/nucleon (above the balance energy), where reaction dynamics are governed by NN collisions only. Li [29] has showed that symmetry energy varies with isospin content of nucleons and plays a

significant role at low energy. Motivated from both the studies, in this chapter [18], author has addressed the isospin dependent properties of nuclear matter (symmetry energy and NN cross-section) via directed transverse flow. To study the relative effect of mean field and NN collisions, the following results are displayed in Fermi energy region at E = 80 MeV/nucleon for different form of symmetry energy and its density dependence.

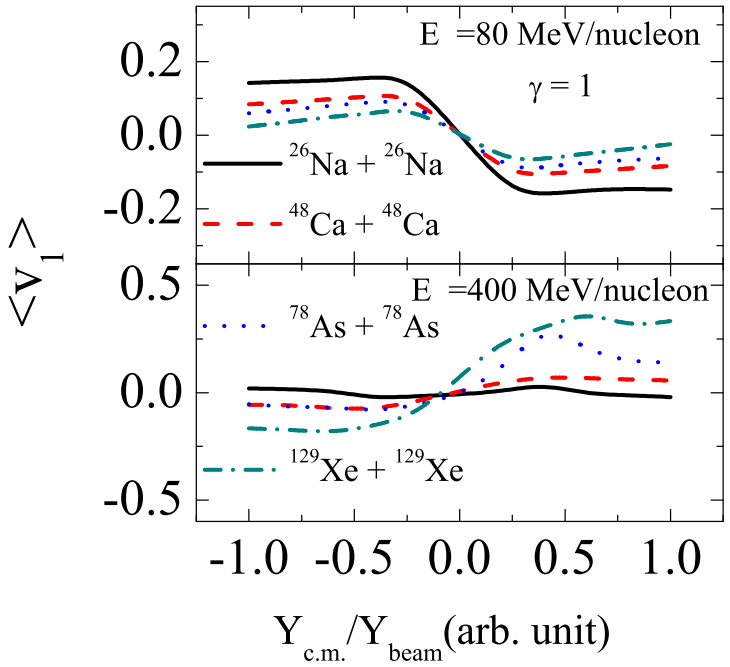

Figure 3.3: $\langle v_1 \rangle$ *dependence with rapidity distribution for different system mass at* $\gamma = 1$.

3.2.4 Transverse momentum dependence of directed flow

The isospin effects are visible in mid-rapidity zone. Thus, to study the isospin effect, author display the parameterized $\langle v_1 \rangle$ as a function of transverse momentum (p_t) in mid-rapidity zone [18]. The directed transverse flow showed a peak around the TL as well as PL region. The $v_1(p_t)$ dependence for symmetric systems form a mirror image on either side of the participant zone [13]. Considering that, author displays the following results for particular TL particle. In Fig. 3.4, one can see that the effect of density dependent symmetry energy increases with system mass. The peak of p_t-differential transverse flow get shifted toward the lower transverse momentum with system mass (as shown by lines with arrows).

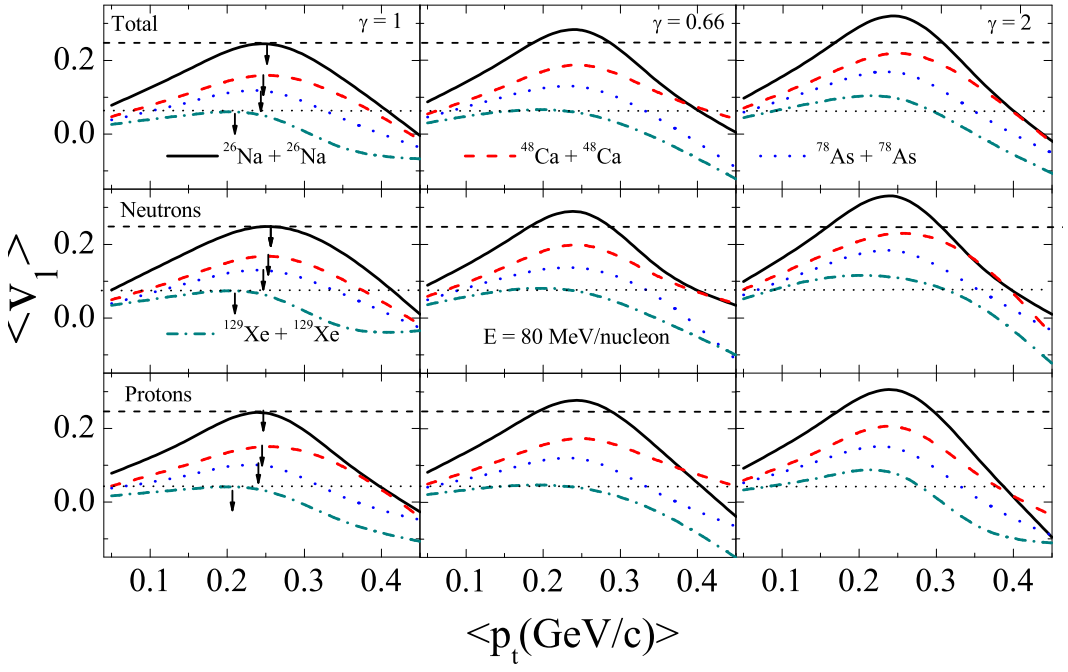

Figure 3.4: *Systematic representation of $v_1(p_t)$-dependence for the reactions of ^{26}Na + ^{26}Na, ^{48}Ca + ^{48}Ca, ^{78}As + ^{78}As, ^{129}Xe + ^{129}Xe and ^{145}Pm + ^{145}Pm. Different columns represent the results for different forms of density dependent symmetry energy and different rows represent $v_1(p_t)$-dependence for total nucleons, neutrons and protons, respectively.*

This happens because one need large incident energy to achieve sufficient initial compression in heavier systems. Moreover, the p_t-differential flow shows peak value in Fermi momentum region i.e. between 0.2 and 0.3 GeV/c ($v_1|_{P_F}$) and maximum sensitivity toward the density dependence of symmetry energy has been observed in this region. To study the isospin effects, author display p_t-differential transverse flow for total nucleons, neutrons and protons. One can see that flow is slightly more for the neutrons compared to the protons [30]. This is because the symmetry energy is repulsive for neutrons and attractive for protons [29].

To study the effects of density dependent symmetry energy on p_t-differential transverse flow for whole mass range, in Fig. 3.5, the transverse directed flow as a function of system mass in Fermi momentum region ($v_1|_{P_F}$) is shown. One can see that $\gamma = 1$ generates less directed transverse flow compared to $\gamma = 0.66$ (soft density dependence). This happens because the strength of symmetry energy with density for $\gamma = 0.66$ shows a rise (below normal nuclear matter density) and fall (above normal nuclear matter density), whereas for $\gamma = 1$, it shows a linear dependence. The flow is generated by pressure gradient, which is related

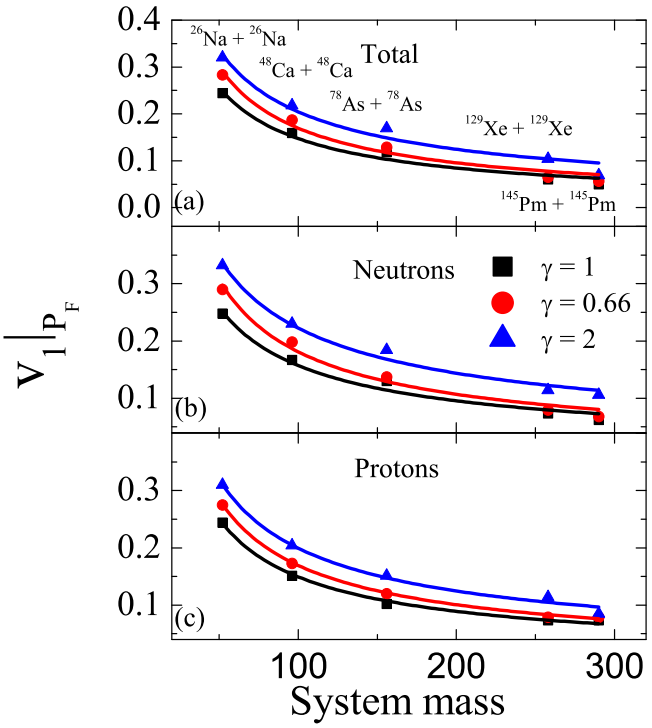

Figure 3.5: $v_1|_{P_F}$ *dependence as a function of system mass for different forms of density dependence of symmetry energy.*

to the density gradient, for $\gamma = 0.66$, the contribution of symmetry energy is more below normal nuclear matter density compared to the $\gamma = 1$, however, reverse trend is observed above the normal nuclear matter density. The trend might be due to the large contribution from low density region for soft density dependence of symmetry energy, which enhances the flow for the $\gamma = 0.66$ compared to the $\gamma = 1$. However, $v_1|_{P_F}$ further increases for the super-stiff form ($\gamma = 2$) of density dependent symmetry energy. This happens because for super-stiff form of density dependent symmetry energy, in general, enhances the pressure gradient of the colliding nuclei. At high density (above normal nuclear matter density), the strength of symmetry energy is more for $\gamma = 2$, which deflects the nucleons away from participant zone. The p_t-differential transverse flow is sensitive toward the various forms of density dependent symmetry energy, which is connected to the NEOS. Therefore, one can say that p_t-differential transverse flow provides a possible tool for extracting the information about the NEOS.

The system mass dependence of the difference of neutron-proton directed transverse flow in Fermi momentum region reflects the role of density dependent symmetry energy in more appropriate way, because the isospin difference enhance the effects of isospin dependent part

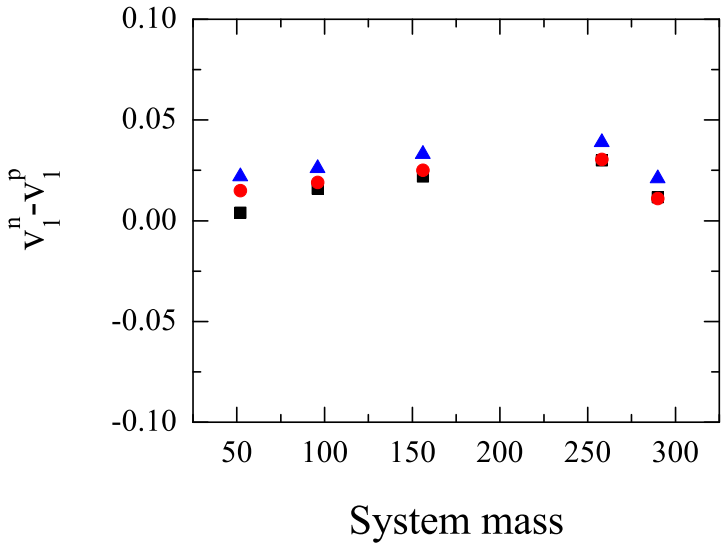

Figure 3.6: *The difference of neutron-proton directed transverse flow as a function of total system mass for different forms of density dependence of symmetry energy.*

and reduce the effects of isospin independent part i.e. the isoscaler part of the NEOS [31]. In Fig. 3.6, the effect of density dependent symmetry energy is studying via the difference of neutron-proton directed transverse flow over the whole mass range by keeping fix N/Z ratio of the colliding nuclei. From Fig. one can observe a small difference in various form of density dependent symmetry energy in whole mass range. It shows that the effect of density dependent symmetry energy is independent from system mass at fixed N/Z ratio of the colliding nuclei.

The symmetry energy is basically the energy difference of pure neutron matter and symmetric nuclear matter. Due to this, in following study N/Z ratio of colliding nuclei is varied to study the effect of density dependent symmetry energy.

3.2.5 N/Z dependence of colliding nuclei on p_t-differential transverse flow

In previous results author has studied the effect of density dependent symmetry energy on p_t-differential transverse flow for whole mass range by keeping neutron to the proton ratio

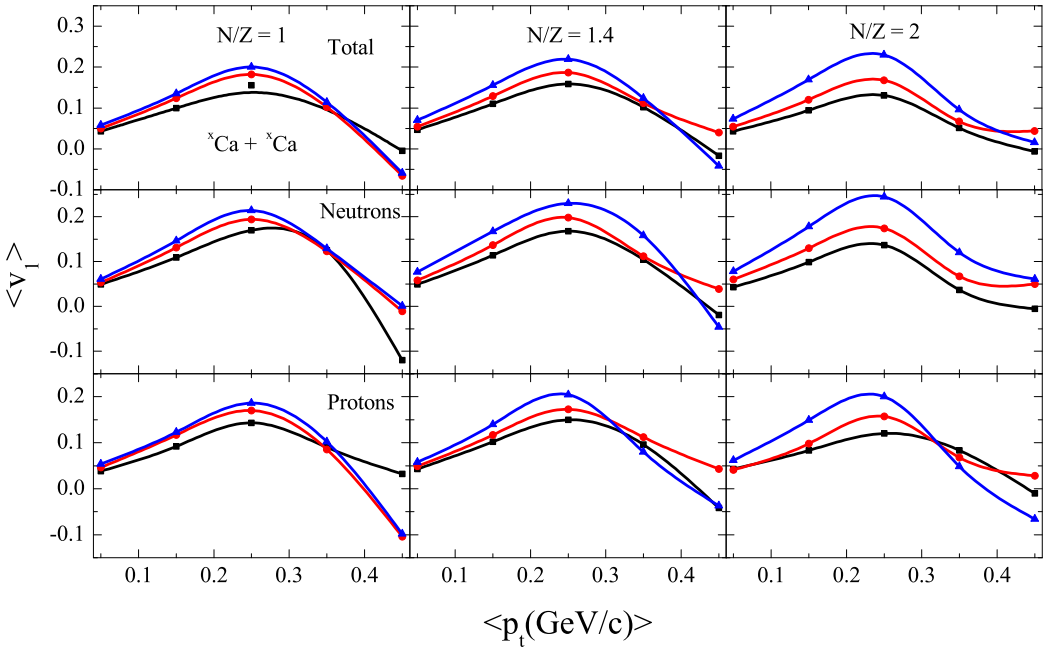

Figure 3.7: *p_t-differential transverse flow for the reaction of $^{x}Ca + {}^{x}Ca$ series for different forms of density dependent symmetry energy. Different rows represent the results for total nucleons, only for neutrons and protons, respectively.*

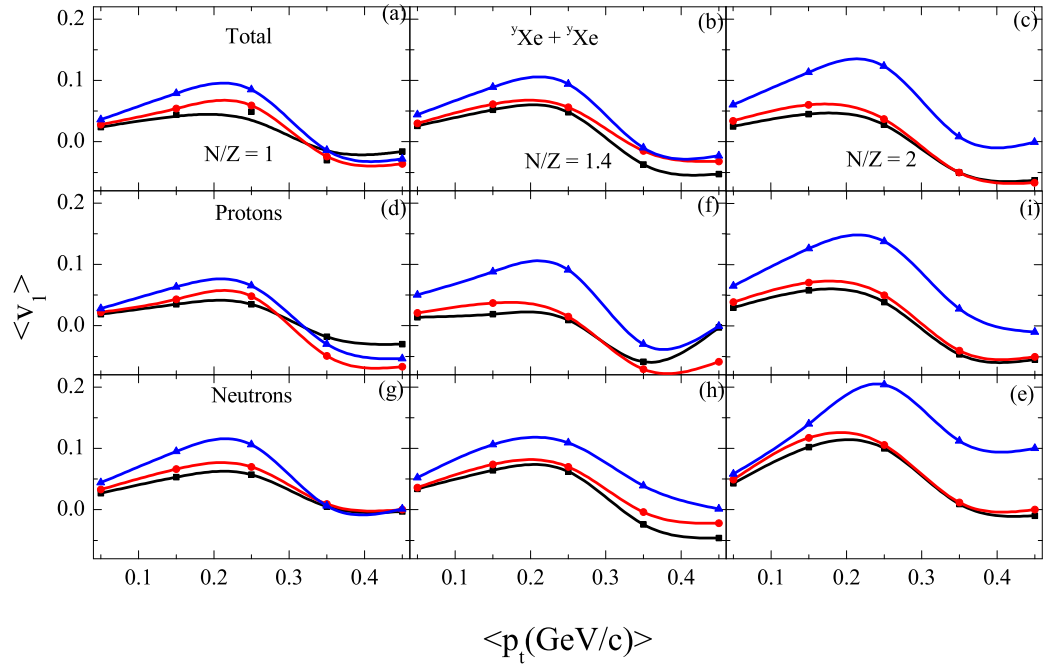

Figure 3.8: *Same as in Fig. 3.7, but for the reaction of $^{y}Xe + {}^{y}Xe$.*

fixed i.e. N/Z $\approx$ 1.4 of the colliding nuclei. However, the effect of symmetry energy increases with neutrons content, therefore, to study the contribution of N/Z ratio of the colliding nuclei, author has extended the study by taking the isotopic series of ^{x}Ca + ^{x}Ca (here x varies from 40 to 60) and ^{y}Xe + ^{y}Xe (here y varies from 108 to 162) shown in Figs. 3.7 and 3.8, respectively. Author has studied the isotopic pairs (Coulomb potential remain the same) in which mass increases due to the addition of neutrons. Therefore, decrease/increase (soft and stiff/super-stiff) in p_t-differential transverse flow reflects the influence of symmetry energy. To check the relative importance of these two mechanisms, Figs. 3.7 and 3.8, p_t-differential transverse flow for all nucleons, neutrons and protons in top, middle and bottom panels, respectively is displayed. From both the figures, we observe that:

(i) The p_t-differential transverse flow for various form of density dependent symmetry energy follow the same trend for various N/Z ratio of colliding nuclei, as shown in previous figures, i.e, flow increases with stiffness parameter. This is because the super-stiff density dependence of symmetry energy enables the early emission of nucleons from the participant zone. The relative strength of symmetry potential behave differently for different γ values below and above the normal nuclear matter densities. Above normal nuclear matter density, the strength of symmetry energy keeps on increasing for $\gamma = 2$ and it shows a fall, for $\gamma =$ 0.66, as explained in the previous figure.

(ii) On considering the N/Z ratio of the colliding nuclei, the effect of density dependent symmetry energy increases with N/Z ratio of the colliding nuclei in both the Figs. 3.7 and 3.8. This happens because increase in N/Z ratio means increase in neutrons number by keeping fix protons number and symmetry potential is highly repulsive for neutrons.

(iii) On comparing the results from top to bottom in both the Figs., author find that p_t-differential transverse flow shows large value for neutrons and relatively small value for protons in whole p_t range. This happens due to highly attractive(repulsive) symmetry potential between protons(neutrons). Thus, attractive force between protons decrease the flow value. However, the p_t-differential transverse flow for whole colliding system (all nucleons) lie between the neutron and proton p_t-differential transverse flow.

(iv) Again, in all conditions density dependent symmetry energy shows maximum sensitivity toward the p_t-differential transverse flow in Fermi momentum region.

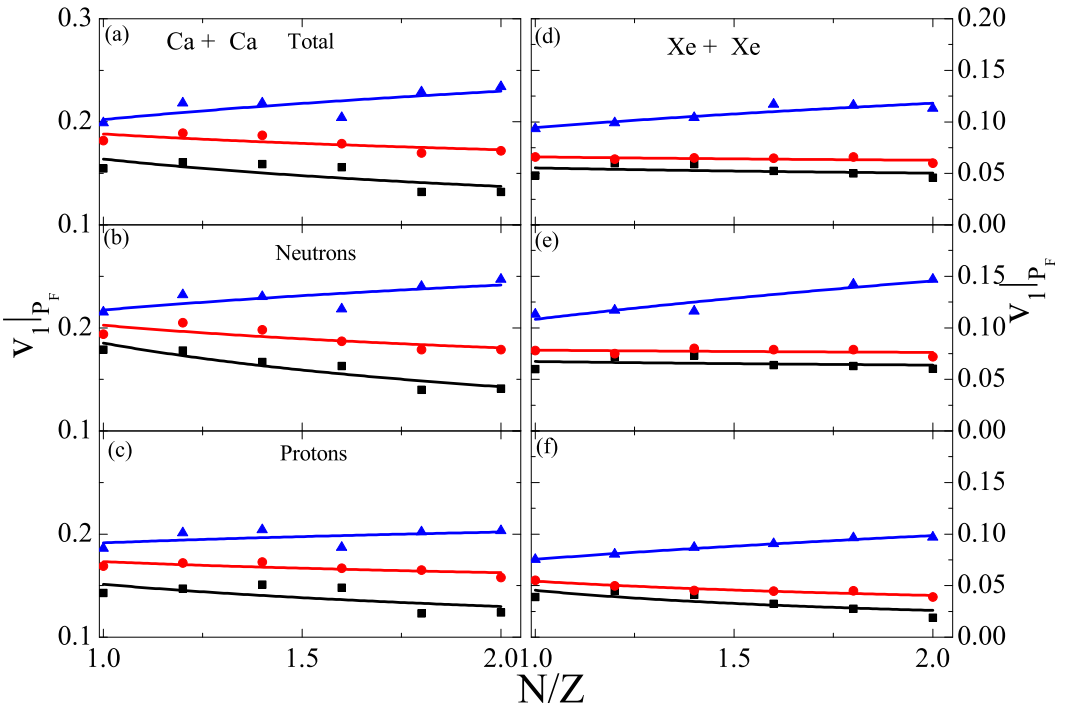

Figure 3.9: *$v_1|_{P_F}$ dependence as a function of N/Z ratio for Ca + Ca (left side) and Xe + Xe (right side) series for different forms of density dependent symmetry energy. Panels from top to bottom display the results for total nucleons, neutrons and protons, respectively. Different symbols are corresponding to different γ values as used in Fig. 3.5.*

To study the comparative effect of system mass and N/Z ratio of colliding nuclei, in Fig. 3.9, we represent $v_1|_{P_F}$ as a function of N/Z which varies between 1 to 2 for the reaction of Ca + Ca (left side) and Xe + Xe (right side). On comparing the results of p_t-differential transverse flow for both the colliding systems, we find that the slope (which signifies the N/Z dependence of colliding nuclei) of $v_1|_{P_F}$ is higher for heavier system (Xe). However, the value of flow is smaller in heavier system. Thus, one can conclude that symmetry energy and its density dependence shows large sensitivity toward the N/Z ratio of heavier system. This is due to the effect of symmetry potential.

In better way to study the effect of symmetry energy and its density dependence for different neutron-proton content in whole periodic table. The Fig. 3.10 represents the difference of neutron-proton directed transverse flow for isotopic series of Ca (upper panel) and Xe (lower panel). From Fig. 3.10, one can see that the super-stiff form of density dependent symmetry energy shows large flow difference in whole isotropic series. Moreover, the effect of isospin dependent part is more prominent in heavier system than the lighter system.

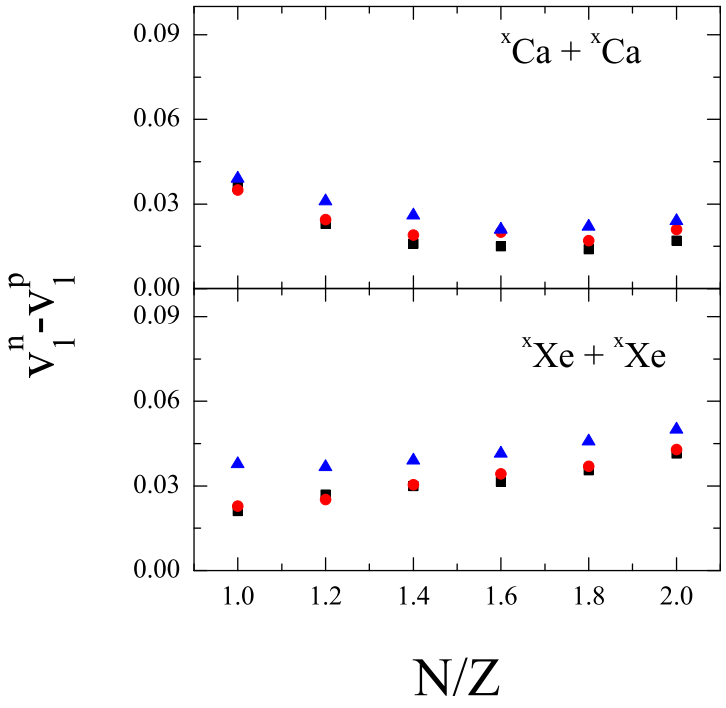

Figure 3.10: *Comparison of the difference between neutron-proton directed transverse flow in semi-central ($\hat{b} = 0.3$) collisions of isotropic series of Ca in upper panel and Xe in lower panel at the energy of 80 MeV/nucleon with different forms of symmetry energy having γ = 1, 0.66 and 2.*

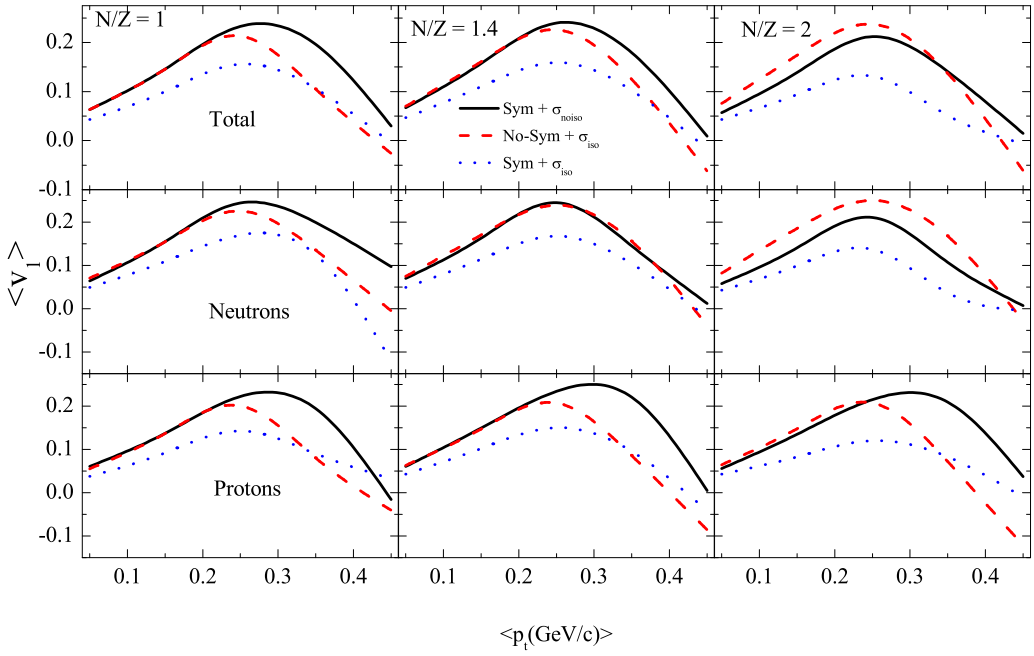

Figure 3.11: *p_t-differential transverse flow for $\gamma = 1$ for the reaction of ^{x}Ca+^{x}Ca. Solid lines and dash lines represent the p_t-differential transverse flow in the absence of isospin dependent cross-section and symmetry energy. Dotted lines represent the results with symmetry energy and isospin dependent cross-section.*

This support the previous Fig. 3.9. However, the difference of neutron-proton directed transverse flow reduces the isospin independent parts (isoscaler part and NN cross-section) and enhance the isospin dependent part of NEOS. Thus, one can conclude that the isotopic series of heavier colliding systems can better explain the isospin dependent part of NEOS.

Till now, author has studied the influence of density dependent symmetry energy on p_t-differential transverse flow for whole system (all nucleons) and its constituent (neutron and proton) individually. The isospin effects also influence the NN cross-section. Therefore, as a next step to study the behavior of p_t-differential transverse flow in more detail. In Figs. 3.11 and 3.12, author compared the results of p_t-differential transverse flow in the absence of isospin dependent NN cross-section (solid lines) (Sym + σ_{noiso}) and symmetry energy (dash lines) (No-Sym + σ_{iso}) with the results of p_t-differential transverse flow in presence of both the effects (isospin dependent NN cross-section and symmetry energy) and is represented via dotted lines (Sym + σ_{iso}) for the reaction of Ca + Ca (Fig. 3.11) and Xe + Xe (Fig. 3.12) for different N/Z ratio of colliding nuclei as taken in previous Figs.

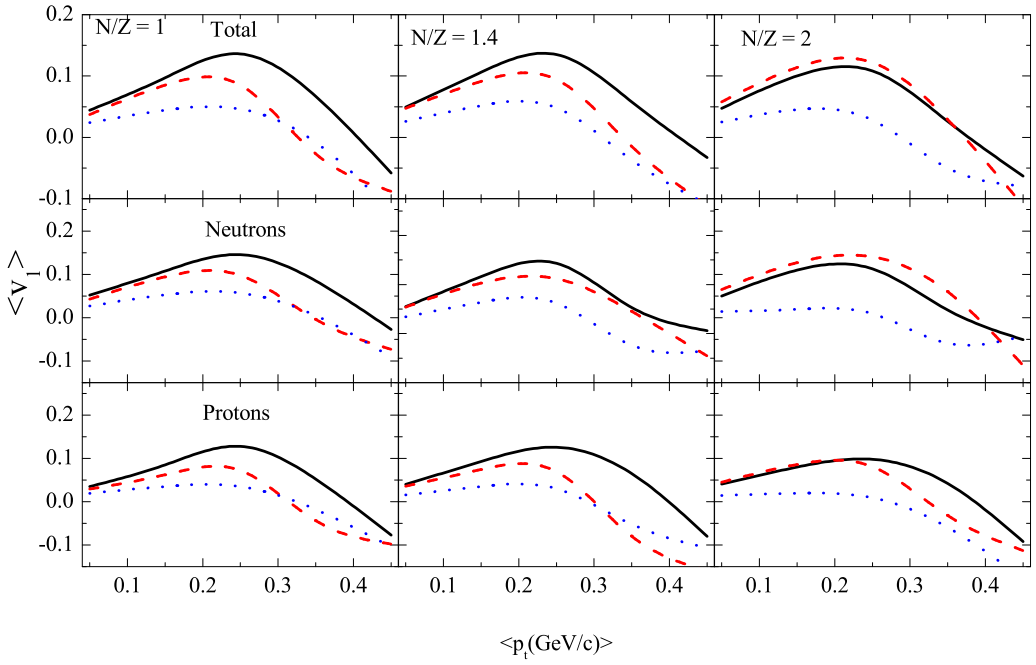

Figure 3.12: *Same as in Fig. 3.11, but for the reaction of* $^{y}Xe +^{y} Xe$.

3.8 and 3.9. From figures 3.11 and 3.12, we observed that on p_t-differential transverse flow the inclusion of isospin effect in calculations take place by symmetry energy and by isospin dependent NN cross-section. However, the influence of isospin effect via symmetry energy is more prominent than the isospin dependent NN cross-section in both figures. The isospin effect increases with N/Z ratio of colliding nuclei. This happens due to increase in neutrons content of colliding nuclei. As already stated that the symmetry energy is repulsive for neutron, thus due to repulsive neutron-neutron interactions, the flow value increases on the inclusion of symmetry energy. However, in isospin dependent NN cross-section, the probability of neutron-proton collisions is nearly three times compared to the neutron-neutron and proton-proton collisions. Thus, due to the inclusion of isospin dependent NN cross-section, p_t-differential transverse flow increases. Again, the increase in the peak value is more for the neutrons rich system compared to neutrons deficient system. The small change in slope is observed when one switch off the symmetry energy contribution, which shows that the sensitivity of N/Z dependence of p_t-differential transverse flow to the strength of symmetry energy and its insensitiveness to the isospin dependence of NN cross-section far away from the mid-rapidity zone. From above discussion, one can conclude that the symmetry energy

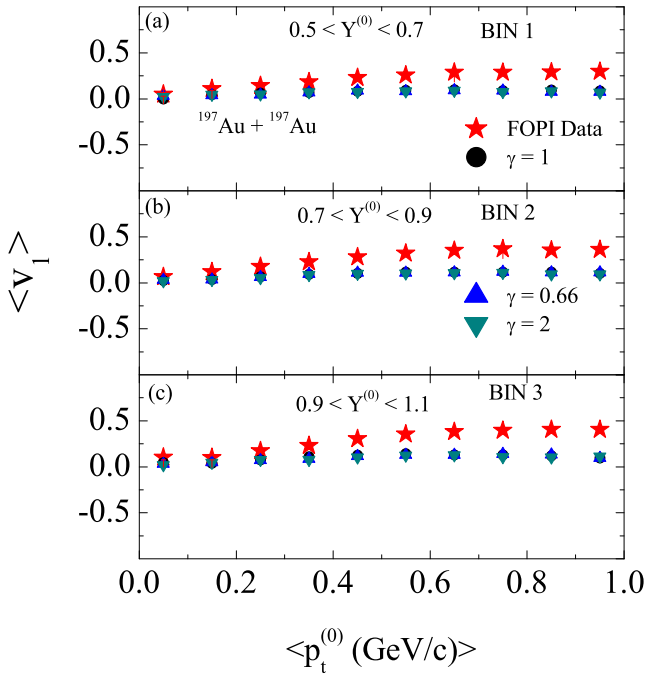

Figure 3.13: *Scaled transverse momentum dependence of directed flow for free protons at E = 250 MeV/nucleon and b varies from 3-6 fm for different scaled rapidity bins, panels (a)-(c) shows the comparison of experimental finding of FOPI collaboration with theoretical calculations for the reaction of ^{197}Au + ^{197}Au.*

plays a dominant role for the enhancement of p_t-differential transverse flow with neutron content throughout the mass range. Again, large slope is observed for heavier masses, which indicates that the N/Z dependence of p_t-differential transverse flow for heavier systems act as a good probe to constrain the density dependent symmetry energy.

On comparing the observed results with Ref. [12], author found that relative change in slope for different γ values is more pronounced at maximal value of p_t-differential transverse flow compared to the balance energy. This signifies that $v_1(p_t)$-dependence of transverse flow is a more sensitive probe compared to the energy of vanishing flow (EVF) to study the effect of symmetry energy and its density dependence. These finding are in confirmation with Ref. [17].

3.2.6 Comparison with experimental data

For more practical interpretation of our results, author has compared the experimental findings of FOPI collaboration [32, 33, 34] with theoretical calculations. Author has used

isospin dependent cross-section and other conditions are chosen according to the availability of the experimental data. The normalized center-of-mass (c.m.) transverse momentum and rapidity is defined as:

$$p_t^{(0)} = p_t/p_{c.m}^{proj}, \qquad Y^{(0)} = (Y/Y_{proj})^{c.m.} \tag{3.4}$$

where the *proj* denotes the projectile.

Fig. 3.13, shows p_t-differential transverse flow of free protons for three different rapidity bins at E = 250 MeV/nucleon. Panels (a)-(c), show the results for the reaction of ^{197}Au + ^{197}Au under the conditions imposed by FOPI [32, 33, 34] collaboration. Author could find that directed transverse flow shows a rise with $p_t^{(0)}$. This happens because transverse momentum transfer to the particles is not uniformly distributed. Moreover, the high-p_t particles emitted at pre-equilibrium stage, therefore, they do not undergo maximum compression stage and thus show large value of flow. The p_t-differential transverse flow shows lesser sensitivity for different form of density dependence of symmetry energy because the effect of symmetry energy vanishes for spectator matter. One can see that, the positive value of flow increases as one move from rapidity $0.5 < Y^{(0)} < 0.7$ (BIN 1) to $0.9 < Y^{(0)} < 1.1$ (BIN 3). This is because, on moving from top to bottom, the transverse momentum associated with the nucleons decreases due to increase of spectator zone, this increases the transverse flow. Moreover, directed transverse flow shows a linear dependence with $\langle p_t^{(0)} \rangle$ at low value of the transverse momentum, but shows deviation from the straight line at higher $\langle p_t^{(0)} \rangle$ [22]. This happens due to the transverse radial expansion. Our theoretical results follow the similar trend as given by experimental findings. However, one can reduce the gap between the experimental data and theoretical calculations by introducing momentum dependent interactions in the potential [13, 35, 36].

3.3 Summary

Theoretical investigation of p_t-differential transverse flow by using the Isospin-dependent Quantum Molecular Dynamics (IQMD) model has been performed. Study shows that the maximum value of p_t-differential transverse flow act as a more suitable probe to study the effect of symmetry energy and its density dependence than the EVF. The sensitivity of symmetry energy towards the p_t-differential transverse flow with is found to be much higher

for heavy system, indicating that the N/Z dependence of p_t-differential transverse flow of heavy systems can act as a suitable probe to constrain the density dependence of symmetry energy at supra-saturation region. The N/Z dependence of p_t-differential transverse flow is sensitive to the symmetry energy and its density dependence and showed insensitivity to isospin dependence of NN cross-section far away from the mid-rapidity zone. Moreover, the theoretical calculations follow the similar trend as given by the experimental findings in different rapidity bins.

Bibliography

[1] I. Tanihata, Nucl. Phys. A **685**, 80 (2001).

[2] M. Di Toro *et al.,* Prog. Part. Nucl. Phys. **42**, 125 (1999).

[3] B. A. Li, C. M. Ko and W. Baur, Int. J. Mod. Phys. E **7**, 147 (1998).

[4] W. Reisdorf and H. G. Ritter, Ann. Nucl. Part. Sci., **47**, 663 (1997).

[5] A. Jain, K. S. Vinayak and S. Kumar, Ann. of Phys. **334**, 334 (2013).

[6] R. Bansal and S. Kumar, Phys. of Part. and Nucl. Lett. **10**, 693 (2013).

[7] K. S. Vinayak and S. Kumar, Phys. Rev. C **83**, 034614 (2011).

[8] H. Stöcker, J. A. Maruhn and W. Greiner, Phys. Rev. Lett. **44**, 725 (1980).

[9] W. Reisdorf *et al.,* Phys. Rev. Lett. **92**, 232301 (2004).

[10] M. L. Miller *et al.,* Phys. Rev. Lett. **82**, 1399 (1999).

[11] J. F. Dempsey *et al.,* Phys. Rev. C **54**, 1710 (1996).

[12] S. Gautum, Ph.D Thesis, Panjab University, Chandigarh (2013).

[13] A. Jain *et al.,* Ann. of Phys. **334** 334 (2013).

[14] A. Andronic *et al.,* Phys. Rev. C **64**, 041604(R) (2001).

[15] J. Lukasik *et al.,* Phys. Lett. B **608**, 223 (2005).

[16] Z. Kohley *et al.,* Phys. Rev. C **82**, 064601 (2010).

[17] B. A. Li and A. T. Sustich, Phys. Rev. Lett. **82**, 5004 (1999).

[18] R. Bansal, A. Jain and S. Kumar, Inter. Jour. of Mod. Phys. E **23**, 1450062 (2014).

[19] J. Aichelin, Phys. Rep. **202**, 233 (1991).

[20] K. S. Vinayak and S. Kumar, Phys. of Part. and Nuclei Lett. **9**(8), 583 (2012).

[21] K. S. Vinayak and S. Kumar, Eur. Phys. J. A **47**, 144 (2011).

[22] S. A. Voloshin, Phys. Rev. C **55** 1630(R) (1997).

[23] R. Bansal, A. Jain and S. Kumar, Ind. Jour. Phys. **89**, 1077 (2015).

[24] B. A. Li, Phys. Rev. C **48**, 2415 (1993).

[25] M. B. Tsang *et al.,* Phys. Rev. Lett. **57**, 559 (1986).

[26] B. Zhang, M. Gyulassy and C. Ko, Phys. Lett. B **455**, 45 (1999).

[27] J. Aichelin, Phys. Report **202**, 233 (1991).

[28] R. Bansal and S. Gautam, Phys. Rev. C **91**, 024615 (2015).

[29] B. A. Li, Phys. Rev. C **69**, 034614 (2004).

[30] B. A. Li, L. W. Chen and C. M. Ko, Phys. Rep. **464**, 113 (2008).

[31] B. A. Li, Phys. Rev. Lett. **85**, 4221 (2000).

[32] A. Andronic *et al.,* Phys. Rev. C **67**, 034907 (2003).

[33] A. Andronic *et al.,* Phys. Lett. B **612**, 173 (2005).

[34] M. Di Toro, S. J. Yennello and B. A. Li, Eur. Phys. J. A **30**, 153 (2006).

[35] A. D. Sood, R. K. Puri, Phys. Rev. C **69**, 054612 (2004).

[36] A. D. Sood, R. K. Puri, Phys. Rev. C **73**, 067602 (2006).

Chapter 4

Correlation between nuclear stopping and collective flow

4.1 Introduction

The investigation of HIC throw light on various rare phenomena like multifragmentation, collective flow and nuclear stopping. The reaction dynamics depends strongly on both incident energy as well as impact parameter. The ability of nuclear matter to dissipate the initial longitudinal momentum into transverse degree of freedom is termed as nuclear stopping. There are various independent parameters in literature that are able to explain the nuclear stopping [1]-[5].The nuclear stopping has been studied extensively both experimentally and theoretically. Bass *et al.* [6] proposed the idea of nuclear stopping phenomena via the "isospin-mixing" method. It also shed light on the entropy of the reaction. Nuclear stopping is related to the question, whether the thermalization (equilibrium) state can be attained or not during the collision. Nevertheless, nuclear stopping is highly influenced by in-medium NN cross-section, Pauli blocking and Fermi motion. Bauer [7] addressed the importance of attractive mean field and in-medium NN cross-section on nuclear stopping in intermediate energy region. Liu *et al.* [4] have proposed the investigation of nuclear stopping for symmetric reactions with different neutron to proton ratio for whole energy range. Their study revealed that nuclear stopping depends on both in-medium NN cross section and mean field. Moreover, it also increases with the system mass. Li and coworkers [8] studied the effect of in-medium NN cross-section and EOS on nuclear stopping. Similarly, Yuan *et al.* [9] have studied the effect of excitation function of nuclear stopping on light mass fragments for the reaction of ^{197}Au + ^{197}Au and reported that the stopping is influ-

enced by stiffness of EOS and in-medium NN cross-section. Kaur *et al.* [5] have studied the effect of mass asymmetry on nuclear stopping by keeping total mass of the colliding nuclei fixed at E = 250 MeV/nucleon. Their study revealed that nuclear stopping decreases with the mass asymmetry. The nuclear stopping can also be correlated with other observables of intermediate energy HIC, such as multifragmentation and collective flow.

Residorf *et al.* [10] showed a linear relation between the directed flow and nuclear stopping for symmetric reactions of ^{197}Au + ^{197}Au, ^{131}Xe + ^{132}Cs, ^{101}Ru + ^{101}Ru, ^{59}Ni + ^{59}Ni and ^{40}Ca + ^{40}Ca at incident energy varying between 150 and 1930 MeV/nucleon (above the balance energy). Zhang *et al.* [11] also demonstrated a linear dependence between the nuclear stopping and the magnitude of directed & elliptic flows for same set of reactions at E = 250 and 400 MeV/nucleon. Recently, Jain and Kumar [12] studied the nuclear stopping around the E_{bal} for symmetric systems. The study does not show a visible effect on nuclear stopping at E_{bal}.

All the above studies are limited for the dynamics of symmetric and nearly-symmetric colliding systems. Little attention has been paid to study the correlation between nuclear stopping and directed transverse flow for asymmetric reactions. Till now, only linear dependence of both the quantities (collective flow and nuclear stopping) is reported at higher incident energies. But, little attention has been paid to study such dependence at lower incident energy. Andronic *et al.* [13] reported that below 150 MeV/nucleon, the correlation between the directed transverse flow and nuclear stopping does not follow the linear dependence, but, still no one has reported the correlation between the directed transverse flow and nuclear stopping at low energy (E < 100 MeV/nucleon). Moreover, Zhang *et al.* [11] have also studied the correlation between elliptical flow and nuclear stopping for symmetric and nearly symmetric reactions at E = 250 and 400 MeV/nucleon. The study reported that a positive correlation holds between the nuclear stopping and the elliptical flow. Motivated from the above discussions, aim in the present chapter [14] is at least five fold:

i) To study the influence of mass asymmetry as well as system mass of colliding nuclei on nuclear stopping under different reaction conditions.

ii) To study the influence of colliding geometry on the correlation between directed transverse flow and nuclear stopping.

iii) To study the nuclear stopping of different mass fragments.

iv) To study the correlation between directed transverse flow and nuclear stopping for the mass asymmetric colliding nuclei at both low as well as high energy.

v) To study the effect of fragment masses on the correlation between elliptical flow and nuclear stopping at and around the transition energy.

4.2 Parameters of nuclear stopping

There are various parameters existing in literature to estimate the degree of nuclear stopping. The nuclear stopping can be investigated via rapidity distribution, anisotropy ratio, quadrupole momentum and relative momentum. The various parameters of nuclear stopping are defined as:

i) The rapidity distribution ($Y(i)$) that helps to calculate nuclear stopping is defined as [1]:

$$Y(i) = \frac{1}{2} ln \frac{E(i) + p_z(i)c}{E(i) - p_z(i)c}, \tag{4.1}$$

where, $p_z(i)$ and $E(i)$ are longitudinal momentum and total energy of i^{th} particle, respectively. In rapidity distribution, for complete stopping a single Gaussian shape distribution is envisage. The width of Gaussian distribution decides the nuclear stopping. The narrow Gaussian indicates better thermalization compared to broader one.

ii) The strength of nuclear stopping from rapidity distribution is further calculated by the stopping parameter $varxz$ [3], which is the ratio of transverse (x) and longitudinal (z) variances of the rapidity distributions. The stopping parameter $varxz$ is defined as:

$$\langle varxz \rangle = \frac{\sigma^2(x)}{\sigma^2(z)}. \tag{4.2}$$

The value of $\langle varxz \rangle = 1$ indicates complete stopping.

iii) The next is quadrupole moment $\langle\ Q_{ZZ}\ \rangle$ [4], which is defined as:

$$\langle Q_{ZZ} \rangle = \sum_i \left[2p_z^2(i) - p_x^2(i) - p_y^2(i) \right]. \tag{4.3}$$

For complete stopping $\langle\ Q_{ZZ}\ \rangle = 0$.

In this chapter, we use the parameter namely anisotropic ratio $\langle R \rangle$ to study the nuclear

stopping [5]. It is defined as

$$\langle R \rangle = \frac{2}{\pi} \frac{(\sum_i p_\perp(i))}{(\sum_i p_\parallel(i))}, \tag{4.4}$$

where $p_\perp = \sqrt{p_x^2(i) + p_y^2(i)}$ and $p_\parallel = p_z(i)$, and p_x, p_y & p_z have their usual meanings.

4.3 Results and discussion

In the present study, starting with the simulations have been carried out for mass symmetric and mass asymmetric reactions i.e. η = 0.0 to 0.5. In particular, we simulate the reactions of ^{40}Ca + ^{40}Ca ($\eta = 0$), ^{36}Ar + ^{44}Ca ($\eta = 0.1$), ^{32}S + ^{48}Ti ($\eta = 0.2$), ^{28}Si + ^{52}Cr ($\eta = 0.3$), ^{24}Mg + ^{56}Fe ($\eta = 0.4$) and ^{20}Ne + ^{60}Ni ($\eta = 0.5$), having A_{tot} = 80 units, ^{80}Kr + ^{80}Kr ($\eta = 0$), ^{70}Ge + ^{90}Zr ($\eta = 0.1$), ^{62}Ni + ^{98}Mo ($\eta = 0.2$), ^{54}Fe + ^{106}Cd ($\eta = 0.3$), ^{45}Sc + ^{115}In ($\eta = 0.4$) and ^{40}Ca + ^{120}Te ($\eta = 0.5$), having A_{tot} = 160 units and ^{120}Te + ^{120}Te ($\eta = 0$), ^{108}Cd + ^{132}Ba ($\eta = 0.1$), ^{96}Mo + ^{144}Nd ($\eta = 0.2$), ^{84}Sr + ^{156}Dy ($\eta = 0.3$), ^{71}Ga + ^{169}Tm ($\eta = 0.4$) and ^{60}Ni + ^{180}W ($\eta = 0.5$), having A_{tot} = 240 units, where $A_{tot} = A_T + A_P$. The whole analysis is carried out with soft equation of state along with an isospin energy dependent reduced cross section i.e. $\sigma = 0.8\sigma_{nn}^{free}$ [15, 16].

4.3.1 System mass dependence of nuclear stopping in Fermi energy region

Fig. 4.1, displays the energy dependence of nuclear stopping for mass asymmetric collisions. Different panels represent the different sets of reactions having total mass A_{tot} = 80, 160 and 240 in panels (a), (b) and (c), respectively. The system mass dependence for whole range of Fermi energy region is analysed.

Figure reveals that:

i) The nuclear stopping decreases with increase in mass asymmetry of colliding nuclei. This happens because $\langle R \rangle$ is ratio of transverse to the longitudinal momentum. The transverse momentum increases with mass asymmetry [5], which result in the decreases in nuclear stopping.

ii) The nuclear stopping increases with system mass (from top to bottom) because the stop-

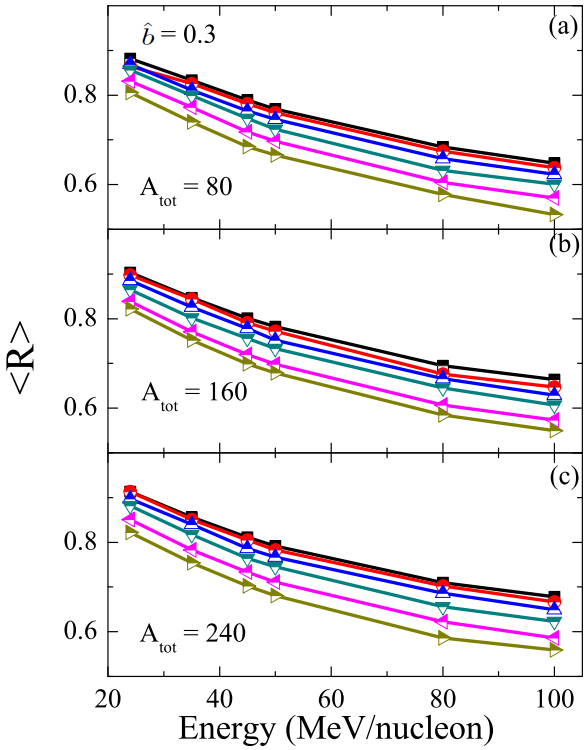

Figure 4.1: *Energy dependence of nuclear stopping at $\hat{b}$ = 0.3. Panels (a), (b) and (c) represent for different system masses A_{tot} = 80, 160 and 240, respectively, whereas different lines represent different mass asymmetries (η).*

ping phenomena is related to the collision zone, and the number of collisions increases with system mass.

iii) The behavior of nuclear stopping remain same (decreases with incident energy) for different sets of system mass in Fermi energy region.

iv) In literature, the maximum stopping is reported for the symmetric system of ^{197}Au + ^{197}Au [17]. A closer look at Fig. 4.1 shows that for the mass asymmetric collisions, the nuclear matter does not achieve complete thermalization. This result is in agreement with Ref. [18].

4.3.2 Effect of colliding geometry on nuclear stopping

Till now, author has studied the effect of mass asymmetry on nuclear stopping for nearly central collisions i.e. for $\hat{b}$ = 0.3. Depending on incident energy the behavior of nuclear stopping is also influenced by collision geometry [19, 20]. In Fig. 4.2, author studies the effect of colliding geometry on nuclear stopping for mass symmetric/asymmetric collisions

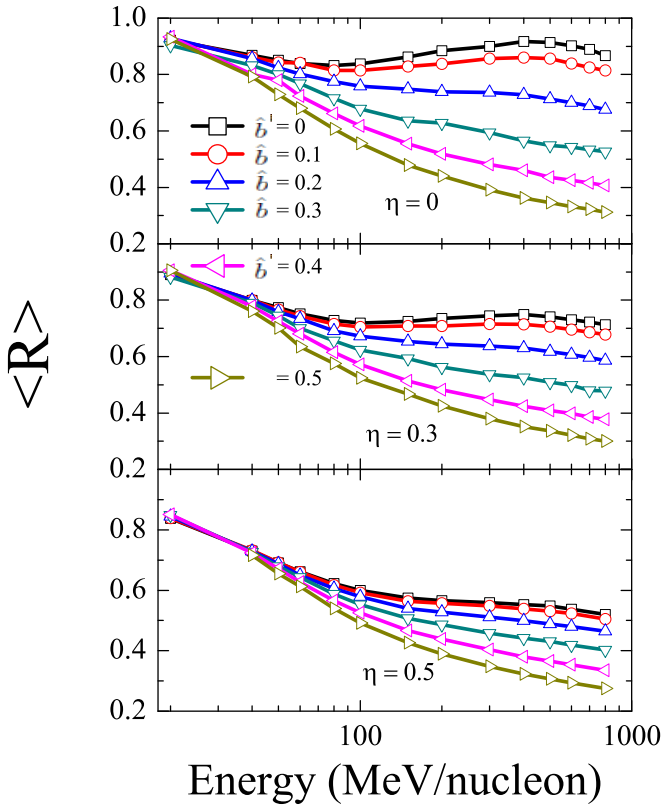

Figure 4.2: *Energy dependence of nuclear stopping in whole range of intermediate energy region for A_{tot} = 240. Panels (a), (b) and (c) represent the different mass asymmetric η = 0, 0.3 and 0.5, respectively, whereas different lines represent different collision geometry varying from $\hat{b}$ = 0 to 0.5.*

over the whole range of intermediate energy region. Figure reveals that the effect of colliding geometry on nuclear stopping for different mass asymmetric collisions is energy dependent. At low energy, the impact of colliding geometry keeps on decreasing with increase in mass asymmetry of colliding nuclei (from top to bottom). Moreover, the effect of colliding geometry on nuclear stopping keeps on increasing with incident energy.

In central ($\hat{b} = 0$) and nearly central ($\hat{b} = 0.1$, 0.2 and 0.3) collisions of mass symmetric reaction, one observes a negative slope till E $\sim$ 100 MeV/nucleon (in Fermi energy region). This happens because at low energy for symmetric collision ($\eta = 0$), residue of both target and projectile moves slowly toward the parallel and perpendicular momentum near their initial positions, thus stopping decreases. Moreover, at low incident energy one observe a dip, which vanishes with increase in mass asymmetry of colliding systems. This happens because in Fermi energy region, NN collisions suppressed by the Pauli blocking and nucleons tend to attain their initial properties [21, 22]. Moreover, in mass asymmetric collisions, because of lighter mass projectile, insufficient energy is pumped to break the target nucleus and projectile nucleus itself decay into fragments [23]. Thus, due to lack of backward scattering of target nucleus in mass asymmetric collisions, one gets small dip for mass asymmetric collisions around Fermi energy region. As one further increases the energy from E $\sim$ 100 to 400 MeV/nucleon, stopping again shows a positive slope, because above Fermi energy region, NN collisions are sufficient to break the initial correlations among the nucleons, which further transfer the initial longitudinal momentum in other directions and hence enhance the nuclear stopping.

Above E $\sim$ 400 MeV/nucleon, the mean free path and the time taken between the successive NN collisions become very small, which leads to suppressing the longitudinal component of momentum in transverse direction. Therefore, the nuclear stopping again decreases (known as transparency). The maximum stopping value is observed around E $\sim$ 400 MeV/nucleon for all central and semi-central collisions. These results are in agreement with the experimental data of FOPI collaboration [10].

Moreover, in semi-central collisions ($\hat{b} = 0.3$ and 0.4), one observe that $\langle R \rangle$ decreases with increase in incident energy for whole range of intermediate energy region. This happens because the nuclear stopping is directly connected to the participant zone, and participant

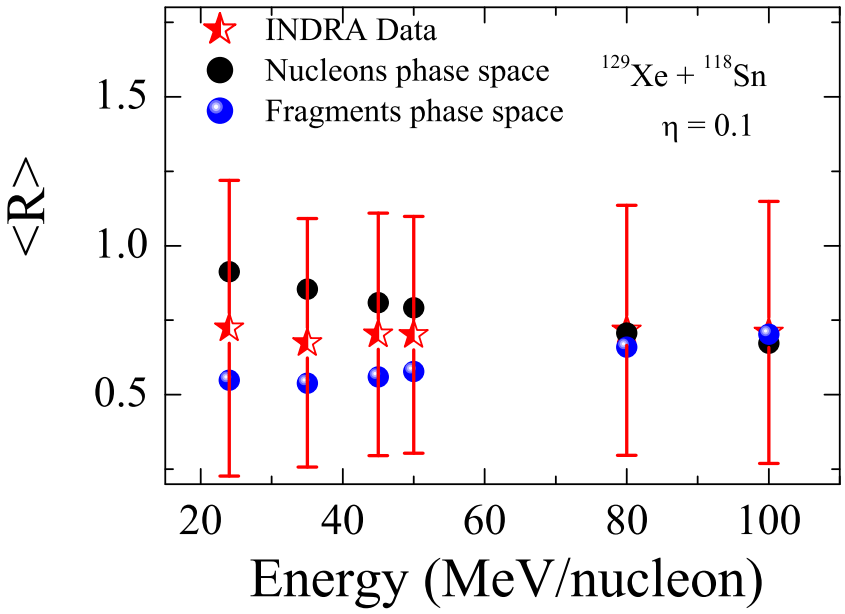

Figure 4.3: *Comparison between experimental (INDRA collaboration [24]) nuclear stopping with theoretical calculations of IQMD model in nucleons phase space (black circle) and fragment phase space (blue sphere) for the central collision of nearly symmetric reaction (^{129}Xe + ^{120}Sn).*

zone decreases with increase in colliding geometry.

4.3.3 Comparison between the nuclear stopping of nucleons and fragments phase space

Fig. 4.3, displays the energy dependence of nuclear stopping for free nucleons and fragments phase space for nearly asymmetric colliding system ($\eta = 0.1$). The stopping calculated for nucleons phase space is higher than that of fragments phase space because most of the free nucleons originate from the participant zone. Below E $\sim$ 50 MeV/nucleon, the nuclear stopping due to fragments phase space behave differently from that of free nucleons, because the emission of fragments is not isotropic in phase space.

To further strengthen our theoretical results, a comparison between theoretical calculations of IQMD model (nucleons phase space as well as fragments phase space) with experimental results [24] of INDRA collaboration is shown in Fig. 4.3. Zhang *et al.* [11] have theoretically proved that the fragments phase space with hard EOS and distance between nucleons of fragments i.e. $\triangle$r = 3.5 fm can better explain the INDRA's experimental data

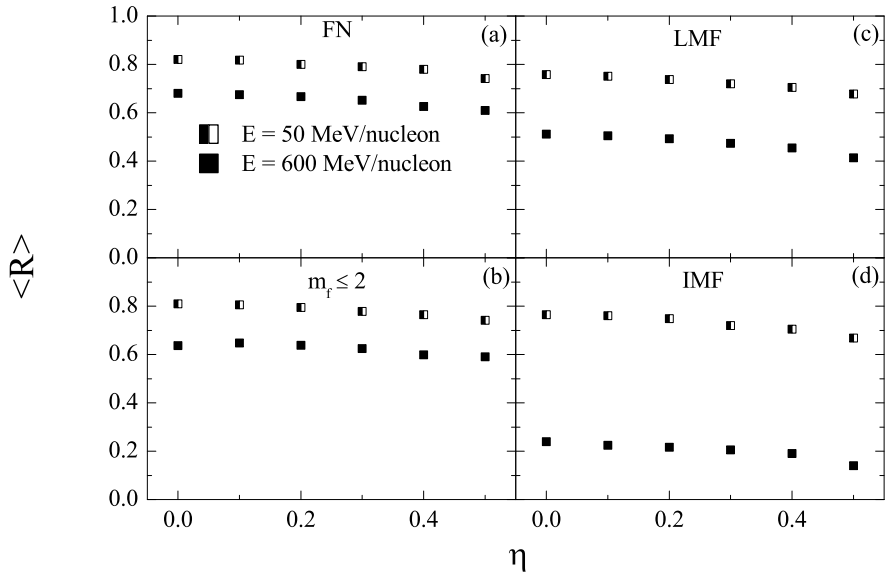

Figure 4.4: *Mass asymmetry dependence of nuclear stopping for (a) FN's, (b) fragments of mass less than and equal to 2 ($m_f \leq 2$), (c) LMF's and (d) IMF's.*

rather than nucleons phase space. Moreover, on comparing the experimental data with our calculations (calculated for soft EOS and $\triangle$r = 4 fm), both the nucleons as well as fragments phase space lie with in the range of INDRA's experimental data. Moreover, the nuclear stopping for fragment phase space shows a dip at E $\sim$ 35 MeV/nucleon as displayed for experimental data. However, such dip is not observed in nuclear stopping calculations for the case of free nucleons. Such findings encourage us to study the nuclear stopping of various fragments.

Till now, no one has reported the effect of fragment masses (FNs, $m_f \leq 2$, LMFs ($2 \leq m_f \leq 4$) and IMFs ($5 \leq m_f \leq A_{tot}/6$)) on nuclear stopping. Thus, it would be interesting to calculate the effect of mass asymmetry on nuclear stopping for different fragment masses.

4.3.4 Effect of mass asymmetry on fragments nuclear stopping

In Fig. 4.4, author has compared the effect of collision energy on the contribution of fragments towards the nuclear stopping (FN's ($m_f = 1$), $m_f \leq 2$, LMF's and IMF's, where

m_f is mass of fragments) for different mass asymmetries. The mass asymmetry of colliding nuclei varies between 0.0 to 0.5. From Fig. 4.4, one can clearly see the effect of collision energy on fragments stopping throughout the mass asymmetry. At low energy, different fragments undergo almost same thermalization. However, at high energy, nuclear stopping keeps on decreasing with fragment masses. In previous Figs. 4.1-4.3, author has showed that the nuclear stopping decreases with increase in incident energy. Thus, from Fig. 4.4, one can conclude that the decay of nuclear stopping at high energy is due to the larger contribution of heavy fragments (IMF's), those are originated from the decay of spectator matter.

The flow is generated by the pressure gradients established in the compressed matter and achieved density is hooked up to the degree of stopping. Lots of efforts have been made in the literature (theoretically and experimentally) to study the correlation between collective flow and nuclear stopping [10]-[13]. Thus, in the next step, author have discussed the results of directed transverse flow and its correlation with nuclear stopping under different reaction conditions (mass asymmetry and incident energy).

4.4 Transverse directed flow

The directed transverse flow is governed by the combined effects of attractive mean field and NN interactions. Depending on incident energy, the reaction outcome may lead to either negative or positive flow. At low incident energies, attractive mean field dominates the reaction dynamics, which leads to the negative flow. On the other hand, at higher energies repulsive NN interactions are responsible for the conflicting nature of the reaction dynamics. In fact, above E_{bal}, the positive values of mean transverse momentum results from kinetic pressure built up during the high density compressional stage of the collision. On the other side, at a particular energy, both attractive mean field interactions and repulsive NN interactions counterbalance with each other resulting into no net flow. This energy is dubbed as balance energy (E_{bal}) [25, 26]. The overlapping region does not expand preferentially along a particular angle at E_{bal}. In other words, the E_{bal} does not signifies the anisotropic emission of particles in transverse direction. Thus, in this section, author has studied the effect of mass asymmetry on directed transverse flow at below and above the E_{bal}. The

directed transverse flow is defined as [1]

$$\langle P_x^{dir} \rangle = \frac{1}{A_{tot}} \sum_i sign\{Y(i)\} p_x(i), \tag{4.5}$$

where A_{tot} refers to the sum of the masses of projectile and target, $p_x(i)$ is the transverse momentum of i^{th} nucleon and *Y(i)* is rapidity distribution, which is defined in eq. 4.1.

The origin of anisotropy for particles momentum distribution lies in the initial asymmetry and collision geometry of colliding nuclei. Because the spatial asymmetries rapidly decreases with time, flow can develop only in the first few fm/c. From this, one can conclude that flow must be sensitive to the NN interactions in the early stage of system evolution. The achieved density at this time is connected to the extent of nuclear stopping. It has been reported many times in the literature [10, 11] that there exists a strong correlation between the directed transverse flow ($\langle p_x^{dir} \rangle$), measured for non-central collisions and the nuclear stopping measured at central collisions $\langle R_{(0)} \rangle$. For symmetric and nearly symmetric collisions, the correlation between the directed transverse flow and nuclear stopping follow a linear behavior at high energies [10, 11]. But the correlation between nuclear stopping and directed transverse flow for mass asymmetric HIC below and above the E_{bal} is still unknown. Author has attempted to explain their correlation in proceeding sections.

4.4.1 Time evolution of transverse directed flow

Fig. 4.5 displays the time evolution of directed transverse flow ($\langle p_x^{dir} \rangle$), for various mass asymmetric collisions at E = 50 (upper panel) and 200 (lower panel) MeV/nucleon with total system mass, A_{tot} = 240 units. From Fig. 4.5, it is clear that below E_{bal} transverse flow is always negative. This shows that below E_{bal} reaction, the attractive mean field governs the reaction dynamics. These interactions turn repulsive (or positive) with increase in incident energy. From figure, one can see that at low energy, $\langle p_x^{dir} \rangle$ shows weak dependence on mass asymmetry of colliding systems. This happens because with increase in mass asymmetry of colliding system, low NN collisions take place, which results in lower saturation density and therefore, weak response occurs for variation in flow. On the other hand, at high energy, the NN collisions increases linearly with participant zone, therefore, huge difference of mass asymmetry can be seen. Moreover, the value of flow gets saturated after t = 100 fm/c

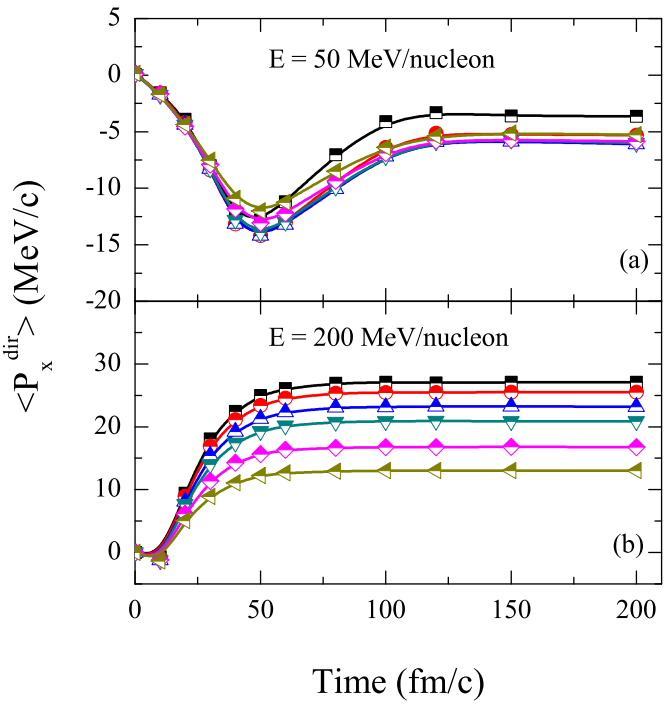

Figure 4.5: *Time evolution of transverse directed flow for different mass asymmetric collisions below (E = 50 MeV/nucleon, shown in upper panel) and above (E = 200 MeV/nucleon, shown in lower panel) the E_{bal}. Different lines represent different mass asymmetries (η).*

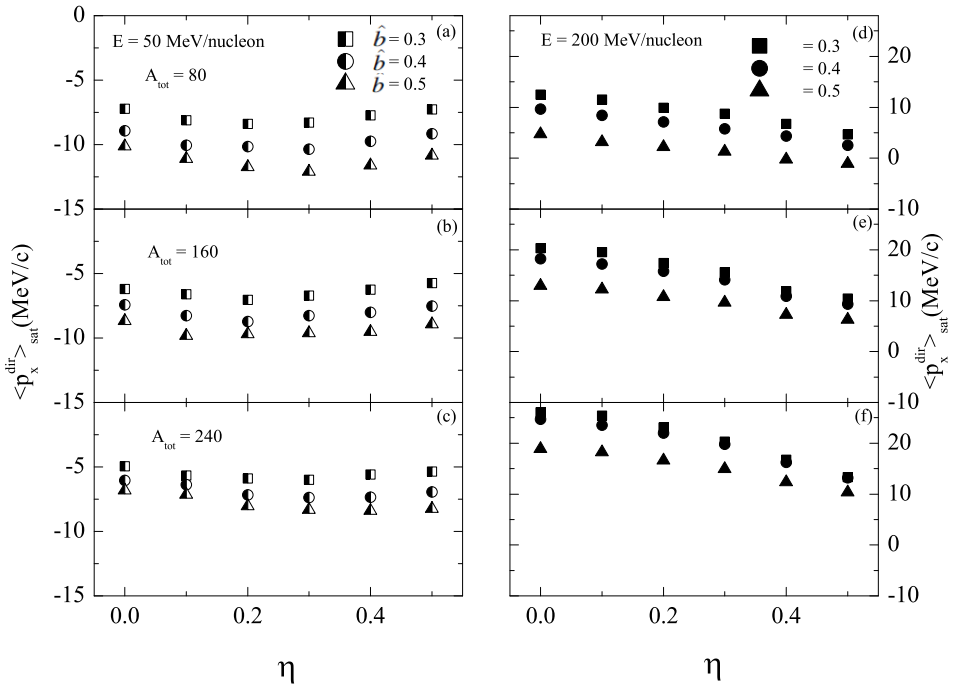

Figure 4.6: *Transverse directed flow as a function of mass asymmetry at different scaled impact parameter, $\hat{b}$ = 0.3, 0.4 and 0.5 and at incident energies E = 50 (left side) and 200 (right side) MeV/nucleon for three sets of total system mass A_{tot} = 80 units ((a) & (d)), A_{tot} = 160 units ((b) & (e)) and A_{tot} = 240 units ((c) & (f)).*

at both energies. The change in flow till 200 fm/c is negligible. Therefore, in following discussion, the results are shown at t = 200 fm/c and the value of directed transverse flow at this time is denoted by $\langle p_x^{dir} \rangle_{sat}$.

4.4.2 Mass asymmetry dependence of transverse directed flow

In Fig. 4.6, the transverse directed flow is calculated at saturation time i.e. t = 200 fm/c denoted by $\langle p_x^{dir} \rangle_{sat}$ as a function of mass asymmetry of colliding nuclei at E = 50 (below E_{bal}) and 200 (above E_{bal}) MeV/nucleon with $\hat{b}$ = 0.3, 0.4 and 0.5. From the figure one can observe that:

i) The $\langle p_x^{dir} \rangle_{sat}$ is negative for E = 50 MeV/nucleon and positive for high incident energy (E = 200 MeV/nucleon) which has been discussed many times in the literature [29, 30].

ii) At low incident energy, $\langle p_x^{dir} \rangle_{sat}$ shows a decrease till η = 0.2 and then shows a rise with further increase in mass asymmetry. This happens because, at low incident energy, with increase in mass asymmetry of colliding nuclei, the projectile nucleus completely merges

into the target nucleus and distribute its energy among the target nucleons. The collective motion of nucleons at low beam energies occur due to the rotation of participant zone, which force the nucleons to preferentially emitted near the reaction plane on target and projectile sides. The azimuthal anisotropy created by this motion is distinct as well as stronger due to the directed transverse momentum of the system. Moreover, the parabolic behavior at low energies is also due to the combined effect of the participant and the spectator matter. At low incident energy, with increase in mass asymmetry, fragments originated from the bounce-off region have small transverse as well as forward momentum, whereas non-destructive target nucleus (target residue) moves toward the projectile side. Therefore, due to the motion of target residue, one can observe more positive flow in highly mass asymmetry reactions.

iii) As the beam energy changes from 50 to 200 MeV/nucleon, the reaction dynamics changes completely. At high energy, $\langle p_x^{dir} \rangle_{sat}$ shows a decrease with mass asymmetry of the colliding nuclei. This happens because with increase in mass asymmetry, the projectile nucleus completely merges into the target nucleus as explained above. At E = 200 MeV/nucleon larger energy is boosted during the collision compared to the E = 50 MeV/nucleon, which enhances the NN collisions and decay the target residue due to this even after $\eta = 0.2$ at E = 200 MeV/nucleon, $\langle p_x^{dir} \rangle_{sat}$ shows a decrease with mass asymmetry of the colliding nuclei.

iv) The colliding geometry is the second factor that can vary the compression of the participant zone. The flow become more negative as one switches from semi-central to peripheral collisions. This happens because for semi-peripheral collisions, pressure gradient is more which leads to more negative value of flow compared to the semi-central collisions.

4.4.3 Correlation between nuclear stopping and transverse directed flow

To study the correlation between nuclear stopping and transverse directed flow, in Fig. 4.7, the nuclear stopping, $\langle R_{(0)} \rangle$ (measured at central collision) vs transverse directed flow ($\langle P_x^{dir} \rangle_{sat}$) measured at non-central collisions below (left side) and above (right side) the E_{bal} is displayed.

Figure reveals that at E= 50 MeV/nucleon the correlation between the $\langle R_{(0)} \rangle$ and $\langle p_x^{dir} \rangle_{sat}$

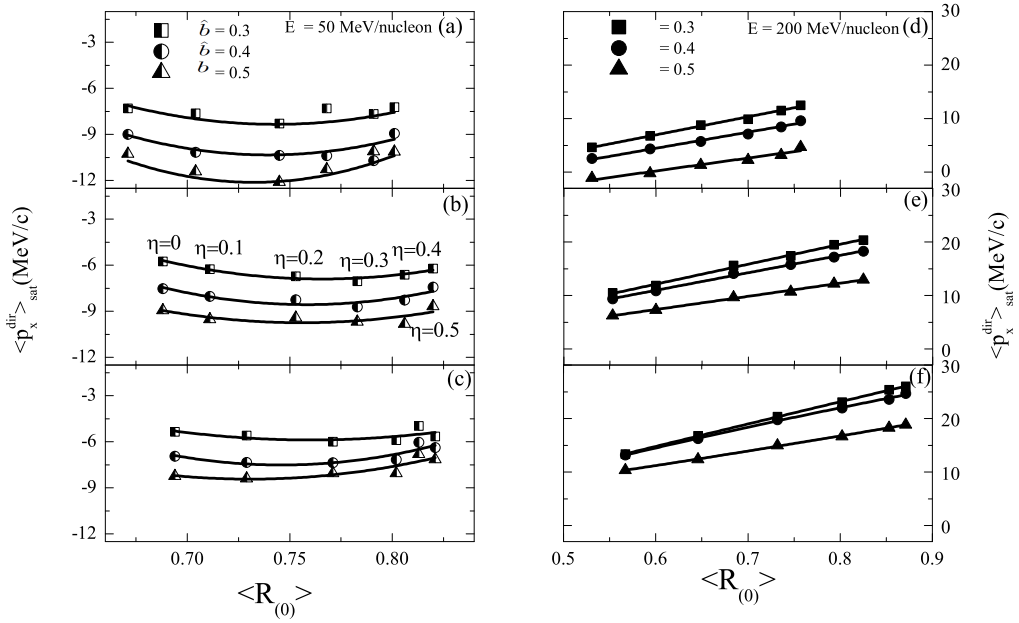

Figure 4.7: *Correlation between transverse directed flow calculated at scaled impact parameter, $\hat{b}$ = 0.3, 0.4 and 0.5 as a function of nuclear stopping which is calculated for central collisions (b = 0) at E = 50 (left side) and 200 (right side) MeV/nucleon for three sets of total system mass A_{tot} = 80 ((a) & (d)), A_{tot} = 160 ((b) & (e)) and A_{tot} = 240 ((c) & (f)).*

shows a parabolic behavior. The reason behind this has been explained earlier. Moreover at E = 200 MeV/nucleon the correlation between the nuclear stopping and transverse directed flow shows a linear dependence. This result is in agreement with Refs. [10, 11, 13]. This result is also in agreement with earlier predictions of Diogene collaboration [32] on charged pions for the reaction of Ne + Pb at an incident energy of 800 MeV/nucleon.

From Fig. 4.7, one can see that the correlation between nuclear stopping and flow remain same as colliding geometry is changed. The effect of colliding geometry keeps on decreasing as one increase the system mass (as one moves from top to bottom). Moreover, the effect of collision geometry decrease as one move toward large mass asymmetric collisions. This happens due to the effect of participant zone, where the projectile nucleus hits the target nucleus. It can be understood by considering an example as when one collide the Ne nucleus of radius 3.0 fm on Ni nucleus of radius 4.4 fm, the change of impact parameter does not affect the collision zone, rather it will shift only from position. Due to this, the rotational motion of participant zone come into picture [33] in highly asymmetric systems due to small

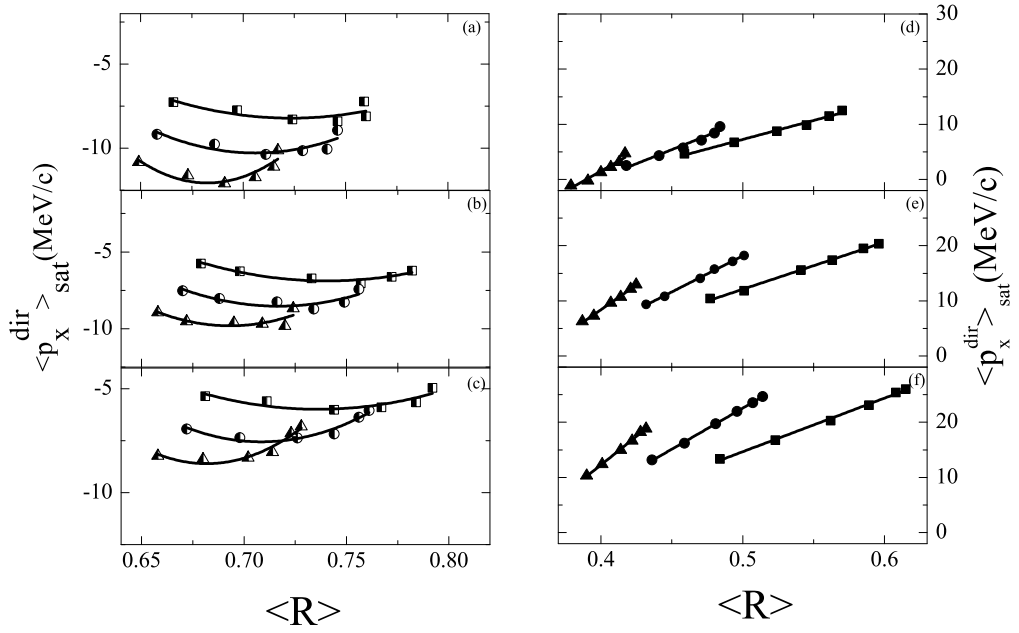

Figure 4.8: *Same as Fig. 4.7, but nuclear stopping is taken at same impact parameter where the directed flow is calculated. Left panels represent results at E = 50 MeV/nucleon and right panels represent results at incident energy E = 200 MeV/nucleon for three sets of total system mass A_{tot} = 80 ((a) & (d)), A_{tot} = 160 ((b) & (e)) and A_{tot} = 240 ((c) & (f)).*

size of projectile.

The curves (lines) at low (high) energy shows that the correlation between transverse directed flow and nuclear stopping shift toward the right on increasing the system mass. The shifting of curves (lines) is due to the nuclear stopping which increases with increase in system mass as shown in Fig. 4.1.

So far we have discussed the correlation between transverse directed flow (measured at non-central colliding geometries) and stopping parameter (measured at central collisions). It would be of interest to study whether this correlation follow the similar behavior (linear dependence at high energy and parabolic fit at low energy), if we study the correlation between directed flow and nuclear stopping, measured at non-central collisions. To study this fact, Fig. 4.8, the correlation between the above said observables for mass asymmetric systems measured at non-central collisions is shown. One can see that the correlation between these two quantities remains unaltered. Only difference is the shifting of parabolic curves (in low energy) and lines (in high energy) toward left with an increase in impact

parameter. This shifting is due to the existing correlation between these two observables.

Since all the calculations with different total mass show the similar behavior below and above the E_{bal}, therefore, one can say that this correlation is stout and is independent from system mass of colliding nuclei and dependent on both incident energy as well as colliding geometry. Till now, we have explored the correlation between the transverse directed flow and nuclear stopping.

In the next section, we will discuss the second harmonic of flow i.e. elliptical flow of different fragments and study the effect of in-plane and out-of-plane fragments flow on nuclear stopping.

4.5 Elliptical Flow

The nuclear flow generated due to the anisotropic distribution of nuclear matter in non-central collisions resulting in orthogonal asymmetry in configuration of space is known as elliptical flow. It is termed as elliptic because at mid-rapidity shape of ϕ-distributions resemble like an ellipse with a major axis along the x-axis (in-plane emission) or y-axis (out-of-plane emission). The elliptical flow is also known as squeeze-out, rotational motion, or anisotropic flow. Initially, the elliptical flow of overlap region is characterized by the eccentricity (ϵ), which is defined as [34]:

$$\epsilon = \frac{y^2 - x^2}{y^2 + x^2}. \tag{4.6}$$

The elliptical flow is quantitatively defined as the difference between the minor and the major axis. The elliptical flow is counted as second-order Fourier expansion given by Voloshin [35]:

$$v_2 \;=\; \langle \cos 2\phi \rangle = \left\langle \frac{p_x^2 - p_y^2}{p_x^2 + p_y^2} \right\rangle, \tag{4.7}$$

where p_y and p_x are y and x components of momentum. The direction of p_x is in the reaction plane, while p_y is perpendicular to the reaction plane, and ϕ is azimuthal angle of emitted particle's momentum relative to the x-axis. The positive elliptical flow explain the eccentricity of an ellipse-like distribution that indicates the in-plane particle emission. For the case of in-plane particle emission, due to smaller NN collisions most of the spectator matter prominent along the reaction plane. The negative value of flow indicates the out-of

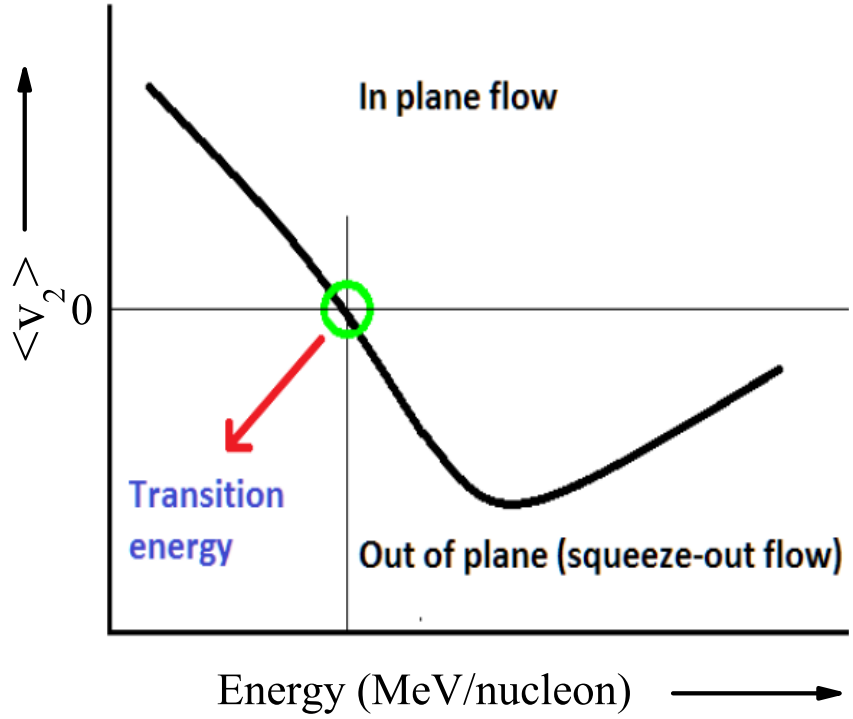

Figure 4.9: *Pictorial view of energy dependence for elliptical flow [36].*

plane particle emission. The particular energy at which nuclear matter transfer from in-plane to out-of-plane is known as transition energy (E_T) [37, 38, 39] as shown in Fig. 4.9. The zero value of v_2 corresponds to isotropic distribution of nucleons around the reaction plane. The transition energy depends on particles emission and shadowing of the spectator matter.

The phenomena of elliptical flow is generated from the participant zone where projectile and target nuclei are shattered to produce squeeze-out of nuclear matter perpendicular to the reaction plane, whereas phenomena of nuclear stopping is also generated from the participant zone. Thus, one can correlate these two observables with each other. In literature, various independent studies are reported that point toward the correlation between transition energy and nuclear stopping. Jain *et al.* [37] studied the effect of charge asymmetry on E_T of different fragment masses, and reported that the E_T of fragments is independent from the isospin content of colliding systems. Vinayak and Kumar [38], reported that there is a correlation between the behavior of LMFs, elliptical flow and nuclear stopping. Cao *et al.* [39] studied the excitation function of elliptical flow for FNs and LMFs in case of spherical

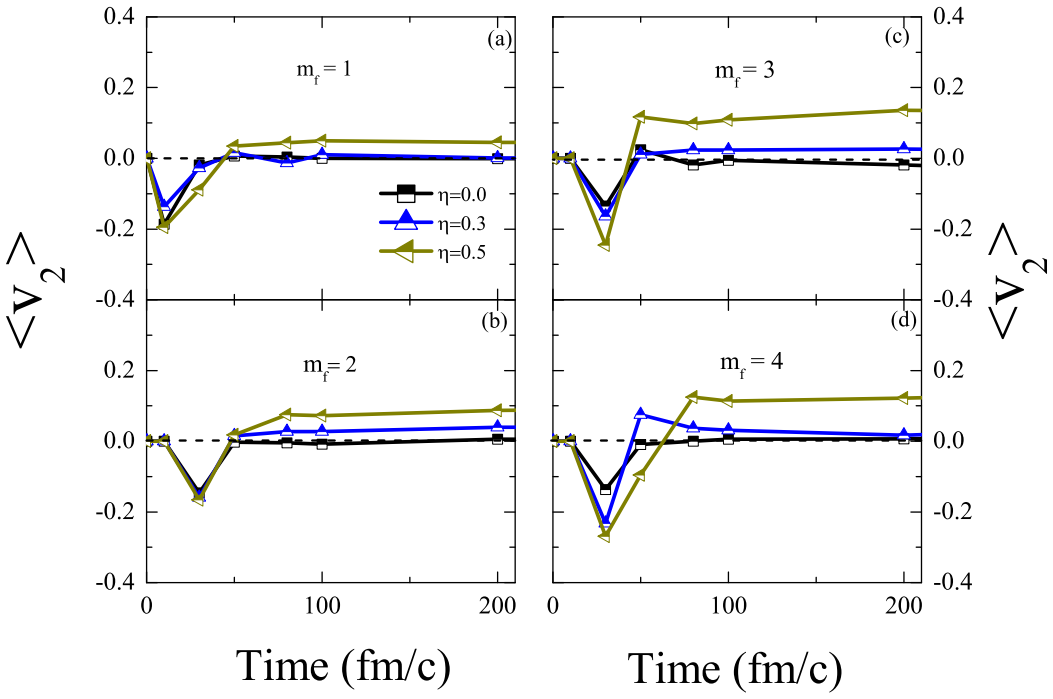

Figure 4.10: *Time evolution of elliptical flow for various mass asymmetric collisions at E = 200 MeV/nucleon. Different panels represent for different fragment masses.*

and deformed configuration of colliding nuclei for different forms of EOS. From these studies, one can clearly see that E_T depend on the fragment masses. Zhang *et al.* [11], reported a positive correlation between the elliptical flow and nuclear stopping for symmetric and nearly symmetric reactions.

In following sections, elliptical flow is calculated for different fragments free nucleon (FN) (mass of fragment, $m_f = 1$), $m_f = 2$, 3 and 4. A systematic study of mass asymmetry is performed by considering the reactions of ^{120}Te + ^{120}Te ($\eta = 0$), ^{108}Cd + ^{132}Ba ($\eta = 0.1$), ^{96}Mo + ^{144}Nd ($\eta = 0.2$), ^{84}Sr + ^{156}Dy ($\eta = 0.3$), ^{71}Ga + ^{169}Tm ($\eta = 0.4$) and ^{60}Ni + ^{180}W ($\eta = 0.5$), having $A_{tot} = 240$ units, on transition energy of fragments. The fragments are constructed by using Minimum Spanning Tree (MST) method [1, 2].

4.5.1 Time evolution of elliptical flow

In Fig. 4.10, the time evolution of the elliptical flow for different fragment masses ($m_f = 1$ (a), $m_f = 2$ (b), $m_f = 3$ (c) and $m_f = 4$ (d)) is displayed. Different lines represent the results for different mass asymmetry of colliding systems. A considerable difference due to

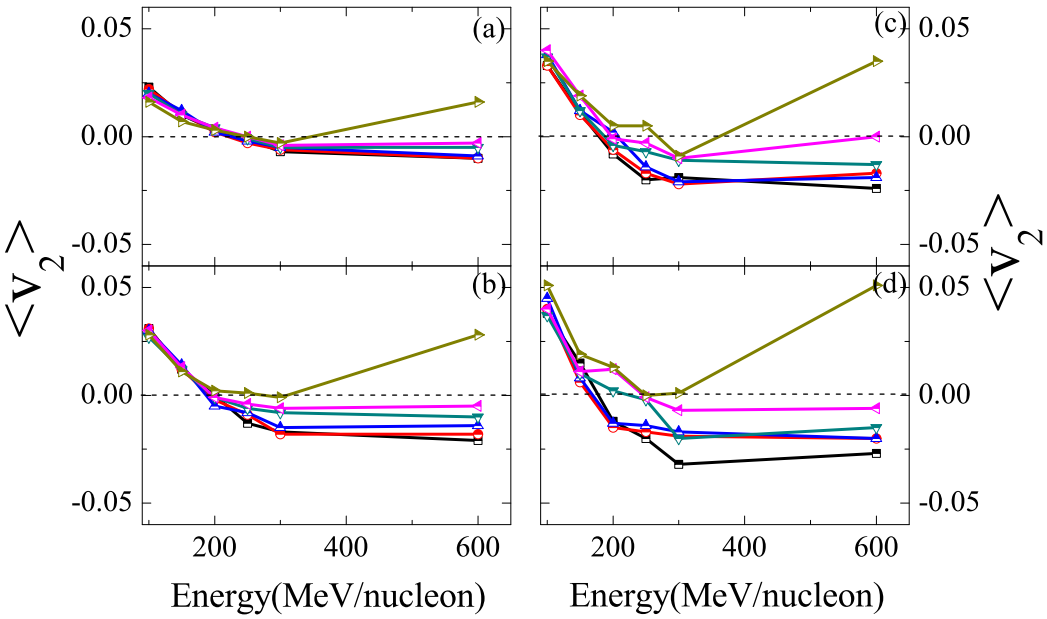

Figure 4.11: *Energy dependence of* $\langle v_2 \rangle$ *for different fragment masses. Different panels are represent for different fragment masses as taken in Fig. 4.10.*

mass asymmetry can be seen throughout the time span. One can see that in initial phase of collisions the elliptical flow is always negative. After t = 100 fm/c, flow becomes more positive with increase in mass asymmetry of colliding nuclei and saturates. Moreover, the flow become more positive as one moves toward heavy fragments.

4.5.2 Effect of mass asymmetry on E_T of different fragments

Fig. 4.11 represents the energy dependence of elliptical flow $\langle v_2 \rangle$ for different fragments as considered in Fig. 4.10. In Fig. 4.11, the positive value of $\langle v_2 \rangle$ at low energies signifies the in-plane particles emission and negative value at higher energies signifies the out-of-plane particles emission. This happens due to dominant role of mean field at low energies. At high energies large compression in participant zone increases the squeeze-out of nuclear matter and shadowing effect due to the spectator matter, turns the flow negative. The energy at which $\langle v_2 \rangle$ changes its sign is known as transition energy (E_T). The E_T increases with mass asymmetry of colliding nuclei. This happens because with increase in mass asymmetry participant matter decreases and spectator matter increases. Moreover, E_T shows large

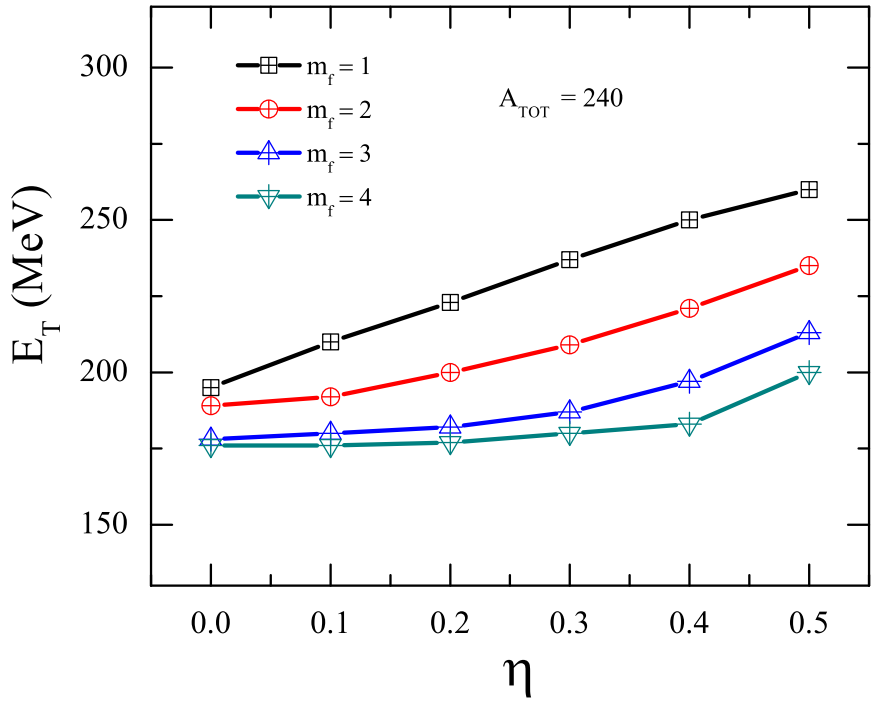

Figure 4.12: *Effect of mass asymmetry on E_T of different fragment masses.*

sensitivity toward the different fragment masses. Thus, to study the mass asymmetry effect on E_T of various fragment masses, in Fig. 4.12, author displays E_T as a function of η for different fragment masses. It is clear from the figure that E_T is influenced by fragment masses. The transition energy depends on three competing components, first is rotation of nucleus, second is expansion of the hot and compressed nuclear matter and last is shadowing of the cold spectator matter [41]. The study of fragment's transition energy for mass asymmetric collisions, reflect the effect of above three components. With increase in mass asymmetry, size of projectile become small and when it hits the target, the non colliding part of target nucleus (target residue) separates from the participant zone. Moreover, slope of E_T with mass asymmetry is varied for fragment masses. This happens because the fragments of mass $m_f = 1$ are produced from the expansion of hot and compressed nuclear matter. Whereas other fragments are originated from both participant as well as spectator matter.

4.5.3 Study of nuclear stopping at and around the transition energy

Vinayak and Kumar [38] have shown that the multiplicity of LMFs, nuclear stopping and elliptical flow resembles with each other and reported that of LMFs at and around the transition energy give us an idea about the reaction dynamics. Moreover, LMFs are correlated with nuclear stopping. Thus, in Fig. 4.13, author study the contribution of in-plane (below E_T) and out-of-plane (above E_T) emission of particles on nuclear stopping via considering the mass asymmetric collisions. To study the behavior of nuclear stopping at and around the transition energy, the reactions are simulated at energies below (with decrement of 25 MeV/nucleon from E_T) and above (with increment of 25 MeV/nucleon from E_T) the transition energy. From Fig. 4.13, author find that $\langle R \rangle$ decreases with increase in mass asymmetry for various fragment masses. This happens due to decrease in participant zone. The $\langle R \rangle$ of fragments having mass $m_f = 1$ do not show any variation at and around the transition energy. The $m_f = 1$ fragments have a larger contribution towards stopping value, which indicates that most of the small mass fragments are originating from participant zone. However, there exist a positive correlation between the nuclear stopping and the elliptical flow [39] i.e. larger stopping value indicates large elliptical flow. Moreover, stopping shows measurable difference at and around the transition energy for heavy fragments. It is clear that during the collision most of positive flow (in-plane) is contributed by the fragments that are originated from the participant zone. Moreover, role of spectator matter increases as one moves toward the heavy fragments. However, in previous Fig. 4.4, author has proved that the heavy fragments are responsible for decrease in nuclear stopping. Moreover, for different η, one can see a considerable change in magnitude of elliptical flow. This is due to the larger momentum associated with heavy fragments.

4.6 Summary

Author has studied the effect of mass asymmetry on nuclear stopping and nuclear flow under various reaction conditions. The study reveals that in intermediate energy region, behavior of nuclear stopping in central and semi-central collisions is entirely different from the semi-peripheral collisions. In mass asymmetric collisions, the non-colliding matter is

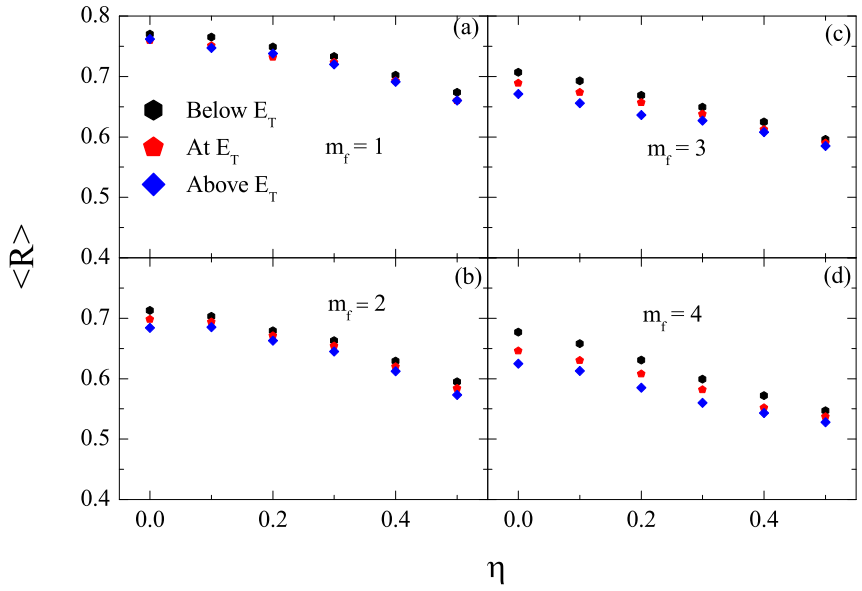

Figure 4.13: *Mass asymmetry dependence of nuclear stopping for different fragment masses at and around the E_T.*

responsible for decrease in stopping value. The flow is generated via the pressure gradient established in the compressed matter and the achieved density is hooked up to the degree of stopping. Author has also studied the correlation between the transverse directed flow with nuclear stopping below and above the balance energy. The correlation between transverse directed flow and nuclear stopping shows a significant change with incident energy as well as colliding geometry. At higher incident energies, it shows a linear dependence, while at low incident energy one can see a parabolic behavior between flow and stopping. The correlation between stopping and flow is stout and is independent of the A_{tot} for different mass asymmetries. Moreover, there are considerable difference between the stopping of free nucleons and fragments phase space.

In addition to this, author has also showed that fragment's transition energy exhibit large sensitivity toward the mass asymmetry of the colliding nuclei. Moreover, the fragments transition energy act as a good probe to understand the reaction dynamics. The study gave an evidence that most of the positive flow (in-plane flow) occurs due to the small fragment masses that are originated from participant zone, whereas negative flow (out-of-plane flow)

occur due to the heavy fragments that are produced from spectator zone.

Bibliography

[1] J. Aichelin, Phys. Rep. **202**, 233 (1991).

[2] P. B. Gossiaux and J. Aichelin, Phys. Rev. C **56**, 2109 (1997).

[3] W. Reisdorf *et al.,* Phys. Rev. Lett. **92**, 232301 (2004).

[4] J. Y. Liu, W. J. Guo, S. J. Wang, W. Zuo, Q. Zhao and Y. F. Yang, Phys. Rev. Lett. **86**, 975 (2001).

[5] V. Kaur, S. Kumar and R. K. Puri, Nucl. Phys. A **861**, 37 (2011).

[6] S. A. Bass *et al.,* GSI Scientific Rep. **94**, 66 (1995).

[7] W. Bauer, Phys. Rev. Lett. **61**, 2534 (1988).

[8] B. A. Li, C. M. Ko and W. Bauer, Int. J. of Mod. Phys. E **7**, 147 (1998).

[9] Y. Yuan, Q. Li, Z. Li and F. H. Lui, Phys. Rev. C **81**, 034913 (2010).

[10] W. Residrof *et al.* Phys. Rev. Lett. **92**, 232301 (2004).

[11] Y. Zhang, Z. Li and P. Danielewicz, Phys. Rev. C **75**, 034615 (2007).

[12] A. Jain and S. Kumar, J. Phys. G: Nucl. Part. Phys. **41**, 105105 (2014).

[13] A. Andronic, J. Lukasik, W. Residrof and W. Trautman, Eur. Phys. J. A **30**, 31 (2006).

[14] R. Bansal, A. Jain and S. Kumar, Indian J. Phys. **89**, 1077 (2015).

[15] S. Gautam, A. D. Sood, R. K. Puri and J. Aichelin, Phys. Rev. C **83**, 034606 (2011).

[16] S. Kaur and R. K. Puri, Phys. Rev. C **87**, 014620 (2013).

[17] S. Kumar and S. Kumar, Chin. Phys. Lett. **27**, 062504 (2010).

[18] J. Liu, W. Guo, S. Wang, W. Zuo, Q. Zhao and Y. Yang, Phys. Rev. Lett. **86**, 975 (2001).

[19] S. Kumar, S. Kumar and R. K. Puri, Phys. Rev. C **81**, 014601 (2010).

[20] Q. F. Li and Z. X. Li, Chin. Phys. Lett. **19**, 321 (2002).

[21] G. Q. Zhang *et al.,* Phys. Rev. C **84**, 034612 (2011).

[22] M. D. Toro, V. Baran, M. Colonna and V. Grece, Jour. of Phys. G: Nucl. Part. Phys. **37**, 083101 (2010).

[23] H. Stöcker, J. A. Maruhn and W. Greiner, Phys. Rev. Lett. **44**, 725 (1980).

[24] G. Lehaut *et al.,* Phys. Rev. Lett. **104**, 232701 (2010).

[25] D. Krofcheck *et al.,* Phys. Rev. Lett. **63**, 2028 (1989).

[26] R. Bansal, S. Gautam, R. K. Puri and J. Aichelin, Eur. Phys. J. A **51**, 2 (2015).

[27] C. Hartnack, R. K. Puri, J. Aichelin, J. Konopka, S. A. Bass, H. Stöcker and W Greiner Eur. Phys. J. A **1**, 151 (1998).

[28] C. Hartnack, H. Oeschler, Y. Leifels, E. L. Bratkovskaya, J. Aichelin Phys. Rep. **510**, 119 (2012).

[29] Y. M. Zheng, C. M. Ko, B. A. Li and B. Zhang, Phys. Rev. Lett. **83**, 2534 (1999).

[30] B. A. Li and A. T. Sustich, Phys. Rev. Lett. **82**, 5004 (1999).

[31] G. Q. Zhang *et al.,* Phys. Rev. C **84**, 034612 (2011).

[32] J. Gosset *et al.,* Phys. Rev. Lett. **62**, 1251 (1989).

[33] Y. G. Ma, W. Q. Shen, J. Feng and Y. Q. Ma, Phys. Rev. C **48**, 1492(R) (1993).

[34] B. Alver *et al.,* Phys. Rev. C **77**, 014906 (2008).

[35] S. A. Voloshin, Phys. Rev. C **55**, 1630(R) (1997).

[36] K. S. Vinayak, Ph.D. thesis, India (2013).

[37] A. Jain, S. Kumar and R. K. Puri, Phys. Rev. C **85**, 064608 (2012).

[38] K. S. Vinayak and S. Kumar, Phys. Rev. C **83**, 034614 (2011).

[39] X. G. Cao *et al.,* Phys. Rev. C **81**, 061603(R) (2010).

[40] R. K. Puri *et al.,* Phys. Rev. C **45**, 1837 (1997).

[41] A. Andronic *et al.,* Phys. Lett. B **612**, 173 (2005).

Chapter 5

Summary and outlook

5.1 Summary

This thesis contains a theoretical study of collective flow and nuclear stopping in intermediate energy heavy-ion collisions. The isospin-dependent quantum molecular dynamics (IQMD) model have been used to generate the nucleonic phase-space. The phase space has been analyzed using the minimum spanning tree (MST) method of clusterization to get the useful information about different phenomena's mentioned above.

In **Chapter 1** starting with the introduction of heavy-ion physics and its phenomena's like multifragmentation, collective flow, nuclear stopping, author discussed the various experimental and theoretical attempts to study the above phenomena. The details of isospin-dependent (IBUU and IQMD) models has been discussed in **Chapter 2**. Author also discussed the secondary model, minimum spanning tree (MST) method that is used to analyse the phase space of nucleons.

In **Chapter 3**, using Isospin-dependent Quantum Molecular Dynamics (IQMD) model, author discussed the role of density dependent symmetry energy on p_t-differential transverse flow for symmetric reactions in Fermi energy region. The study showed that the effect of density dependent symmetry energy is highly prominent in Fermi momentum region i.e. $0.2 < p_t < 0.3$ GeV/c, thus Fermi momentum region can act as a good probe to study the effects of density dependent symmetry energy. Author has also proved that the N/Z dependence of p_t-differential transverse flow of heavier systems can act as a good probe to constrain the density dependent symmetry energy in supra-saturation region. Maximum value of p_t-differential transverse flow act as a more suitable probe compared to the EVF to

study the effect of density dependent symmetry energy. The theoretical calculations follow the similar trend as given by the experimental findings of FOPI collaborations for different rapidity bins, whereas the role of density dependent symmetry energy is negligible away from the mid-rapidity region.

In **Chapter 4**, author has studied the effect of mass asymmetry on nuclear stopping under various reaction conditions. The behavior of nuclear stopping showed a minima and maxima in central and semi-cental collisions only. In asymmetric collisions, the non-colliding matter (IMF) are responsible for decrease in stopping value. The correlation between transverse directed flow and nuclear stopping show a significant change with incident energy as well as colliding geometry. At higher incident energies, it shows a linear dependence, while at low incident energy, author observe a parabolic behavior. The correlation between stopping and flow is stout and is independent of the system mass for various mass asymmetries. The study gave an evidence that most of the positive flow (in-plane flow) occurs due to the small fragment masses $m_f = 1$, whereas heavy fragments are contributing to the negative flow (out-of-plane flow).

5.2 Outlook

Though, author has studied the role of isospin content of colliding nuclei, density dependence of symmetry energy and isospin dependent NN cross-section on p_t-differential transverse flow. In addition, the influence of mass asymmetry on nuclear stopping has been studied in detail both below and above the Fermi energy region. There are many challenges yet to be solved. One can study why the number of particles decreases with increase in transverse momentum. One can estimate the energy dissipation in mass asymmetric collisions through nuclear stopping. Rotational effects of nuclear matter in mass asymmetric collisions will be of great use to study the production of giant monopole resonant. One can also develop the equation of state for isospin asymmetric nuclear matter. Moreover, one can expand the study of fragments stopping to understand the NEOS. The study of mass asymmetric collisions could be of great use for the new facility called ANURIB (Advanced National facility for Unstable & Rare-Isotope Beams) at VECC Kolkata.